STUDY OF NITROUS ACID (HONO) FORMATION MECHANISM AND ITS IMPACT ON PHOTOCHEMISTRY IN HONG KONG

WU JUEQI

M.Phil

The Hong Kong Polytechnic University

2014

The Hong Kong Polytechnic University

Department of Civil and Environmental Engineering

STUDY OF NITROUS ACID (HONO) FORMATION MECHANISM AND ITS IMPACT ON PHOTOCHEMISTRY IN HONG KONG

A thesis submitted in partial fulfillment of

the requirements for the degree of

Master of Philosophy

By

WU Jueqi

February 2014

CERTRIFICATE OF ORIGINALITY

I hereby declare that this thesis is my own work and that, to the best of my knowledge and belief, it reproduces no material previously published or written nor material which has been accepted for the award of any other degree or diploma, except where due acknowledgement has been made in the text.

Name: Wu Jingqi

Signature:

ABSTRACT

Nitrous acid (HONO) is an important trace gas in the atmosphere. It is a key precursor of the hydroxyl radical (OH) which is one of the most significant oxidants in the atmosphere. Therefore, HONO plays an important role in atmospheric chemistry and formation of air pollution. There has been a growing amount of research in the recent decade on the HONO sources and its environmental impacts, but the daytime formation mechanism of HONO still remains under debate.

Hong Kong is a coastal city in southern China which suffers from severe photochemical air pollution. Due to the lack of field measurements, little is known about the abundances, sources, and atmospheric consequences of HONO in Hong Kong. In this study, the first continuous measurements of ambient HONO in Hong Kong, as well as measurements of other related gases and aerosols were conducted by researchers in the Hong Kong Polytechnic University. In order to better interpret the observed HONO data, a box model coupled with an explicit Master Chemical Mechanism (MCM, version 3.1) is applied to a strong photochemical episode during the comprehensive field campaign. The model is constrained by real-time observation data, including O_3, CO, NO, NO_2, VOCs, etc., which helps to improve the model performance. Based on the numerical simulations, daytime potential HONO sources and the impact of HONO on photochemistry are investigated. The major findings include: (1) High daytime HONO concentrations (over 1 ppbV) were frequently measured, which is among the highest HONO level in the existing records. (2) Nighttime HONO accumulation is mainly

attributed to NO_2 heterogeneous reaction on ground surfaces, while the high daytime HONO level cannot be explained by the already known gas-phase reaction (NO+OH). Only a significant extra daytime source(s) (P_{extra}) of 1.12 pptV/s would sustain the observed HONO levels. Correlation analysis further indicates that a heterogeneous reaction of NO_2 on aerosol appears to be a significant source of daytime HONO at the site, which is different from the results in many other studies. (3) HONO photolysis is found to be an important OH source throughout the day. If we only considered the homogenous source (NO+OH) in the MCM model, as is the case in most current air quality models, the OH concentration would be underestimated by up to 20%.

This study has proved that there exists strong unknown HONO source(s) in the daytime at our study site. Moreover, modeling results suggest that a comprehensive HONO formation mechanism should be coupled into the chemical mechanism so as to get a better model performance of OH radical and other related species. Since this is the very first piece of effort on HONO study in Hong Kong, more focus should be put on this topic in the future, in order to obtain a whole picture of HONO in Hong Kong.

Acknowledgements

I would like to express my heartfelt gratitude to my chief supervisor, Professor Tao Wang, for his continuous guidance, encouragement, care, support, and patience throughout my entire graduate study. He provided me with an invaluable opportunity to conduct this research. In overcoming the difficulties of working with numerical model, I developed skills in problem solving and data interpretation. In addition, the many helpful discussions with Professor Wang throughout my study period gave me important insights that shaped my research style and improved my scientific perspective on atmospheric chemistry.

I would like to sincerely thank Mr. Steven Poon for his generous help whenever I have problems with both my work and daily life. I am also very grateful to my group-mates: Dr. Xue Likun, Dr. Wang Zhe, Guo Jia, Xu Zheng, Zhou Shenzhen, Zha Qiaozhi, Tham Yee Jun, Zhang Li, Yan Chao for their continuous help and discussions on my research topic. It is wonderful to have you guys in my life at PolyU. In addition, thank you so much to Prof. S. C. Lee, Dr. K.S. Lam and Dr. Hai Guo for their support and advice on both my study and life over the years. Finally and most importantly, I would like to sincerely thank my parents and family for their unconditional love, support, and tolerance. My thesis would not have been possible without having these people in my life. I truthfully appreciate them.

This project was funded by a studentship provided by the Hong Kong Environment and Conservation Fund (Project No. 7/2009), the Hong Kong Environmental Protection Department (HKEPD), and the Niche Area Development Program of the Hong Kong Polytechnic University (PolyU) (1-BB94). I really acknowledge the financial support from HKEPD and PolyU.

TABLE OF CONTENTS

LIST OF FIGURES

LIST OF TABLES

Chapter 1 Introduction

Rapid industrial expansion and development of science and technology have been observed in the past few decades. Unquestionably, these developments accelerate the growth of global economy and benefit the quality our daily life. However, resulting pollutants released into the atmosphere are also increasing. For example, emission of massive amount of primary pollutants, such as NO, NO_2, CO, SO_2, and VOCs, are mainly resulted from human-related activities. These activities include urbanization, industrialization, transportation, and fossil combustion processes (Figure 1.1) (Wang et al., 2002). After emitted into the atmosphere, these primary pollutants undergo complex chemical reactions and lead to production of numerous secondary pollutants such as ozone (O_3), peroxyacyl nitrate (PAN), nitric acid (HNO_3), nitrous acid (HONO), and some non-methane VOCs.

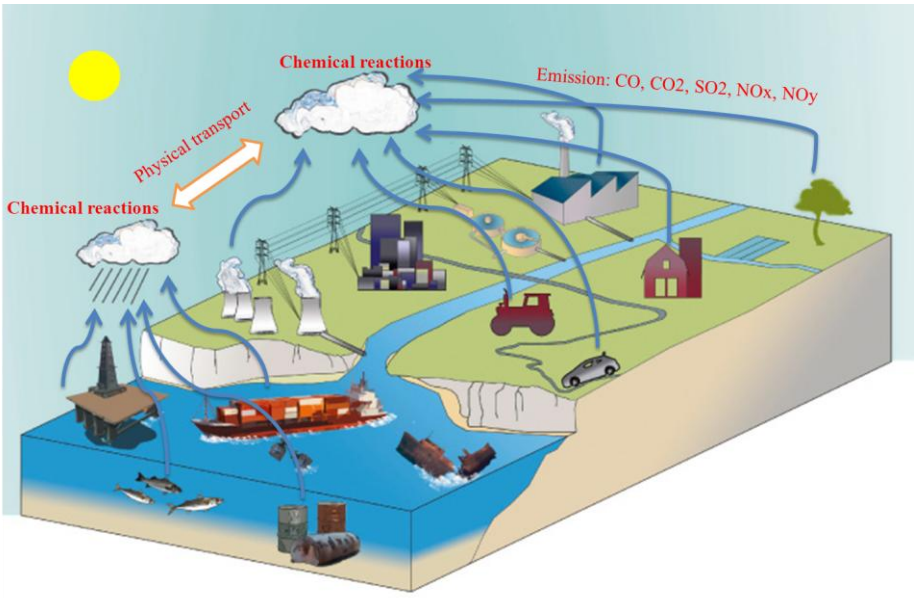

Figure 1.1 Schematic of pollutants emission from vehicles and industries.

Among all secondary pollutants, O_3, especially tropospheric ozone, has gained widespread attention because of its negative impacts to both environment and human health. Since the very early times, numerous studies have been carried out to reveal the formation and decomposition mechanisms of tropospheric ozone (Krupa and Manning, 1988; Finlayson-Pitts and Pitts Jr, 1993). Up to now, its long-term trends, diurnal and seasonal variation characteristics, source and sink pathways are well understood (Wu and Chan, 2001; Wang et al., 2003; Vingarzan, 2004; Oltmans et al., 2006; Cooper et al., 2010; Zheng et al., 2010). Meanwhile, along with the in-depth understanding of O_3, effective control strategies on O_3 pollution in the troposphere have been proposed and widely adopted (Sillman, 1993; Ryerson et al., 2001; Chou et al., 2006).

Compared to O_3, another secondary pollutant, nitrous acid (HONO), is still not clear to the public. Ever since the first unequivocal detection of HONO in the atmosphere by Perner and Platt (1979), HONO has aroused the interests of many scientists. It is an important trace gas in atmosphere. Yet, it is usually present in small quantities, typically up to a few ppbV at night, which only makes up a small portion of the total amount of gaseous nitrogen oxides (Lammel and Cape, 1996). In spite of such low concentration in atmosphere, it plays a significant role in the atmospheric chemistry. To be specific, its importance reflects on the strong impact to hydroxyl radical (OH). In the presence of sunlight, HONO can photo-dissociate to OH and NO (Seinfeld and Pandis, 1998):

$$\mathrm{HONO} + \mathrm{hv} \rightarrow \mathrm{OH} + \mathrm{NO}\ (300\mathrm{nm} < \lambda < 400\mathrm{nm}) \qquad \text{(R1.1)}$$

Therefore, HONO is considered as a reservoir for both NOx (NOx=NO+NO_2) and HOx (HOx=HO_2+OH). Its photolysis is believed to be an important OH source especially in the early morning, when other OH precursors are still small (Jenkin et al., 1988; Seinfeld and Pandis, 1998; Kleffmann, 2007; Zhang et al., 2012).

OH radical is one of the major oxidants in the atmosphere. Due to its high reactivity, OH radical can react with trace species, which will then lead to the production of various reactive radicals and intermediates. These propagating reactions initiate the photochemistry, resulting in formation of series of secondary pollutants (Levy 2nd, 1971; Brasseur et al., 2003; Hofzumahaus et al., 2009).

Given the strong relation between HONO and OH radical, impact of HONO to photochemistry is non-negligible. Therefore, ambient HONO has been measured in many field campaigns (Stutz et al., 2002; Kleffmann et al., 2003; Su et al., 2008b). In most of these measurements, similar HONO diurnal patterns have been observed, with the highest concentration appeared at night and the lowest in the daytime. The daytime trough mainly results from fast photolysis of HONO, (R1.1). Based on this sink path way together with another two reactions (R1.2) and (R1.3), a theoretical gas-phase photo-stationary-state (PSS) concentration of HONO can be calculated (Kleffmann et al., 2005; Kleffmann, 2007). The calculated PSS concentration is usually around several tens of pptV.

$$HONO + OH \rightarrow NO_2 + H_2O \qquad (R1.2)$$

$$NO + OH + M \rightarrow HONO + M \quad \text{(R1.3)}$$

However, in many field measurements, high daytime HONO concentrations have often been observed which cannot be explained by the gas-phase PSS concentrations (Zhou et al., 2002; Kleffmann et al., 2003; Vogel et al., 2003; Kleffmann et al., 2005; Acker et al., 2006a; Wong et al., 2012; Michoud et al., 2013; Spataro et al., 2013). The discrepancy between calculated PSS and observed HONO level indicates that there still exists missing daytime HONO sources, except the gas-phase reaction, (R1.1) (Zhou et al., 2003; George et al., 2005; Stemmler et al., 2006; Kleffmann, 2007; Zhou et al., 2011). Therefore, this discrepancy stimulates worldwide interests on daytime nitrous acid chemistry. There are now increasing number of studies conducted to investigate the daytime 'unknown sources' of HONO. Various research approaches have been adopted, including laboratory studies, numerical simulations as well as field measurements.

Despite the strong influence of HONO on photochemistry, only limited research in China are related to HONO. Most of them mainly focus on SO_2 or NOx-involved pollution processes. This is possibly due to the following factors: (1) high SO_2/NOx concentration recorded in many mega cities in China; (2) lack of HONO instrumentation in most field campaigns; and (3) challenges existing in measuring daytime HONO concentration, due to the fact that it is usually close to or lower than the detection limit of measuring instrument. In addition, the limited studies carried out in China are unequally distributed in region. Most of them centers on developed areas, such as

Beijing, Shanghai and Pearl River Delta (PRD) region (Su et al., 2008a; Su et al., 2008b; Qin et al., 2009; Li et al., 2011a; Su et al., 2011; Zhang et al., 2012). Thus, it is very important and urgent to improve our understanding on HONO-related chemistry in different parts of China.

Hong Kong is one of the large cities in PRD region. Compared to other cities in this region, Hong Kong has a low CO/NOy ratio, around 3.3 (ppbV/ppbV). This is attributed to large quantities of diesel vehicles (Wang and Kwok, 2003). In other words, Hong Kong is characterized by higher NOx concentration and its pollution type is quite different from some big cities in China. This high-NOx atmosphere will favor the production of nitrogen compounds, including HONO. Under such circumstance, HONO is worth the research attention. Yet, few scientists pay attention to HONO-related processes in Hong Kong.

In this study, a comprehensive summer field campaign has been carried out at a suburban coastal station in Hong Kong. The thorough data obtained are used to investigate HONO characteristics, its formation mechanism, and impact to atmospheric chemistry. In addition, for the first time, a zero-dimensional observation-based box model coupled with an explicit chemical mechanism MCM (Master Chemical Mechanism) is utilized in this study to achieve the research objective.

This thesis is divided into seven chapters.

1. Chapter 1 gives a brief introduction about the research background and objective, as well as the framework of this thesis.

2. Chapter 2 presents a comprehensive literature review of potential daytime HONO sources. Results from laboratory studies, field measurements and numerical simulations are presented and discussed. Existing debates on this topic as well as knowledge gap are also displayed.

3. Chapter 3 emphasize the research objective and significance of this study.

4. Chapter 4 describes the experiments site and introduces the instrumentation of various trace gases and meteorological parameters.

5. Chapter 5 reviews the most widely used chemical mechanisms in current air quality models and discusses the development of an observation-based nitrous acid box model used in our study. Both advantages and disadvantages of the explicit and condensed chemical mechanisms are discussed.

6. Chapter 6 presents the general observation results and detailed data analysis of HONO from the perspectives of both measurements and numerical simulations.

7. Chapter 7 summarizes the main conclusions of this study and gives some recommendations on future studies.

Chapter 2 Literature review

Nitrous acid (HONO) is an important trace gas and a secondary pollutant in the atmosphere. Its impact to photochemistry is non-negligible, especially in polluted areas. HONO has long been recognized as an important reservoir of both HOx and NOx. Within the wavelength of sunlight range from 300 to 400 nm, photolysis of HONO lead to the production of OH and NO, following (R1.1) (Harrison et al., 1996; Seinfeld and Pandis, 1998). After a whole night's accumulation of HONO in the dark, the impact of it to OH in the early morning is further enhanced. Therefore, HONO photolysis provides a significant source of OH in the early morning, especially when O_3 concentration is still low and photolysis of O_3 is small (Seinfeld and Pandis, 1998; Li et al., 2010):

$$O_3 + h\nu \rightarrow O(^1D) + O_2(\lambda < 319\text{nm}) \quad \text{(R2.1)}$$

$$O(^1D) + H_2O \rightarrow 2OH \quad \text{(R2.2)}$$

As discussed in chapter 1, OH can react with most of the trace gases and initiate a series of photochemical chain reactions, which will further result in the formation of O_3 and other secondary pollutants (Li et al., 2010). Considering the significance of HONO to photochemistry and the existing large discrepancy between observed daytime HONO and its PSS concentration, it is of great importance to determine the source and sink pathways of daytime HONO. In this chapter, sources and sinks of HONO have been reviewed (Figure 2.1). Besides, two kinds of HONO instrumentations have been presented.

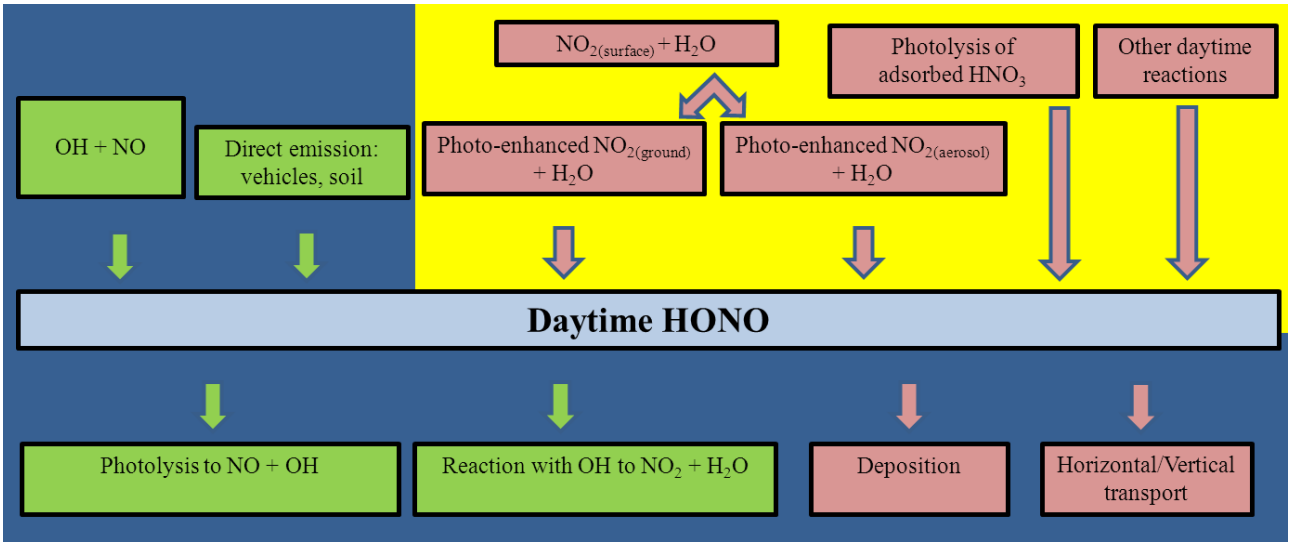

Figure 2.1 Sources and sink pathways of HONO, cited from Li et al. (2012).

2.1 Source Pathways of HONO

2.1.1 Homogenous Sources

The most well-known homogenous source of HONO is the reaction between NO and OH, (R1.3), as mentioned in chapter 1. When NO and OH are high, especially in some polluted areas, this gas-phase reaction can be substantial in the daytime. Yet, it contributes little to the nighttime HONO build up, due to the low concentrations of both NO and OH (Kleffmann, 2007; Li et al., 2011a; Zhang et al., 2011).

$$NO + OH + M \rightarrow HONO + M \qquad \text{(R1.3)}$$

However, in many field measurements, reaction rate of (R1.3) alone is too small to sustain the elevated HONO mixing ratios in the daytime (Harrison et al., 1996; Aumont et al., 1999; Vogel et al., 2003; Acker and Möller, 2007). Therefore, scientists have

proposed many other potential HONO sources, including both chemical and physical origins, to explain the discrepancy.

In addition to (R1.3), Stockwell et al. (1983) have proposed another homogenous source of HONO under dark conditions. That is the reaction between NO_2 and HO_2:

$$NO_2 + HO_2 \rightarrow HONO + O_2 \quad \text{(R2.3)}$$

This source helps to reproduce the observed HONO profiles in their modeling study. Yet, laboratory-based rate constant of this reaction has a wide range, from $5*10^{-16}$ $cm^3molecules^{-1}s^{-1}$ to $3*10^{-15}$ $cm^3molecules^{-1}s^{-1}$ (Howard and Evenson, 1977; Tyndall et al., 1995). Assuming a high NO_2 and HO_2 concentration of 10ppbV and 10^9 molecules/cm^3, production rates of 18 pptV/h and 108 pptV/h can be derived under two different rate constants. In most studies, $5*10^{-16}$ $cm^3molecules^{-1}s^{-1}$ have been chosen as the rate constant for estimation, which results in a small contribution of 18 pptV/h. Therefore, this source has often been ignored when high HONO level up to several hundreds of pptV has been observed (Ren et al., 2003; Kleffmann et al., 2005; Kleffmann, 2007).

Besides, some other gas-phase reactions can also lead to the production of HONO:

$$NO + NO_2 + H_2O \rightarrow 2HONO \quad \text{(R2.4)}$$

$$HNO_3 + \text{hv} \rightarrow HONO + O(\,^3P) \quad \text{(R2.5)}$$

$$2NO_2 + H_2O + NH_3 \rightarrow 2HONO + NH_4NO_3 \quad \text{(R2.6)}$$

However, these reactions are often considered of negligible importance in the atmosphere, due to either low reaction rate constant or lacking laboratory confirmation (Yarwood et al., 2005; Zhang and Tao, 2010; Li et al., 2012; Zhang et al., 2012).

All the homogenous sources mentioned above involve only inorganic species, such NO, NO_2, HNO_3, etc. In fact, except inorganic gas-phase reactions, HONO can also come from organic sources. For example, photolysis of some aromatic compounds has recently been proved to be the daytime HONO sources. In a flow tube photo-reactor, Bejan et al. (2006) have observed that photolysis of ortho-nitrophenols is a non-negligible daytime HONO source for urban atmosphere during the day. In the presence of 1ppbV of nitrophenols, a HONO formation rate of 100 pptV/h could be estimated for a maximum J_{NO2} value of $10^{-2}s^{-1}$. This type of photochemical gas-phase source can help to explain why there is no pronounced daytime vertical gradient of HONO or [HONO]/NOx observed in some field campaigns (Trick, 2004; Kleffmann, 2007; Villena et al., 2011; Wong et al., 2012).

Apart from chemical sources, direct emission from vehicles is another important source that contributes greatly to HONO accumulation, especially under polluted urban scenario. The reported direct emission ratio of HONO/NOx from tunnel studies has a wide range, from 0.3% to 2.3% (Kirchstetter et al., 1996; Kurtenbach et al., 2001; Gutzwiller et al., 2002; Gonçalves Ageitos et al., 2010; Li et al., 2012). In fact, this ratio

depends highly on the composition of the vehicle fleet. Generally, gasoline powered cars usually have low HONO/NOx ratio compared to diesel powered cars. Kirchstetter et al. (1996) observed a relatively low HONO/NOx ratio of 0.29%(±0.05%) in tunnel of San Francisco, where over 99% of all vehicles were gasoline-fueled. Kurtenbach et al. (2001) measured HONO and NOx concentrations in a high traffic density tunnel in Germany. A HONO/NOx direct emission ratio of 0.8% was calculated, which was based on a fraction of 6.0% heavy-duty trucks, 6.0% commercial vans, 74.7% gasoline powered and 12.3% diesel powered passenger cars, and 1% motorcycles on a working day. In addition to these two tunnel studies, a much higher HONO/NOx emission ratio up to 2.3%(±0.6%) was recorded by Gutzwiller et al. (2002). They found that semi-volatile and/or water-soluble species contained in diesel exhaust could contribute to the secondary HONO formation. Thus, primary together with secondary HONO emitted from diesel exhaust lead to a HONO/NOx ratio three times larger than the primary HONO emission ratio of 0.8%. From the wide range of HONO emission ratio presented above, we can deduce that contribution from direct emission to HONO accumulation varies from place to place. For instance, in urban area where there is a high density of traffic or high proportion of diesel cars, this source may be of great importance. However, in rural or semi-rural places, HONO direct emission has often been ignored.

Another direct emission source is from soil nitrate, which has been recently proposed by Su et al.(2011). Their observation showed that fertilized soils with low pH were a strong source of HONO and OH radical. They suggested that the highly water-soluble nitrites could undergo the following reversible reaction:

$$NO_2^-(aq) + H^+(aq) \leftrightarrow HNO_2(aq) \leftrightarrow HONO(g) \quad \text{(R2.7)}$$

where (aq) represents aqueous-phase, (g) represents gas-phase. They found that the variation of this soil-related HONO source matched quite well with diurnal pattern of the daytime missing source. Yet, it still needs to be verified whether this source is equally important in high-polluted or non-agricultural areas other than in fertilized areas.

2.1.2 Heterogeneous Sources

After taking the homogenous sources into account, the measured high daytime HONO concentrations in many suburban and urban areas still cannot be reproduced by simulations (Sarwar et al., 2008b; Su et al., 2008b; Li et al., 2010; Li et al., 2011a; Czader et al., 2012a). Hence, some heterogeneous reactions are proposed by scientists to explain the high daytime HONO concentrations.

Svensson et al. (1987) found that heterogeneous reaction involving NO_2 and water vapor leads to the generation of HONO in darkness. Their study has shown that (R2.8) can occur on most uncontaminated surfaces. Its reaction rate has been shown to be of the first order in NO_2 by several laboratory studies (Svensson et al., 1987; Jenkin et al., 1988; Harrison and Collins, 1998; Kleffmann et al., 1998; Finlayson-Pitts et al., 2003).

$$2NO_2 + H_2O \rightarrow HONO + HNO_3 \quad \text{(R2.8)}$$

While this formation pathway reproduces nighttime HONO levels in polluted atmospheres, its strength is not high enough to sustain an elevated daytime concentration. Thus, various light-related HONO sources have been examined. In the presence of light, TiO_2 in mineral dust has been found be a photo-catalyst of (R2.8). Conversion efficiency of NO_2 can be largely improved on irradiated surfaces containing TiO_2 (Gustafsson et al., 2006; Ndour et al., 2008).

In addition to NO_2 hydrolysis on surfaces, Ammann et al. (1998) suggested that interaction between NO_2 and soot particles could contribute to HONO concentrations in polluted air mass, (R2.9). The conversion efficiency is significantly increased when soot is freshly emitted. But deactivation of soot surface occurs quickly, leading to small uptake coefficient of NO_2. Yet, a recent study has shown that oxidized soot surfaces can be reactivated under solar radiation, and conversion of NO_2 to HONO on soot is dramatically enhanced compared to that in dark condition (Monge et al., 2010). Besides, redox reactions of NO_2 on illuminated surfaces containing organics such as phenols, aromatic ketones and humid acid has also been found to be importance sources of daytime HONO (George et al., 2005; Stemmler et al., 2006; Stemmler et al., 2007).

$$NO_2 + red_{ads} \rightarrow HONO + ox_{ads} \quad \text{(R2.9)}$$

Li et al. (2008) reported that electronically excited NO_2 in visible light reacts with water vapor and produces HONO, (R2.10). However, the significance of this source is still under debate. In the study of Carr et al. (2009), they did not observe the occurrence of

this reaction. Moreover, rate constant for this reaction derived by Crowley and Carl (1997) is one order of magnitude lower than that derived by Li et al. (2008), which indicates the insignificant role of this reaction in the troposphere.

$$NO_2^* + H_2O \rightarrow HONO + OH \quad \text{(R2.10)}$$

Several other HONO formation pathways, involving NO_2 as a reactant or product on different surfaces, have been studied (Svensson et al., 1987; Rivera-Figueroa et al., 2003):

$$NO + NO_2 + H_2O(\text{surface}) \rightarrow 2HONO \quad \text{(R2.11)}$$

$$NO + HNO_3(\text{surface}) \rightarrow NO_2 + HONO \quad \text{(R2.12)}$$

Yet, rate constant for (R2.11) is uncertain and differ by two orders of magnitude (Zhang et al., 2011). Knipping and Dabdub (2002) pointed out that (R2.12), renoxification of HNO_3 on surface, would result in additional NOx production in range of tens of ppbV, given enough reaction surface. However, two recent laboratory studies suggested that these two reactions, (R2.11) and (R2.12), are of minor importance in the atmosphere (Kleffmann et al., 1998; Kleffmann and Wiesen, 2004).

In addition to NO_2 involved reactions listed above, Zhou et al. (2003) suggested that adsorbed nitric acid (HNO_3) photolysis on ground and vegetation surfaces, (R2.13), is an effective daytime source of HONO in low-NO_x environments. The rate of this reaction is 1-2 orders of magnitude faster than that in the gas-phase. Zhou et al. (2011)

also observed that deposited HNO_3 could be converted to HONO and NOx at the top forest canopy surfaces through photochemical process. In their study, good positive correlations were found between daytime HONO flux and nitrate loading on leaf surface, and between HONO flux and the rate constant of nitrate photolysis. Even in polluted urban atmospheres, (R2.13) can contribute significantly to daytime HONO buildup, according to the research of Sarwar et al.(2008b).

$$HNO_3(ads) + h\nu \rightarrow HONO + O(\,^3P) \qquad \text{(R2.13)}$$

Though so many sources have been proposed, main daytime HONO sources still differ from place to place. Some important parameters, such as location of monitoring sites, meteorological conditions, and loading of pollutants, can all help determine the major daytime HONO source in specific places. Therefore, until now, there is no standardized formation mechanism that is able to explain elevated daytime HONO everywhere.

2.2 Sink Pathways of HONO

As discussed in chapter 1, the main loss pathway of HONO is its photolysis, (R1.1). Besides (R1.1), HONO can also react with OH, leading to the production of NO_2, (R1.2) (Alicke et al., 2003; Kleffmann et al., 2005; Kleffmann, 2007):

$$HONO + h\nu \rightarrow OH + NO \ (300\text{nm} < \lambda < 400\text{nm}) \qquad \text{(R1.1)}$$

$$HONO + OH \rightarrow NO_2 + H_2O \qquad \text{(R1.2)}$$

Together with the gas-phase reaction between NO and OH, (R1.3), a theoretical gas-phase photo-stationary-state concentration (PSS) of daytime HONO can be calculated according to (E2.1):

$$[HONO]_{pss} = \frac{k_3[NO][OH]}{J_{HONO}+k_2[OH]} \quad \text{(E2.1)}$$

where k_2 and k_3 is the rate coefficient of (R1.2) and (R1.3), respectively. J_{HONO} is the HONO photolysis frequency. Based on this equation, calculated PSS concentration usually ranges from a few to tens of pptV.

Apart from (R1.1) and (R1.2), HONO can also react with itself, serving as another sink pathway:

$$HONO + HONO \rightarrow NO_2 + NO + H_2O \quad \text{(R2.14)}$$

In laboratory studies, when HONO concentration is very high (ppmV level), this homogenous bimolecular decomposition of HONO can play an important role. But it is of negligible importance in the atmosphere, with a rate coefficient $k=1.6*10^{-24}$ $cm^3molecules^{-1}s^{-1}$ as suggested by Atkinson et al (1992). As to the rate coefficient, Mebel et al. (1998) recommended a theoretical value of $k=5.8*10^{-25}*(T^{3.64})*\exp(-6109/T)$ ($cm^3molecules^{-1}s^{-1}$) for kinetic modeling. Notably, published values for this HONO self-reaction rate coefficient vary by 6 orders of magnitude, which gives a lot of uncertainties in calculation (Chan et al., 1976; Kaiser and Wu, 1977; Mebel et al., 1998).

In addition to chemical removal pathways discussed above, dry deposition is an important physical sink for HONO. Harrison et al. (1996) measured a HONO deposition velocity of 2 cm/s. under low-NO_2 concentration, this would result in a deposition rate of 0.02/mixing height(m) (s^{-1}). In existing research, deposition velocity of HONO ranges from 0.077 to 3 cm/s (Harrison et al., 1996; Stutz et al., 2002; Li et al., 2011a). This process is extremely important at night, when there is a shallow boundary layer about several hundred meters height.

Recently, another physical removal process starts to call the attention of scientists. According to the simulation of a 1-D transport model, Wong et al. (2013) suggested that vertical transport is the most important dilution process to HONO in the lower atmosphere. Their modeling studies showed that vertical transport dilution strength was three times more than the photolysis of HONO. This result is reasonable in their specific study, since they have observed strong negative vertical gradient in field measurement, which means that ground surface is a most important source region for HONO (Wong et al., 2012). Yet, this result is different from the traditional idea in which HONO photolysis is the most significant sink pathway. In situations where no strong gradient is observed, the vertical distribution of HONO can be regarded as homogenous. Under such circumstances, vertical transport process is of minor importance to the daytime HONO sink. Beside, weak vertical convection will also suppress the effect of pollutants' vertical transport. Therefore, in order to better estimate the significance of this process, meteorological parameters such as vertical wind speed should be measured simultaneously with other trace gases.

2.3 Overview of HONO Instrumentation

Given the significance of HONO in atmospheric chemistry, it has been measured in many field campaigns for years (Harrison and Kitto, 1994; Andres-Hernandez et al., 1996; Spindler et al., 1999; Zhou et al., 2002; Acker et al., 2006a; Stutz et al., 2013). Currently, there are mainly two types of instruments being widely used to measure HONO concentrations. One is based on spectroscopic techniques, and the other type relies on chemical techniques. Both techniques have their advantages and disadvantages (Kleffmann, 2007). Here, only a brief review on these two kinds of instruments is given. Detailed descriptions of HONO and other trace gases instrumentation in our study are presented in chapter 4.

2.3.1 Spectroscopic Techniques

Nowadays, mainly four spectroscopic techniques have been adopted to detect HONO, including cavity ring-down spectroscopy (CRDS) (Spindler et al., 2003), tunable diode laser spectroscopy (TDLS) (Febo et al., 1996), Fourier transform infrared (FTIR) spectroscopy (Appel et al., 1990), and differential optical absorption spectroscopy (DOAS) (Platt, 1994; Platt et al., 1980). DOAS is one of the most established and reliable spectroscopic techniques. It detects HONO according to its absorption on specific UV band. This spectroscopic technique is free of chemical interferences which exist in chemical methods. But the detection limit of this spectroscopic instrument is in the order of 100 pptV (Simon and Dasgupta, 1995; Acker et al., 2006b; Liao et al.,

2006). In some rural and remote areas, daytime HONO concentrations are usually less than several hundreds of pptV (Zhou et al., 2002; Kleffmann et al., 2003; Zhou et al., 2003; Wong et al., 2012). Under such circumstances, the use of spectroscopic techniques may bring up measurement uncertainties. Besides the sensitivity limitation, spectroscopic-based instruments are also more expensive and difficult to operate than chemical instruments.

2.3.2 Chemical Techniques

Wet chemical methods, such as wetted effluent diffusion denuders and long path absorption photometers (LOPAP) (Simon and Dasgupta, 1995; Kleffmann and Wiesen, 2005; Acker et al., 2006b; Michoud et al., 2014), are widely used in HONO field measurements. Scrubbing solution is used in chemical techniques to collect gas phase HONO and analyze its derivatives selectively. Instruments using wet chemical methods usually have high sensitivity, with detection limits as low as 1 pptV. Besides, they are cheaper and easier to operate compared to spectroscopic techniques based instruments. Yet, these instruments may suffer from sampling artefacts as well as chemical interferences which is likely to be caused by the scrubbing solution or formation of HONO on sampling lines (Su et al., 2008b).

With these advanced techniques developed to measure HONO, discrepancy still exists between different instruments (Appel et al., 1990; Febo et al., 1996; Spindler et al., 2003;

Liao et al., 2006). Therefore, to improve the performances of various instruments, inter-comparisons between commonly used HONO instruments under different locations and atmospheric conditions are strongly suggested in future studies (Kleffmann, 2007).

Chapter 3 Knowledge Gap and Research Objectives

Though so many potential daytime sources are proposed and discussed, there is still uncertainty over whether HONO formation can be mainly attributed to ground- or aerosol-related processes. Modeling studies have shown that heterogeneous reaction on aerosol surface is of minor importance to HONO accumulation, while some recent studies give an opposite view (Aumont et al., 2003b; Sarwar et al., 2008b; An et al., 2009; Li et al., 2010; Ziemba et al., 2010; Li et al., 2011b; An et al., 2013).

Given the different spatial distributions of ground (including building and all additional solid surfaces) and aerosol surfaces, the influence of these surfaces on HONO concentrations is expected to produce different vertical distribution patterns (Liu, 2012). If ground-related processes dominated HONO formation, the fast photolysis in the daytime would lead to a low concentration of HONO in higher altitudes. In several field studies, strong negative HONO gradient have been observed in the lower boundary layer, suggesting that HONO mainly forms on ground surfaces (Stutz et al., 2002; Veitel, 2002; Kleffmann et al., 2003; Trick, 2004; Wong et al., 2011). However, most of the early gradient studies were carried out at night. As there is a larger surface area to volume ratio (S/V) of ground at night, it is reasonable to assume that ground surfaces are more important than aerosol surfaces in HONO formation (Trick, 2004).

Though vertical profiles in nighttime all show strong negative gradients of HONO, different vertical profiles are presented in daytime HONO gradients studies. Both negative and homogenous vertical distribution patterns have been observed. Villena et al. (2011) measured HONO by Long Path Absorption Photometer technique (LOPAP) at 6 m and 53 m simultaneously on an urban building in Chile. Decreasing daytime HONO concentrations with increasing height were recorded, suggesting a ground surface source. Gradient study in three altitude intervals (30-70 m, 70-130 m, and 130-300 m) conducted by Wong et al. (2012) using a Differential Optical Absorption Spectroscopy instrument (DOAS) also showed larger HONO concentrations near ground surface than aloft in Houston. Zhang et al. (2009) conducted aircraft measurements of daytime HONO vertical profiles within 2600 m above ground level (AGL) in a rural region. Strong negative HONO gradients were observed in stable boundary layer, indicating the significance of HONO ground source. Yet, substantial daytime HONO in the upper boundary layer and free troposphere suggested an additional source of HONO in the air column. Similarly, no daytime vertical gradients of HONO in the range of 10-190 m were observed in the study of Kleffmann et al. (2003) at a semi-rural region in Germany. An airborne HONO measured within 1000m and another vertical study on a 200m meteorological tower both showed no strong vertical gradients of HONO in the daytime (Trick, 2004; Häseler et al., 2009). These relatively uniform HONO vertical profiles indicate either strong convection in boundary layer or the existing of additional daytime HONO sources in the air.

In addition to gradient measurements, correlation analysis between the daytime HONO strength from unknown sources and the indicator/proxy of proposed heterogeneous processes is another effective way to investigate the daytime sources. Unknown sources are usually estimated by PSS approach (E2.1), assuming photolysis is the main sink pathway of daytime HONO (Alicke et al., 2002; Zhou et al., 2002; Kleffmann et al., 2003; Vogel et al., 2003; Kleffmann et al., 2005; Acker et al., 2006a; Wong et al., 2012; Michoud et al., 2013). Adopting this approach, recent studies conducted in Southern China by Su et al. (2008b) and Li et al. (2012) suggested that aerosol surfaces have a negligible role in HONO formation, as there was a poor correlation between the HONO strength from unknown sources and proxies of sources on the aerosol surface.

However, as mentioned in chapter 2, Wong et al. (2013) suggested that the PSS approach would lead to underestimation of the unknown source strength of daytime HONO. Because their one-dimensional modeling study showed that vertical transport leaded to more than half of the HONO loss and was three times larger than that from photolysis in the lowest boundary layer. This suggests that vertical transport process may be of great importance to the observed HONO level. Yet, since this term highly depend on the vertical distribution pattern of HONO as well as meteorological factors, its impact to HONO may vary from case to case. Under circumstances where no strong vertical gradients are observed, it is reasonable to assume homogenous distributed HONO in vertical direction. Thus, vertical transport is of minor importance to the observed HONO concentration in this situation. Besides, it is difficult to take vertical transport process into account when using PSS approach, if no gradients studies are

available. Therefore, PSS approach is still widely used to estimate the HONO unknown daytime sources.

Despite the knowledge gap on the daytime source(s) of HONO, there are also other aspects remain further investigations. For OH sources, the relative importance of each OH precursor (HONO, O_3, HCHO, etc.) is under debate. Most scientists believe that HONO photolysis can only affect OH in the early morning when O_3 and HCHO concentrations are low (Seinfeld and Pandis, 1998; Alicke et al., 2002; Gonçalves Ageitos et al., 2010; Li et al., 2010). Yet, some research suggest that under certain circumstances, such as polluted atmosphere, HONO can be a dominant source of OH through whole day (Vogel et al., 2003; Acker et al., 2006a). For research methods of HONO chemistry, transport models implemented with lumped chemical mechanisms are often used for simulations (Sarwar et al., 2008b; Li et al., 2010; Li et al., 2011b; Czader et al., 2012a; Elshorbany et al., 2012; Zhang et al., 2012). However, the existing lumped mechanisms only contain homogenous HONO sources, which will lead to underestimation of both OH and HONO. Besides, to improve numerical efficiency, these lumped chemical mechanisms usually simplify HOx ($OH+HO_2$) and intermediates-related reactions (Whitten et al., 1980; Carter, 1988; Stockwell et al., 1997). Given the close relation between OH and HONO, this simplification will undoubtedly lead to uncertainties during calculation, affecting the simulation results of HOx and HONO (Marcia C, 2000).

In this study, we aim to investigate the possible daytime source(s) of HONO. Based on a summer field campaign at a suburban site of Hong Kong in 2011, we analyze the HONO source budget in a multi-day pollution episode in August, and assess the relative importance of different surfaces in the formation of daytime HONO. During this campaign, various pollutants and meteorological parameters were measured simultaneously. Nighttime conversion rate of NO_2 to HONO, possible sources of daytime HONO, as well as impact of HONO on the OH radical have been discussed in detail.

Chapter 4 Experimental Site and Instruments

4.1 Tung Chung Study Site Description

The field study was conducted at an air-monitoring station operated by the Environmental Protection Department of Hong Kong (HKEPD) at Tung Chung (TC, 22.30^{o}N, 113.93^{o}E). It is a suburban site situated in the southwest of Hong Kong which is about 20 km away from the urban center (Victoria Harbor).

The station locates in a residential area and bordered by the Hong Kong International Airport to the northwest, South China Sea to the northeast and Lantau Island to the south. As shown in figure 4.1, the main vegetation near the station is the plant in Lantau Island. Both local anthropogenic emission and pollution from the highly industrialized Pearl River Delta (PRD) region can affect TC under different meteorological conditions (Xu et al., 2013).

This study makes use of the data measured during the summer, from August 4th to September 7th. Both general observation results and detailed data analysis during this campaign will be presented in chapter 6. The main focus of this study is on the daytime HONO chemistry, especially on data collected between 25 and 31 August 2011, during which time a multi-day photochemical episode occurred.

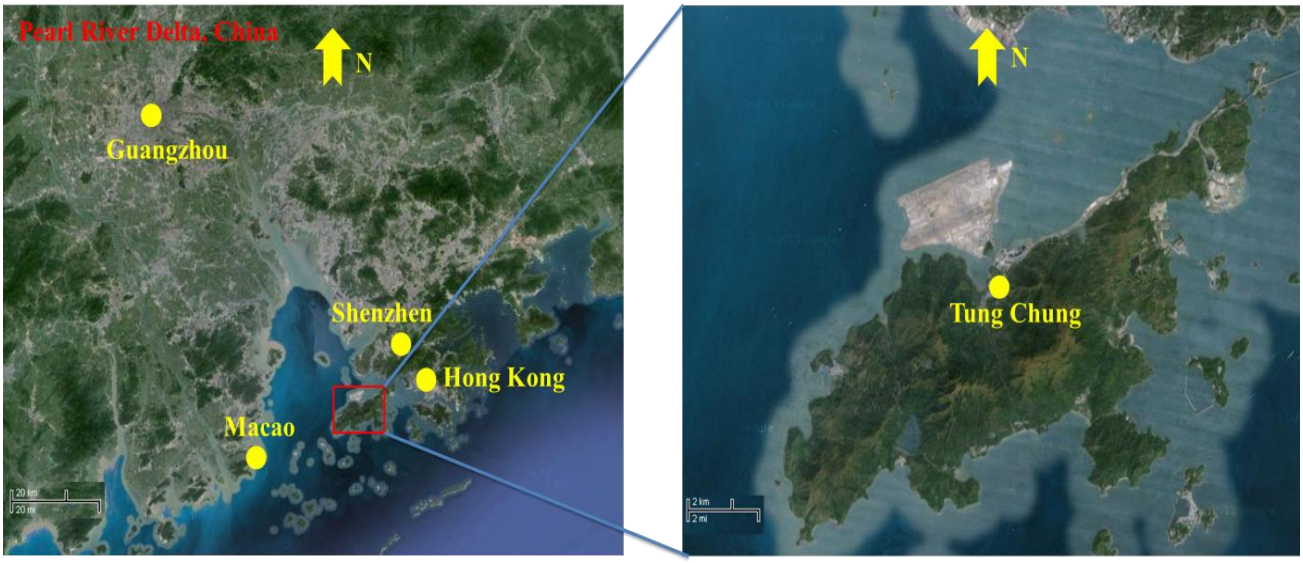

Figure 4.1 Location of Tung Chung Station.

4.2 Instrumentation of HONO

HONO was measured by other members of our research team using a commercial long path absorption photometer instrument (QUMA, Model LOPAP-03) (Kleffmann et al., 2002; Kleffmann and Wiesen, 2008). As described in section 2.3.2, this instrument is based on chemical techniques. The ambient air was sampled in two similar temperature-controlled stripping coils in series by a mixture reagent of 100g sulfanilamide and 1L HCl (37% volume fraction) in 9L pure water. In the first stripping coil, almost all HONO and a fraction of interfering substances, such as NO_2, N_2O_5, were sampled. In the second coil, only little HONO and same amount of interfering species as in the first coil were sampled. After adding a reagent of 1.6g N-naphtylethylendiamine-dihydrochloride in 9L pure water, colored azo dye was formed in the solution, which

was then detected photometrically in long path absorption in special Teflon tubing. Thus, an interference-free HONO signal was derived from the difference between the signals of the two channels.

To correct any small baseline drifts, zero air was sampled every 12 hours. A span check of instrument sensitivity was conducted by sampling 0.04 ug/m^3 NO_2^- solution every three days. The sample flow and the liquid flow were set to 1 L/min and 0.28 ml/min, respectively. Before the experiment, sampling efficiency of HONO in the sampling unit was determined to be 99.95 % with a HONO-source generator (QUMA，Model QS-03). With the above setting, time resolution, detection limit, and accuracy of the measurement during the field measurement period were 10 minutes, 5 pptV and 10%, respectively. The detection limit was determined by three times the deviation of the signal appeared on the panel after injecting the zero air into the instrument.

4.3 Instrumentation of Other Traces Gases and Parameters

NO and NO_2 were measured by a chemiluminescence instrument (TEI model 42i) coupled with a highly selective photolytic converter (Droplet Measurement Technologies, model BLC) (Xu et al., 2013). O_3 was measured with a UV photometric analyzer (TEI model 49i) (Wang et al., 2001). Hourly mass concentration of $PM_{2.5}$ was measured by a tapered element oscillating microbalance (TEOM 1405-DF, Thermo Scientific) with a Filter Dynamic Measurement System (FDMS). VOC were measured

in real-time by an on-line analyzer (Syntech GC 955, Series 600/800, Netherland), with two sampling systems and two column separating systems: GC1 and GC2 for C_2-C_5 and C_6-C_{10} hydrocarbons, respectively (Ling et al., 2012). All instruments were installed on the roof of Tung Chung Health Center. LOPAP-03 was located at an altitude around 16 m AGL, other instruments were located at an altitude around 20 m AGL.

The particle number size distribution in the range of 0.005μm-10μm was measured by a wide-range particle spectrometer (WPS^{TM}, MSP Corporation Model 1000XP). Aerosol surface density (surface to volume ratio) was calculated from the particle number size distributions measured by WPS^{TM}. This instrument combines the principles of differential mobility analysis (DMA), condensation particle counting (CPC) and laser particle spectrometer (LPS), and can measure the particle size distributions ranging from 0.005μm to 10μm in diameter. The DMA and CPC can measure aerosol size distributions in the 0.005μm to 0.5μm particle diameter range in up to 96 channels. The laser particle spectrometer (LPS) covers the 0.35μm to 10μm particle diameter range in 24 additional channels. In our study, we selected a sample mode of 48 channels in DMA, and 24 channels in LPS. It takes about 8 minutes for one complete scan of the entire size range (i.e., 0.005μm to 10μm). The detailed descriptions and operations of the instrument can be found in Gao et al. (2009). To calculate the $(S/V)_a$, the aerosols are assumued to be spherical, and the aerosol surface density is then calculated from the following formula (Su et al., 2008a; Gao et al., 2009; Li et al., 2012):

$$(S/V)_a = 4\pi(d/2)^2/V \quad \text{(E4.1)}$$

where $(S/V)_a$ denotes the aerosol surface density, d is the diameter of the aerosol which can be obtained from the particle number size distribution measurements. V is the volume of the air sampled into the instrument.

NO_2 Photolysis frequency (J_{NO2}) was measured by two optical actinometers (Metcon, Germany), which were set up about 2.5 m above the roof surface. The two actinometers were parallel with each other, but faced in opposite directions. This configuration allows the determination of upward J_{NO2}^{U} and downward J_{NO2}^{D}. J_{NO2} used in model calculation was calculated through upward J_{NO2}^{U} multiplied by the average albedo (1.05). In addition to J_{NO2}, other basic meteorological parameters, such as relative humidity (RH), temperature, wind speed and wind direction have also been measured simultaneously.

Chapter 5 Development of a Nitrous Acid Box Model

5.1 Overview of Condensed Chemical Mechanisms

HONO formation mechanism, especially during the daytime, is not fully understood. In order to have a clear picture of HONO chemistry in atmosphere, model simulations are carried out as a supplement of laboratory and field studies. In most models, only limited chemical species and reactions are represented and included in the chemical mechanisms, so as to make efficient calculation of the chemical reactions, complex meteorological conditions and the emission processes simultaneously. To achieve this, each mechanism comes up with some rules to simplify the chemical reactions and make them representative of the real chemical processes in the atmosphere.

Since inorganic species and reactions are much fewer than that of organic, various mechanisms treat relevant inorganic reactions similarly, but differ mainly in the way dealing with organic chemistry. They make simplification of the organic chemistry mainly through three different ways: lumped structure, lumped molecule and reactivity generalization. Chemical species and reactions of organic compounds included in the model may vary from mechanism to mechanism. Besides, the number of reactions and species ranges from tens to thousands in different mechanisms (Seinfeld, 1988).

Currently, the most widely used mechanisms for modeling tropospheric chemistry include carbon bond mechanism (CBM), the mechanism for Regional Acid Deposition

Model (RADM) and Statewide Air Pollution Research Center (SAPRC) mechanism. They are all condensed chemical mechanisms which have been used for many years and been updated with time for the adaption of new experimental data or special needs.

5.1.1 Carbon Bond Mechanism (CBM) and Its Updated Versions

The carbon bond mechanism (CBM) is a condensed lumped structure mechanism and is a most popular used one. It is a set of generalized reactions and rate constants. CBM groups carbon atoms with similar chemical bonding, e.g., single and double bonding. The mechanism treats the similar-bonding carbon atoms similarly. In other words, it is a condensation of all reactions occurred in atmosphere (Whitten et al., 1980).

After developed in 1970s, it has been updated and modified for many times (version CBM-I, CBM-II, CBM-III, and CBM-EX). The carbon bond IV (CBM-IV) mechanism proposed by Gery et al. (1989) has been a widely used chemical mechanism in urban to regional air quality modeling systems for a long time, which is built on the base of CBM-EX. It consists of 33 chemical species and 81 chemical reactions. 18 function groups are designed to represent primary and secondary organic compounds in the atmosphere. CBM-IV has high computational efficiency and it is among the fastest of the commonly used chemical mechanisms (Sarwar et al., 2008a).

The CBM-IV mechanism has been updated in year 2005 and thus named as CB05 (Yarwood et al., 2005). CB05 has 156 reactions which are nearly two times the number of reactions relative to the previous version, CBM-IV. More detailed treatment of urban areas and new reactions are provided by the updated version, CB05, involving biogenic, toxics, species important to particulate formation and acid deposition. Among those reactions, 89 of them are organic reactions. 51 species are considered in the core mechanism, including 16 inorganic and 35 organic species. This updated version is intended to simulate complex photochemistry process in urban and regional troposphere.

5.1.2 Regional Acid Deposition Model (RADM) and Its Updated Versions

The Regional Acid Deposition Model, version2 (RADM2) mechanism is another widely used generalized species mechanism for regional-scale air quality simulations, which is developed from the first version of RADM (Stockwell, 1986; Stockwell et al., 1990). Most of the organic species are aggregated into the model species based on their similarity in functional groups and reactivity with OH. It has been updated by Stockwell et al. (1997) to Regional Atmospheric Chemistry Mechanism (RACM) and is used in many photochemical transport/transformation atmospheric chemistry models to predict concentrations of oxidants and other air pollutants.

In addition to a general updating of rate constants for many inorganic and organic reactions from RADM2, a completely new reaction scheme for isoprene is included in RACM. 237 reactions are considered in the updated mechanism. Moreover, 17 stable inorganic species, 4 inorganic intermediates, 32 stable organic species and 24 organic intermediates are included in RACM mechanism. Rate constants and products yields from laboratory measurements are used. It is much more detailed and realistic than reactions considered in RADM2. Compared to CBM and SAPRC, RO_2 chemistry in RADM and RACM is treated much more explicitly.

5.1.3 Statewide Air Pollution Research Center (SAPRC) Mechanism and Its Updated Versions

SAPRC is a detailed mechanism for gas phase reactions of volatile organic compounds (VOCs) and oxides of nitrogen (NOx) in urban and regional atmosphere. It has been developed and updated several times by Carter (1988; 2000; 2007; 2010) at Statewide Air Pollution Research Center and thus is referred to SAPRC. It is a lumped molecule mechanism where surrogate species are used to represent organic compounds.

Different from the lump method in CBM, organic species are lumped according to the similarity of reactivity toward OH, which is similar to the approach used in RACM. Inorganic chemistry in this mechanism is very similar to that included in the CBM. But the number of organic species contained in SAPRC is three times more than that in

CBM (Marcia C, 2000). SAPRC-99 was developed in 1999 and is an updated version of SAPRC-90 mechanism, which is now widely used in air quality models. It includes representations of almost 780 types of VOCs atmospheric reactions for reactivity assessment (Carter, 2000). Compared to SAPRC-90, SAPRC-99 updates the reaction rates of some reactions, and treats some species explicitly. The lasted version of SAPRC is named SAPRC-07 which has added the chlorine chemistry as well as some new chemical species such as benzene based on the general structure of SAPRC-99.

5.2 Overview of Air Quality Model Simulations

5.2.1 Model Performance

By adopting condensed chemical mechanisms discussed above, many air quality models are used to investigate the HONO chemistry. Most of these models are one-dimensional (1-D) or three-dimensional (3-D) transport models. The model framework is often comprised of chemical module, meteorological module, and vertical/horizontal transport module.

Generally, modeling studies aim to reach the following three targets: (1) reproducing the observed HONO concentration in simulation; (2) finding the major source(s) of HONO in the nighttime and daytime; (3) estimating the impact of HONO on OH budget and the

photochemistry. Focusing on these three aspects, numerous simulations are conducted, results of which are reviewed in below.

Using a two-layer 1-D box model, Aumont et al. (2003a) conducted simulations to verify the contribution of HONO photolysis to OH radicals, O_3 and NOx budgets in polluted boundary layer. Three additional sources of HONO were included in the model: direct emissions, NO_2 heterogeneous reactions on ground and aerosol surface. Their research showed that the HONO accumulation were mainly resulted from direct emission and ground reactions. They also found that HONO sources contributed a lot to primary OH production in wintertime conditions, which would then affect both NOx and O_3 concentrations throughout the day. But in summer, the impact of HONO sources to NOx/O_3/HOx was only limited at sunrise, which is of minor importance. Vogel et al. (2003) carried out numerical simulations with a 25 layers 1-D model coupled with RADM2 chemical mechanism. Apart from gas phase production, they also introduced direct emissions of HONO, heterogeneous reactions on ground. Besides, a photolytic HONO source was included, the rate of which was proportional to photolysis frequency of NO_2. While nighttime HONO can be explained by direct emissions and the heterogeneous reactions on the surface, daytime HONO can only be reasonably simulated after introducing the photolytic source. Simulation results showed that HONO was the main source of OH radicals when O_3 and humidity were low. Based on a vertical gradient measurement of HONO, a recent 1-D chemistry and transport model study was carried out by Wong et al.(2013). Their study demonstrated that photolytic formation on the ground was the major source of HONO in the lower troposphere,

which was consistent with their measurement where strong daytime gradient of HONO was observed. Moreover, they proposed that vertical transport was served as a dilution pathway of HONO, the proportion of which was 3 times more than HONO photolysis in the total HONO sink strength. This result is quite different from the traditional thought which believes photolysis is the main sink pathway for HONO. It calls scientists' attention to the validity of PSS approach when estimating the unknown daytime HONO sources.

In spite of 1-D transport models, 3-D models such as WRF-CHEM (Weather Research Forecasting Model with Chemistry) and CMAQ (Community Multiscale Air Quality) models are also widely used. A WRF-CHEM model simulation was performed by Li et al. (2010) in Mexico City. Besides the HONO homogenous source, secondary HONO formation from NO_2 heterogeneous reactions with semi-volatile organics and fresh soot, photo-induced NO_2 reactions on aerosol and ground surface were also considered. According to the modeling results, NO_2 reaction with semi-volatile organics contributed to 75% of the observed HONO concentration, followed by the NO_2 heterogeneous reaction on the ground surface (18%). With the additional HONO sources, simulated HOx concentrations increased, yielding a better agreement with observation. Increased HOx in the model helped to convert more NO to NO_2 in the morning, leading to a midday averaged enhancement of O_3 to 6 ppbV in the model. Using WRF-ARW/HERMES/CMAQ model system, Gonçalves et al.(2012) found that direct emission and NO_2 hydrolysis on ground surfaces significantly improved the model performance, with little contribution from NO_2 hydrolysis on aerosol surfaces. In the

early morning in urban areas, HONO photolysis was the main source of OH and its contribution was higher than that of O_3 photolysis. Another kind of 3-D chemistry transport model, CMAQ model, has also been used in many studies to simulate HONO mixing ratios. Sarwar et al. (2008b) added NO_2 heterogeneous reactions, direct HONO emissions as well as photolysis of adsorbed nitric acid (HNO_3) deposited on the ground into CMAQ chemical mechanism, CB05. The study suggested that heterogeneous reactions on ground and photolysis reactions were the major sources, accounting for 86% of the modeled HONO concentrations, while direct emissions and gas phase reactions only accounted for 14%. During the day, surface HNO_3 photolysis was an important source for HONO. However, at night, heterogeneous reaction was the most significant one. Using the same model and chemical mechanism, Zhang et al. (2011) conducted HONO simulations during fall in Pearl River delta, China. Two heterogeneous sources and two surface photolysis sources were included in the model in addition to direct emissions. Yet, after taking all these additional sources into account, simulation case can only explain 36%~40% of the observed HONO. This low simulated concentration indicates that either the parameterization scheme in the model was inappropriate or there exist additional unknown HONO sources.

Most of the above modeling studies tend to support that NO_2 heterogeneous reaction on ground surface is the main HONO source and aerosol surface reaction is of negligible role. Yet, some other studies do not rule out the importance of aerosol reactions and even suggest that this source pathway is the most important one. An et al.(2013) and Li et al.(2011b) both used WRF-CHEM to simulate the HONO concentrations in the

Northern China. Their research suggested that heterogeneous reactions on aerosol are the key contributor to HONO concentrations. This disagreement in various studies may result from the differences in aerosol surface area density $(S/V)_a$ and uptake coefficient of NO_2 on aerosol surface (γ_a) adopted in different models. For example, in the numerical studies of An et al.(2013) and Li et al. (2011b), large γ_a of 10^{-4} was used, which led to reasonable simulation results and to large contribution from aerosol-related sources. Besides, $(S/V)_a$ simulated in their studies are much higher (~10^{-3} m^{-1}) than those in the studies mentioned above (~10^{-4} m^{-1}).

In spite of the discrepancy in the existing simulation results, parameterization scheme for HONO-related reactions in various chemical mechanisms is similar.

$$2NO_2 + H_2O \xrightarrow{aerosol/ground} HONO + HNO_3 \quad \text{(R2.8)}$$

$$NO_2 + red_{ads} \rightarrow HONO + ox_{ads} \quad \text{(R2.9)}$$

$$NO_2^* + H_2O \rightarrow HONO + OH \quad \text{(R2.10)}$$

$$HNO_3(ads) + hv \rightarrow HONO + O(\,^3P) \quad \text{(R2.13)}$$

Based on the first order rate constant of NO_2, the kinetics parameterization for these reactions are as follows:

$$k_{2.8} = \frac{1}{8} * V_{NO_2} * \left(\frac{S}{V}\right) * \gamma \quad \text{(E5.1)}$$

$$k_{2.9} = \frac{1}{4} * V_{NO_2} * (\frac{S}{V}) * \gamma \quad \text{(E5.2)}$$

where $k_{2.8}$ and $k_{2.9}$ denote two reaction rate coefficients for (R2.8) and (R2.9), by assuming 50% yield of (R2.8) and 100% yield of (R2.9). V_{NO2}, (S/V) and γ represent the mean molecular speed of NO_2, surface to volume ratio of the reaction surface and the uptake coefficient of NO_2, respectively. Chemical kinetic of (R2.10) has been examined in the study of Li et al. (2008) which reported that electronically excited NO_2 in visible light reacts with water vapor and produces HONO. Yet, the significance of this source is still being debated. In the study of Carr et al. (Carr, 2009), they did not observe the occurrence of this reaction. Moreover, rate constant for this reaction derived by Crowley and Carl (1997) is one order of magnitude lower than that derived by Li et al.(2008), which indicates the negligible role of this reaction in troposphere. Zhou et al. (2003; 2011) did a series of laboratory and field measurements to test the rate coefficient of (R2.13), and proved that the rate of this reaction is 1-2 orders of magnitude faster than that in the gas-phase.

5.2.2 Shortcomings of Condensed Chemical Mechanisms Based Numerical Simulations

Even though a lot of modeling studies have been done to investigate HONO chemistry, its formation mechanism is still under debate. Large discrepancy still exists between the simulation results and the observed ambient HONO mixing ratio. In the daytime,

discrepancy is even larger than that at night. In addition to the discrepancy between simulation and observation, another aspect which also needs close attention is that the chemical mechanisms in model frameworks are similar. Most of them are highly condensed chemical mechanisms, such as RADM2, SAPRC and CB05 as mentioned above.

All these condensed chemical mechanisms introduced above adopt lumped approaches. CBM is a lumped structure mechanism. SAPRC, RADM and RACM are all lumped species mechanisms. Hundreds of VOC species emitted into the atmosphere are grouped into a few lumped surrogates. All parameters associated with the lumped surrogates, including the reaction rate constants, products yields and the types of produced are held constant throughout the simulation. Typically, parameters selected are those that correspond to t=0 and are derived from emission inventories or from early morning ambient VOC measurements. These fixed parameters and lumped representative surrogates may possibly lead to uncertainties during calculation process and affect the simulation results (Marcia C, 2000).

More specifically, when it comes to HONO chemistry, HONO concentrations are largely influenced by reactions related to radicals and intermediates. However, to improve the numerical efficiency, many intermediates have not been taken into account in those condensed chemical mechanisms. This simplification of intermediates will largely limit the model performance of HONO. Therefore, a more explicit chemical

mechanism is needed to be included in model framework, so as to get more precise simulation results. Meanwhile, comparison between the simulation results of different mechanisms is also strongly suggested. Besides, more experiments and laboratory studies should be done to quantify the kinetic data of various HONO sources.

5.3 The Master Chemical Mechanism Box Model (MCM)

5.3.1 Principles of MCM

Unlike the condensed chemical mechanisms (CBM, RADM, and SAPRC) discussed above, the Master Chemical Mechanism (MCM) is a near explicit chemical mechanism. It defines a series of rules to construct the detailed degradation schemes based on kinetic and measured data which are relevant to the oxidation of volatile organic compounds (VOCs) in troposphere (Jenkin et al., 1997). The resultant generation of ozone and other secondary pollutants are also included in the mechanism. All reactions are gas phase and assumed to occur under conditions appropriate to the planetary boundary layer. On the basis of the known reactions of the small number of similar chemical species, large quantities of unstudied chemical reactions are defined by analogy and with the use of structure-reactivity correlations (Saunders et al., 2003).

The following flow chart, Figure 5.1, denotes the main types of reactions, organic intermediate and product potentially generated. The products generated following this

flow will further degrade within the same framework. This process will continue until CO_2 yields, or until the subsequent chemistry of final product is already represented in the mechanism.

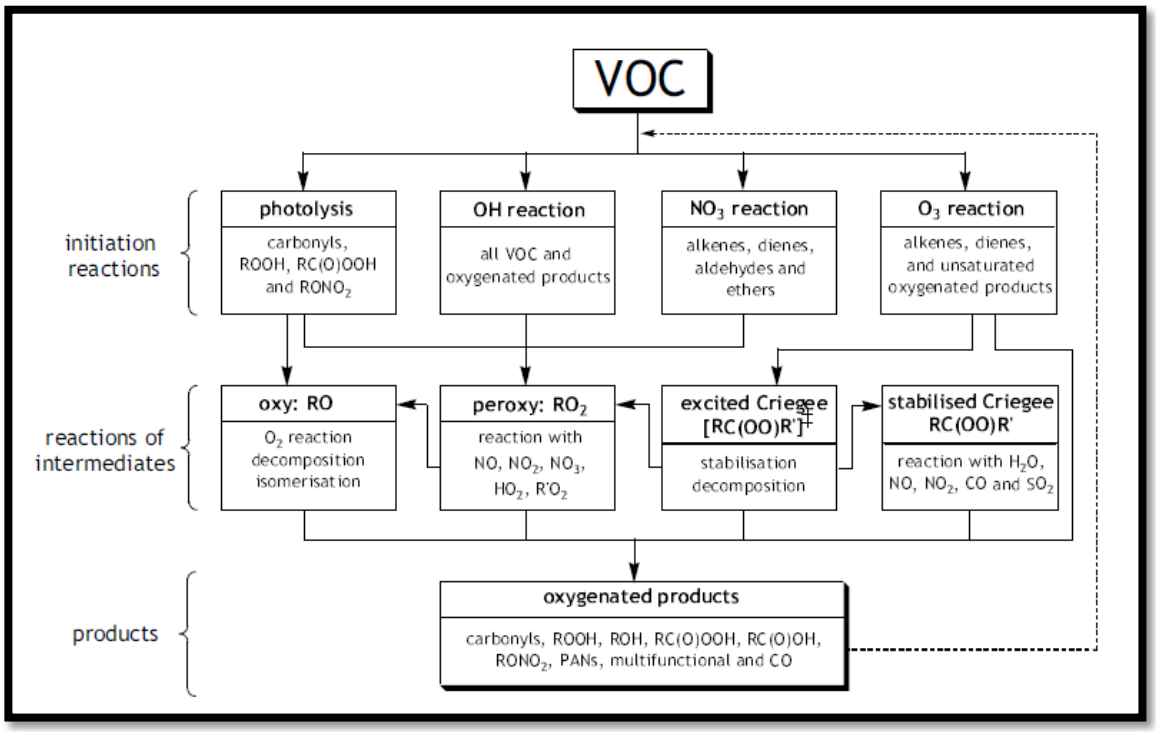

Figure 5.1. Flow chart of VOC degradation framework in the MCM (source from http://mcm.leeds.ac.uk/MCM/home.htt).

5.3.2 Numerical Scheme for Chemical Reactions

MCM code is based on FACSMILE format. FACSMILE provides a powerful platform to solve differential equations. A special high-level programming language is used in

FACSMILE. Ordinary differential equations, chemical reactions, and boundary conditions can be expressed in simple terms by this programming language. Specifically, FACSMILE language is very useful in describing chemical reactions. A complete reaction can be described by one statement in FACSMILE. Two examples are used to illustrate FACSMILE representation of irreversible and reversible reactions.

5.3.2.1 Irreversible Reactions

Assuming that one species A is converted to another species B with a known rate coefficient, which is the simplest irreversible reaction. The chemical notation for this reaction is expressed as:

$$[\mathrm{A}] \xrightarrow{k_f} [\mathrm{B}] \qquad \text{(R5.1)}$$

where [A] and [B] represent the concentrations of species A and B respectively, and k_f is the (known) rate coefficient of the reaction. This can be written mathematically:

$$\frac{\mathrm{d[A]}}{\mathrm{dt}} = -\mathrm{R}_f = -k_f * [\mathrm{A}] \qquad \text{(E5.3)}$$

$$\frac{\mathrm{d[B]}}{\mathrm{dt}} = \mathrm{R}_f = k_f * [\mathrm{A}] \qquad \text{(E5.4)}$$

where $R_f=k_f*[A]$ is the conversion rate of A to B. These differential equations can be solved by FACSMILE. This reaction is written in FACSMILE language using some special notation:

$$\%\ \mathrm{KF}\ :\ \mathrm{A} = \mathrm{B}\ ; \qquad \text{(E5.5)}$$

in which KF represents the rate coefficient of the reaction. Conversion rate R_f can be calculated by adding a RF in front of the notation:

RF % KF : A = B ; (E5.6)

A FACSMILE program can be typed in either upper or lower case characters which have no differences in executing the codes.

5.3.2.2 Reversible Reactions

A more typical reaction would be a reversible reaction in which species A is converted to species B with forward rate coefficient k_f, while B converts back to A with backward rate coefficient k_b. The reversible reaction would be written as:

$$A \underset{k_b}{\overset{k_f}{\leftrightarrow}} B \quad \text{(R5.2)}$$

the forward and backward reaction rates of which are given by:

$$R_f = k_f * [A] \quad \text{(E5.7)}$$

$$R_b = k_b * [B] \quad \text{(E5.8)}$$

The net rate of conversion is:

$$R = R_f - R_b = k_f * [A] - k_b * [B] \quad \text{(E5.9)}$$

The reversible reaction can be defined mathematically by the equations:

$$\frac{\mathrm{d[A]}}{\mathrm{dt}} = -\mathrm{R} = k_b * [\mathrm{B}] - k_f * [\mathrm{A}] \quad \text{(E5.10)}$$

$$\frac{\mathrm{d[B]}}{\mathrm{dt}} = \mathrm{R} = k_f * [\mathrm{A}] - k_b * [\mathrm{B}] \quad \text{(E5.11)}$$

FACSMILE's special syntax enables us to describe the reaction in the following form:

$$\%\ \mathrm{KF}\ \%\ \mathrm{KB}\ :\ \mathrm{A} = \mathrm{B}\ ; \quad \text{(E5.12)}$$

or,

$$\mathrm{R}\ \%\ \mathrm{KF}\ \%\ \mathrm{KB}\ :\ \mathrm{A} = \mathrm{B}\ ; \quad \text{(E5.13)}$$

to obtain the net reaction rate R of this reaction.

These special syntaxes in FACSMILE make it easy to add or change chemical reactions included in MCM, which enable the modification of chemical mechanism to better simulate the tropospheric chemical environment.

5.3.3 Physical Parameters in MCM

Apart from explicit chemical reactions, physics is also an essential aspect that affects pollutants' concentrations. Aerodynamics is one of the most important physical factors. It will lead to transport and diffusion of pollutants. However, MCM does not take horizontal and vertical convection into account. This is because MCM is primarily

developed to study chemical mechanism of specific species in a sealed reaction box. It assumes that all gases are well mixed within the box. Thus, MCM is not the best choice when modeling some species whose life time is very long and the concentrations can be largely affected by long-range transport. In this study, since HONO has a relatively short lifetime, especially in the noontime (around 10 minutes), its concentration is less likely to be influenced by transport and diffusion within short time period. Therefore, using an explicit chemical mechanism, MCM, to investigate HONO chemistry is feasible and reasonable.

Though detailed aerodynamics is not incorporated in MCM, two physical parameters are considered, that is, mixing height and solar zenith angle. In MCM, deposition rate is determined by mixing height. Solar zenith angle is used to calculated photolysis frequencies of photo-dissociable species. In box model, deposition and photolysis are two major physical factors that affect pollutants' concentrations. Therefore, parameterization methods of the two parameters, mixing height and zenith angle, are described in detail below.

5.3.3.1 Mixing Height

Deposition rate can be derived from mixing height by (E5.17). The mixing height in MCM ranges from 300 to 1300 meters. MCM assumes that when sunlight is not available, the mixing height remains at 300m without any changes. But one hour after

dawn, mixing height starts to increase from 300m. At 2 p.m., mixing height reaches its maximum of 1300m. From this moment till dusk, mixing height holds the value of 1300m. Right after dusk, mixing height drops to 300m again. In this process, dawn and dusk are referred to sunrise and sunset time, respectively, which can be calculated as follows:

$$\cos\omega = \tan\varphi * \tan\sigma \quad \text{(E5.14)}$$

$$\text{dawn} = 12\text{hr} * (\frac{\omega}{180}) \quad \text{(E5.15)}$$

$$\text{dusk} = 24\text{hr} - \text{dawn} \quad \text{(E5.16)}$$

ω is hour angle at sunrise which is in the range of 0 to 180 degree. φ represents the latitude of study location. σ is the sun declination angle, which is determined by the specific date in the year.

One hour after dawn, mixing height keeps increasing till 2 p.m., which can be described by the algorithm below:

$$\text{Mixing height} = H_{min} + (T_{cur} - (\text{dawn} + 1)) * \frac{H_{max} - H_{min}}{14 - (\text{dawn} + 1)} \quad \text{(E5.17)}$$

In this equation, H_{min} denotes the minimum of the mixing height which is 300m in this case. H_{max} is set to 1300m, denoting the maximum of the mixing height is this case. T_{cur} is the current time of a specific day in the model. This calculation method of mixing height is highly simplified. Yet, the results of this method agrees quite well with a summer observations in Hong Kong (Chan et al., 2006). Thus, this simplification is

feasible and makes the numerical simulation more efficient. Based on the assumptions above, diurnal pattern of the mixing height in MCM framework is presented in figure 5.2.

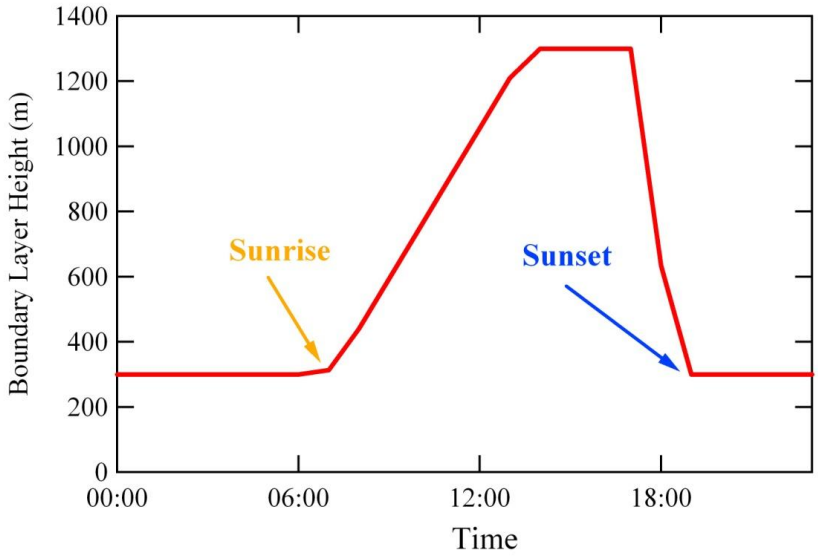

Figure 5.2 Diurnal pattern of mixing height in MCM.

5.3.3.2 Zenith Angle

In MCM, photolysis frequencies are a function of solar zenith angle. Assuming clear sky conditions at an altitude of 0.5 km on 1 July at latitude of 45°N, calculation of photolysis frequency is described by an expression:

$$J = l(\cos\theta)^{m}\exp(-n * \sec\theta) \qquad \text{(E5.18)}$$

where θ is solar zenith angle. The optimized three parameters (l, m and n) for all the core photolysis reactions are suggested by Saunder et al. (2003) .

Zenith angle can be calculated by the formula:

$$\cos\theta = \cos\varphi * \cos\delta * \cos H + \sin\varphi * \sin\sigma \quad \text{(E5.20)}$$

Same as mentioned above, φ represents the latitude of study location. σ is the sun declination angle. H is hour angle, defined as the angular displacement of the sun east or west of the local meridian due to the rotation of the earth. It is zero at solar noon, positive in the afternoon, and negative in the morning.

5.3.4 Advantages of MCM

A near explicit chemical mechanism will reduce the efficiency in numerical models. This may result from an unmanageably large number of reactions, especially for larger VOCs. Thus, MCM make some simplification in degradation schemes. The simplification includes disregarding OH reaction channels of low probability, simplifying treatment of the degradation of a number of minor product classes and parameterizing the representation of the permutation reactions of organic peroxy radicals (Saunders et al., 2003).

Though certain simplification methods are adopted to increase the computational efficiency, MCM describes the detailed gas phase chemical process involved in troposphere. Up to date, the degradation of methane and 142 non-methane VOCs are

represented in this mechanism. In the most updated version MCM3.1 revised by Bloss et al. (2005), 46 inorganic reactions and 13,523 organic reactions are considered. Kinetic data in the mechanism are extracted from literatures and IUPAC (International Union of Pure and Applied Chemistry) report of year 2001 (Jenkin et al., 1997; Jenkin et al., 2003; Saunders et al., 2003; Bloss et al., 2005). With so many species and intermediates taken into account, MCM overcomes the disadvantages of those condensed mechanisms (in section 2.4.2) when modeling HONO chemistry. Previous studies have even shown that OH concentrations simulated by the MCM are comparable with measurements in high-NO_x atmospheres (Mihelcic et al., 2003; Elshorbany et al., 2009; Elshorbany et al., 2012).

5.4 An Observation-based Model

Observation-based model (hereafter referred to OBM) is a model that constrained by observations. Unlike transport models in which all precursors (such as O_3, NOx, and NOy) need to be simulated within the models, an observation-based box model can directly read in data measured in the field campaign. This method can catch up the real-time changes of atmospheric chemical components, which helps to reduce the uncertainties of numerical simulations. For example, if the main pollutants do not agree well with observations in the transport models, the target modeled species are also less likely to be well simulated. Yet, observation-based method can avoid this scenario, since all the real-time major pollutants data obtained in the field campaign can be directly read into the model framework.

In our study, measurements of ambient HONO precursors, several other species along with some meteorological data are used to constrain the model. Different from emission-based model (EBM), OBM does not use emission inventories and does not require the simulation of boundary layer dynamics. Compared to EBM, observation-based method is a more precise method to simulate HONO and to assess the sensitivity of HONO concentrations to its precursors (Cardelino and Chameides, 2000).

5.4.1 Constraint Data

MCM model in this study adopts this observation-based approach. Observation datasets in our study were gathered during an intensive field campaign launched in Tung Chung station for the whole August, 2011. All figures of observation datasets are presented in chapter 6. As described in chapter 4, 10 inorganic species including NO, NO_2, O_3, etc. (Figure 6.1), 24 volatile organic compounds (VOCs) (Figure 6.2, only main VOC species are included), as well as some meteorological parameters such as temperature, solar radiation, photolysis frequency of NO_2 (J_{NO2}) and humidity (changed to water vapor concentration) (Figure 6.3) were used to constrain the model. Surface density of aerosols ($(S/V)_a$) (Figure 6.4) is also use as constrains.

To find a balance between the numerical calculation efficiency and the precision of the calculation, time resolution of the model input and output are all set to ten minutes. All

observed data are scaled to ten minutes' averaged values before read in. Besides, in order to stabilize the intermediates in the model, ten days' pre-run with averaged values are conducted. Time series of main pollutants, radicals and meteorological parameters are presented in the following chapter.

Chapter 6 Results and Discussion

6.1 Data Overview

All data are collected from a suburban site in Hong Kong, Tung Chung, during a summer field campaign. The detailed description of the study site and instrumentation are introduced in chapter 4. The campaign lasted for approximately a month, from August 4 to September 6. (All times series presented in the following figures are data selected during August 10 to 31, due to the simultaneous records of all parameters.) In the first three weeks of August, the prevailing wind was from the South China Sea and the air mass was clean and humid, which leaded to a very good air quality.

This study mainly focuses on data collected in the last week of August. During this period the atmosphere was extremely polluted in Hong Kong. The averaged peak concentrations for NO, NO_2, O_3 and $PM_{2.5}$ were 34 ppbV, 59 ppbV, 150 ppbV and 72.7 $\mu g/m^3$ in TC, respectively. Moreover, high daytime HONO concentrations of over 1 ppbV were frequently observed. This polluted week is a typical photochemical episode.

Before conducting model simulation to investigate the HONO chemistry during the episode, some basic data analysis was carried out to reveal the overall characteristics of various pollutants in both episode and non-episode (clear) days. In this chapter, the time series, diurnal variations of major pollutants and meteorological parameters are presented. Nighttime NO_2 to HONO conversion rates and potential daytime HONO

sources are analyzed. In addition, the impact of HONO to photochemistry is examined through the explicit MCM box model.

6.1.1 Time Series of Main Pollutants and Meteorological Parameters

Figure 6.1, 6.2, 6.3 and 6.4 illustrate the main gas pollutants and meteorological parameters measured in TC during the whole summer campaign. In figure 6.3, we can find that solar radiation was very strong. Except some raining days, solar radiation usually exceeded 600W/m^2 around noontime. This sunny condition was in favor of the daytime photochemistry.

In this study, an episode is defined when the peak one-hour averaged O_3 concentration at TC site exceeded 100ppbV. Figure 6.1 shows that during the field campaign, an episode lasted for successive seven days was observed, from 25th August to 31st. Due to an approaching typhoon, Hong Kong was under the influence of northeast/northwest wind flow which brought various pollutants from the highly industrialized upwind PRD region to Hong Kong. Concentrations of both primary and secondary pollutants such as NO, NO_2, CO, SO_2, PAN, H_2O_2 and HONO all reached quite high levels in the episode. On the early morning of 27th August, HONO concentration was even close to 4 ppbV. This episode occurred when total UV was high, and the wind directions were generally from northeast/northwest, which was consistent with previous observations on episode days (Wang et al., 2003; Zhang et al., 2007).

In figure 6.1, we can see that NOx (NOx=NO+NO_2) concentrations were only slightly increased in episode days compared to non-episode days. Yet, the NO_2 to NOx ratio as well as the NOy concentrations were increased significantly, which suggests that air mass in episode days was aged. Abundant atmospheric oxidants in the aged air mass can turn NO to NO_2, NOx to NOy more efficiently than that in non-episode days, leading to significantly increasing of secondary pollutants. HONO is among one of the secondary pollutants and is a very important trace gas to tropospheric chemistry.

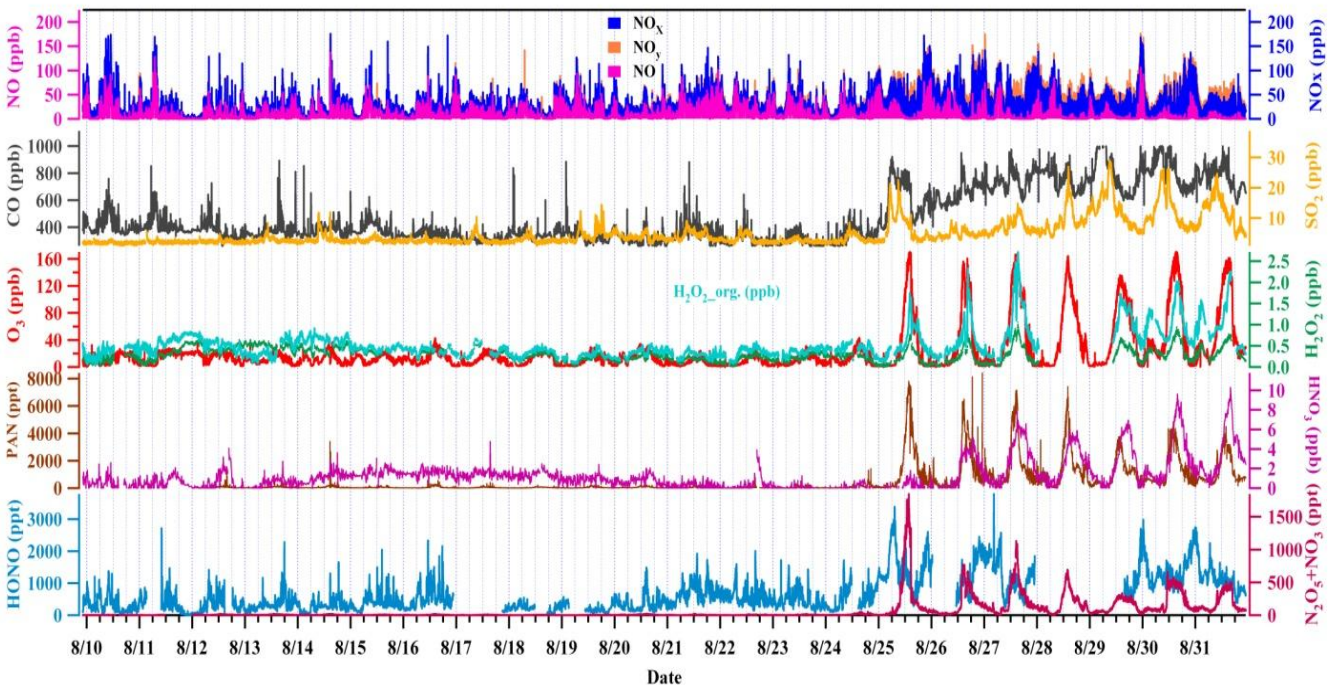

Figure 6.1 Time series of measured major pollutants.

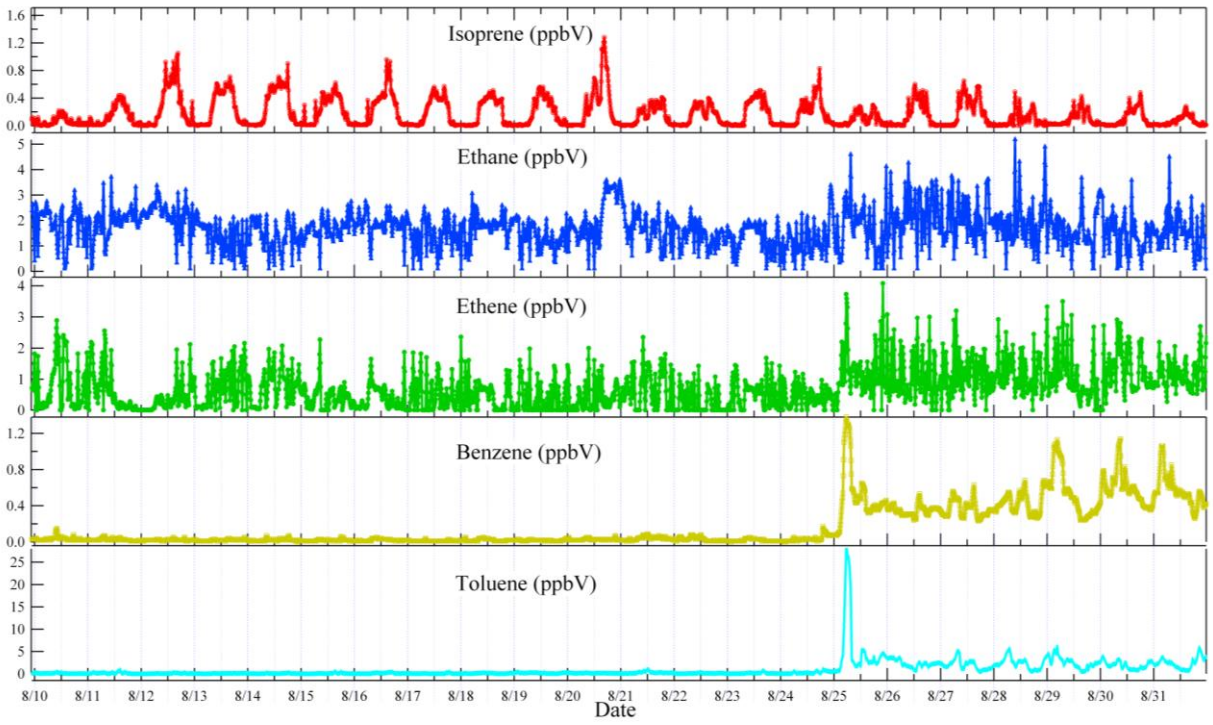

Figure 6.2 Time series of main VOCs species in the summer field campaign.

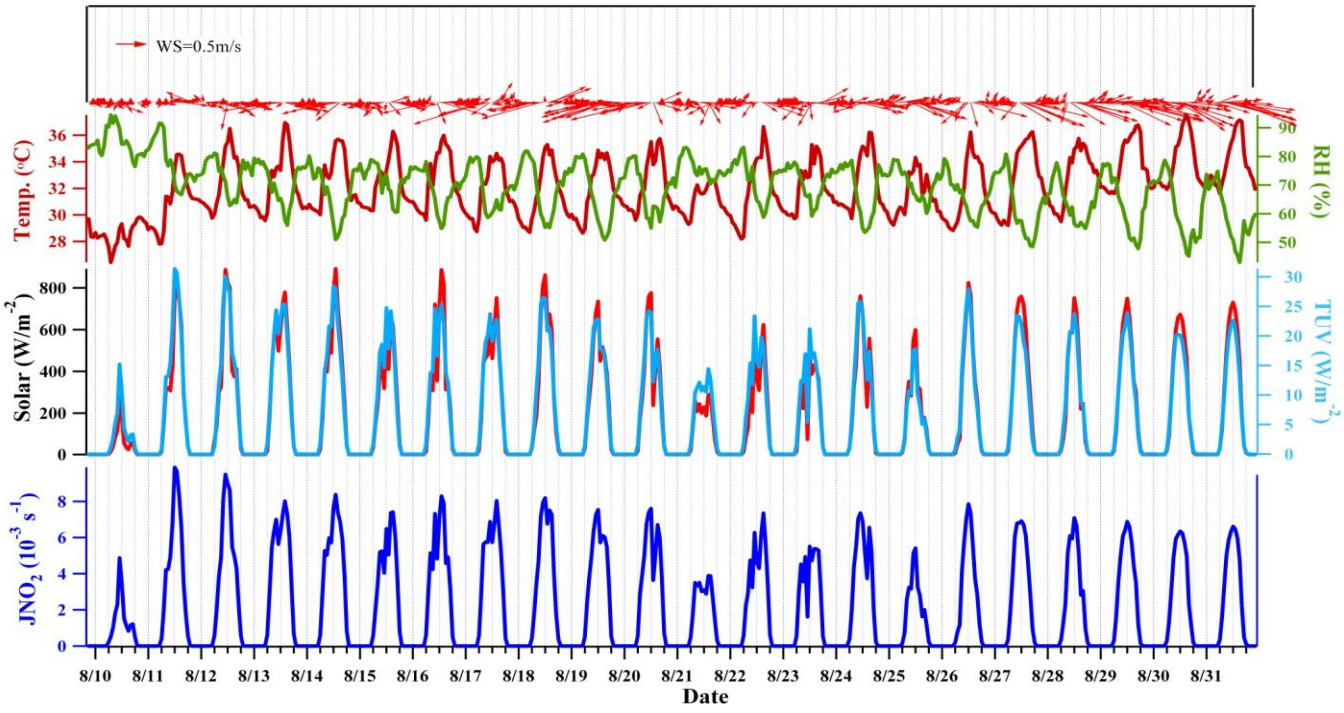

Figure 6.3 Time series of measured meteorological parameters.

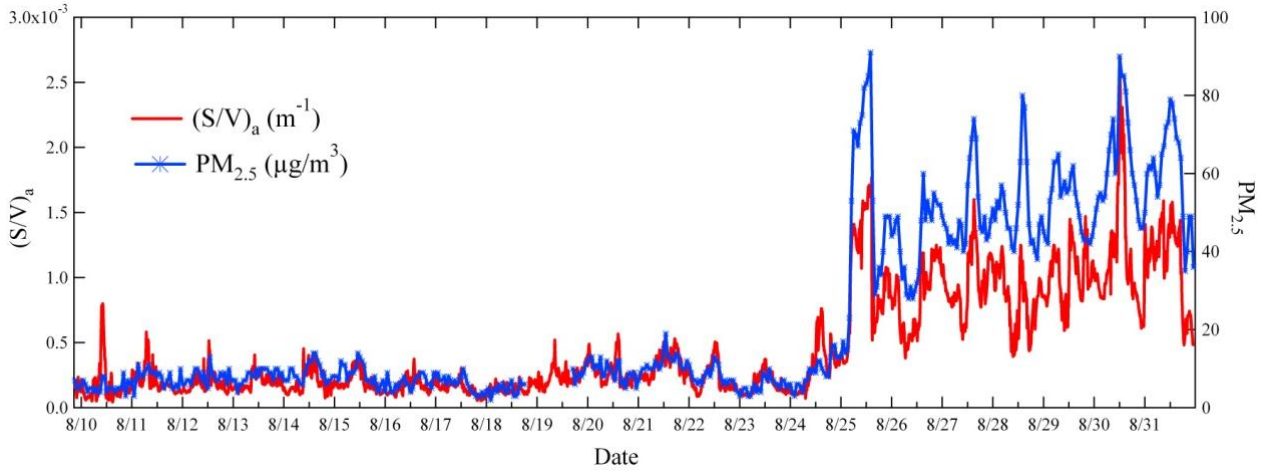

Figure 6.4 Time series of $PM_{2.5}$ (blue) and $(S/V)_a$ (red) measured in the summer field campaign.

6.1.2 Diurnal Patterns of Main Pollutants and Meteorological Parameters

In order to better have an overall picture of these pollutants in the summer campaign, averaged diurnal patterns of main pollutants and parameters in both episode and non-episode days are presented.

Figure 6.5 shows that in non-episode days, concentrations of all major pollutants were very low. NO_2 concentration is around 15 ppbV, and peak O_3 concentration is less than 25 ppbV. This situation is reasonable due to the clean air mass from the South China Sea at this period. Daytime HONO concentration was around 500 pptV, which peaked in the early morning before sunrise. An interesting phenomenon is that daytime concentration of HONO was higher than that in the nighttime, which is different from

the typical diurnal pattern of HONO. One possible reason for this special phenomenon is that in clear days, homogenous reaction between NO and OH radical (R1.3) contributes significantly to the daytime HONO accumulation, and it becomes one of the main daytime sources of HONO. This is resulted from the relatively higher NO and OH concentrations in clear days compared to that in episode days. Simulated OH concentrations in the whole field campaign will be presented in the following section.

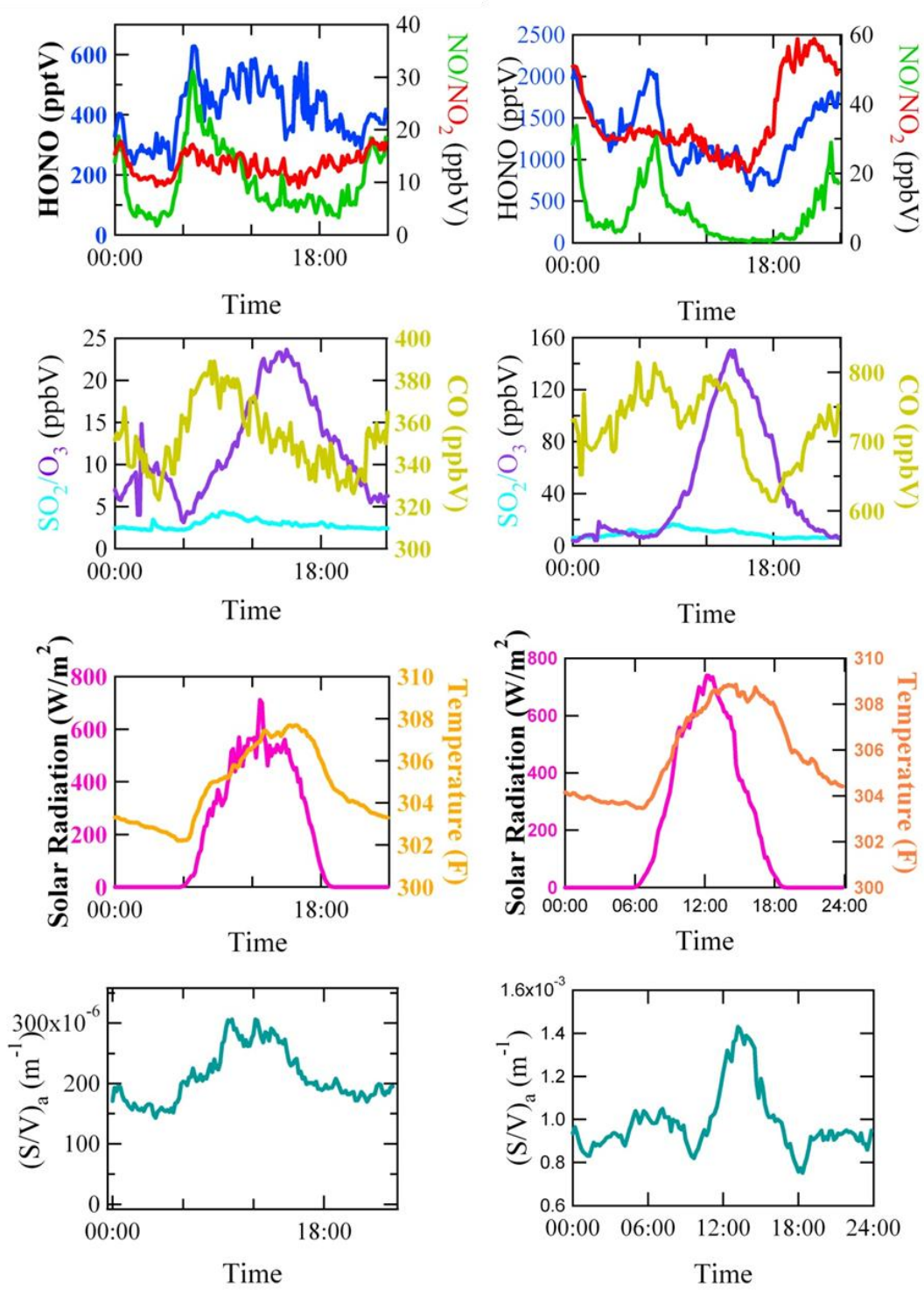

Figure 6.5 Diurnal patterns of main pollutants and parameters in (a) non-episode (left) and (b) episode (right) days.

When in episode days, NO_2/NO ratio has increased a great deal (Figure 6.5), which indicates the aging process of the air mass. Other gas pollutants such as CO, SO_2, O_3 and particles (represented by $(S/V)_a$) all show rather high concentrations. Peak O_3 concentration even reaches 150 ppbV, which is around six times of the peak concentration in non-episode days. Peak $(S/V)_a$ concentration is also increased by five times.

Typical diurnal pattern of HONO have been observed in the episode, with the highest concentration before sunrise, and the lowest around noontime. The accumulation of HONO at night mainly results from the NO_2 heterogeneous reaction with water on ground surfaces (Kleffmann et al., 2003; Li et al., 2010; Wong et al., 2011). The highest averaged concentration of HONO reaches 2 ppbV before sunrise, and then falls to 1.2 ppbV due to the fast photolysis when sunlight is available. Around noontime, its concentration is relatively stable, which means that source and sink strength of HONO are almost equivalent to each other. This high daytime value (≈1.2 ppbV) is comparable to field measurements reported by Su et al. (2008b) at a polluted rural site (≈1.0 ppbV) in the central PRD, and by Sarwar et al. (2008b) at an urban site in the US (≈1.0 ppbV), but is higher than that observed by Li et al. (2012) at a rural site in Southern China (≈0.5 ppbV), and by Kleffmann et al. (2003) at a semi-rural site in Germany (≈0.3 ppbV). The daytime HONO concentration measured in TC site is among one of the highest concentrations in existing records (Harrison et al., 1996; HAO et al., 2006; Zhang et al., 2009; Wong et al., 2012; Lee et al., 2013). Two most obvious reasons leading to this high daytime HONO level may be that: (1) high concentration of HONO precursor, NO_2;

and (2) favorable meteorological conditions such as high humidity and strong radiation. All these factors are in favor of the photochemistry during episode days. Other possible reasons for the high HONO concentration will be discussed in the section 6.4. Before investigating the daytime HONO sources, some analyses on the nighttime HONO are conducted, including NO_2 conversion rate and main heterogeneous reaction surfaces.

6.2 Nighttime Conversion Rate of NO_2 to HONO

It is widely believed that nighttime HONO is mainly from NO_2 heterogeneous reaction on solid surfaces (including building, plant and ground surfaces). This assumption is examined by many field measurements and modeling studies (Harrison and Kitto, 1994; Aumont et al., 2003a; Gonçalves Ageitos et al., 2010; Li et al., 2010). Therefore, the strength of heterogeneous source can be represented by the NO_2 conversion rate.

To estimate NO_2 to HONO conversion rate in TC site, only nighttime data are selected for analysis. This because the absence of both sunlight and heavy traffic helps to reduce calculation uncertainties caused by influence of HONO photolysis and vehicle emission (Alicke et al., 2003). Conversion rates under both fresh and aged air mass are investigated. As shown in figure 6.6a, under aged air mass, both $HONO/NO_2$ and HONO concentration increase steadily after sunset. Assuming a linear increase of HONO concentration during time interval (t_2-t_1), the NO_2 to HONO conversion rate can be estimated (Alicke et al., 2002; Acker et al., 2005; Yu et al., 2009). Since heterogeneous production rate of HONO is in first order of NO_2, the HONO formation

is proportional to NO_2 concentration. Thus, the averaged nighttime conversion rate under aged air mass can be determined by the formula below:

$$C_{NO_2 \rightarrow HONO} = ([HONO]_{t_2} - [HONO]_{t_1})/(t_2 - t_1)[NO_2]_{night} \quad \text{(E6.1)}$$

The calculated value is 0.43%/h between 1830 and 2100 in local time. By the same method, NO_2 conversion rate of 0.31%/h (0200 to 0430 a.m.) in non-episode days is obtained, as shown in figure 6.6b. The NO_2 conversion rate in episode does not change too much compared to that in non-episode days. Assuming a 100% yield of HONO from heterogeneous reaction, and constant solid reaction surfaces under different air mass, the NO_2 uptake coefficients (γ_{NO_2}) will be similar in these two periods.

$$C_{NO_2 \rightarrow HONO} = \frac{1}{4} * V_{NO_2} * \left(\frac{S}{V}\right)_{solid} * \gamma_{NO_2} \quad \text{(E6.2)}$$

As presented in figure 6.7, the conversion rates (0.31%/h and 0.43%/h) estimated in our study site are comparable to the one measured in a semi-rural region in Germany by Kleffmann et al. (2003). Yet, compared to the values in most other monitoring sites such as Xinken, the NO_2 conversion rates in TC are much lower. This suggests that the NO_2 conversion efficiency on solid surfaces in TC may be lower than that in other places listed in figure 6.7, which may be caused by the different chemical and physical qualities of the reaction interfaces in different places.

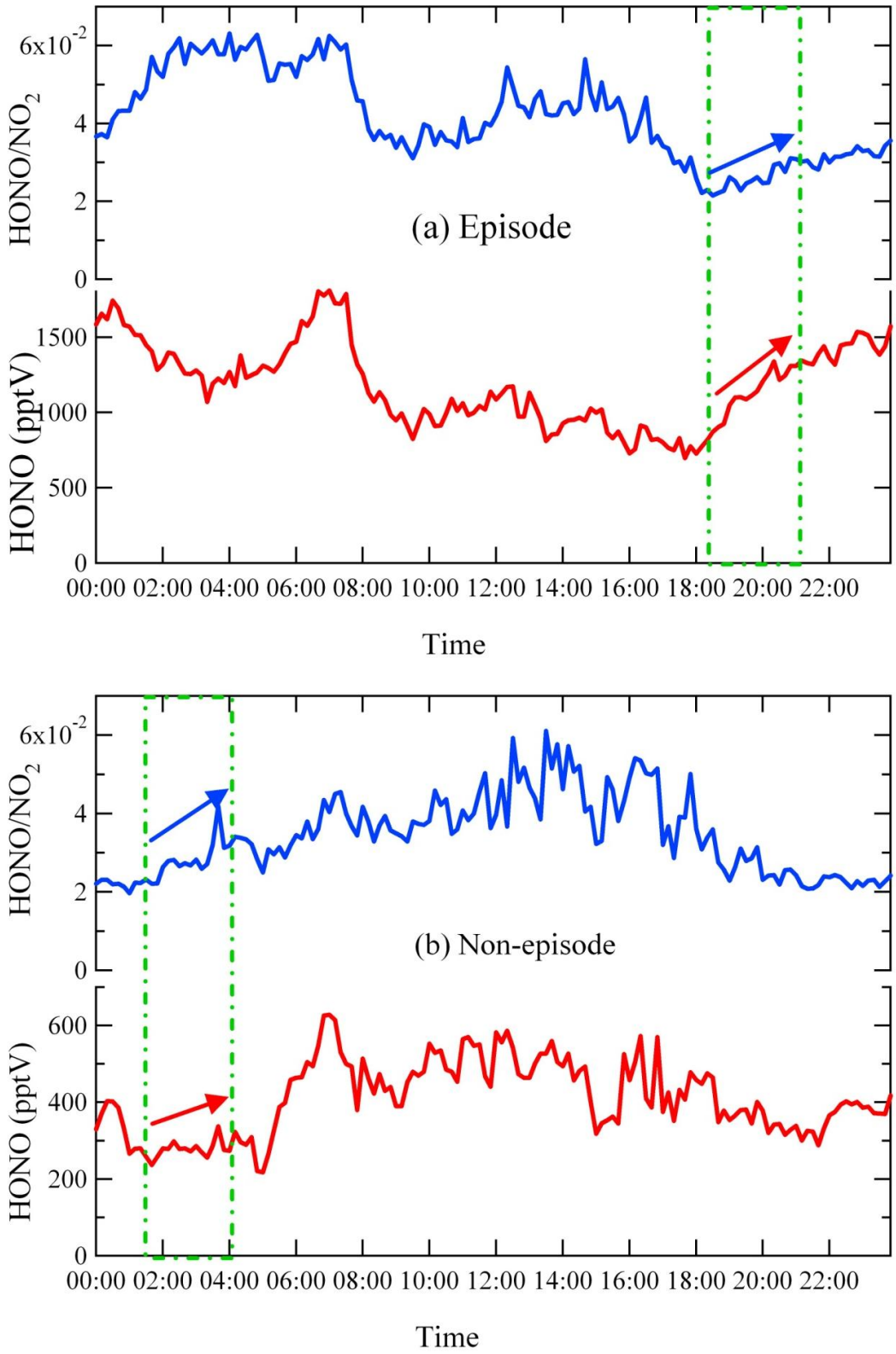

Figure 6.6 Averaged $HONO/NO_2$ and HONO patterns in (a) episode, (b) non-episode days.

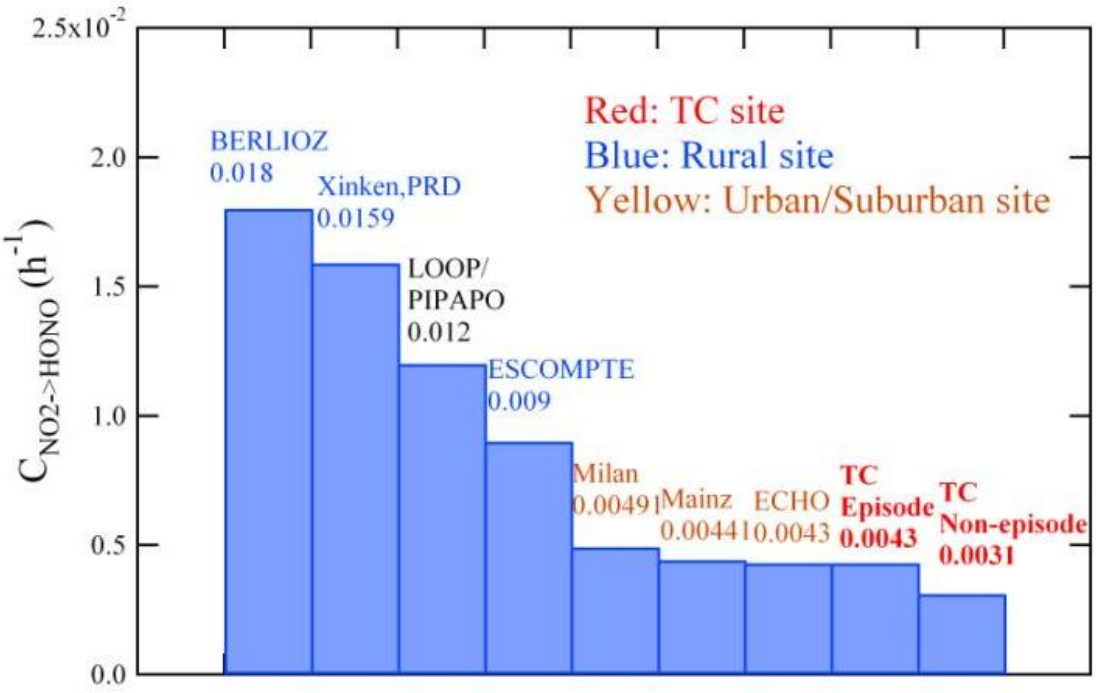

Figure 6.7 NO_2 Conversion Rate in Different Monitoring Sites (for C_{NO2} of other sites, please refer to Kathmadu (Yu et al., 2009), Xinken(Su et al., 2008a), Mainz and Milan(Lammel, 1999), ESCOMPTE(Acker et al., 2005), ECHO(Kleffmann et al., 2003), LOOP/PIPAPO(Alicke et al., 2002), BERLIOZ(Alicke et al., 2003).

Though NO_2 heterogeneous reaction on ground surface has been widely accepted as the major HONO source at night, some scientists have found good correlations between nighttime HONO and aerosol concentration, which indicates that aerosol surfaces may also be one of the important interfaces for NO_2 heterogeneous reactions (Notholt et al., 1992; Andres-Hernandez et al., 1996; An et al., 2009; Li et al., 2011b). Next, we try to figure out whether the nighttime NO_2 conversion process on aerosol surfaces is important or not in TC. Since solid surfaces are usually referred to those building or

ground surfaces, they are considered as constant in both clear and polluted days. Yet, the surface area of aerosol may change a lot due to the increasing aerosol concentration in polluted days. Surface density of aerosol ($(S/V)_a$) in two time periods is presented in figure 6.8 as below.

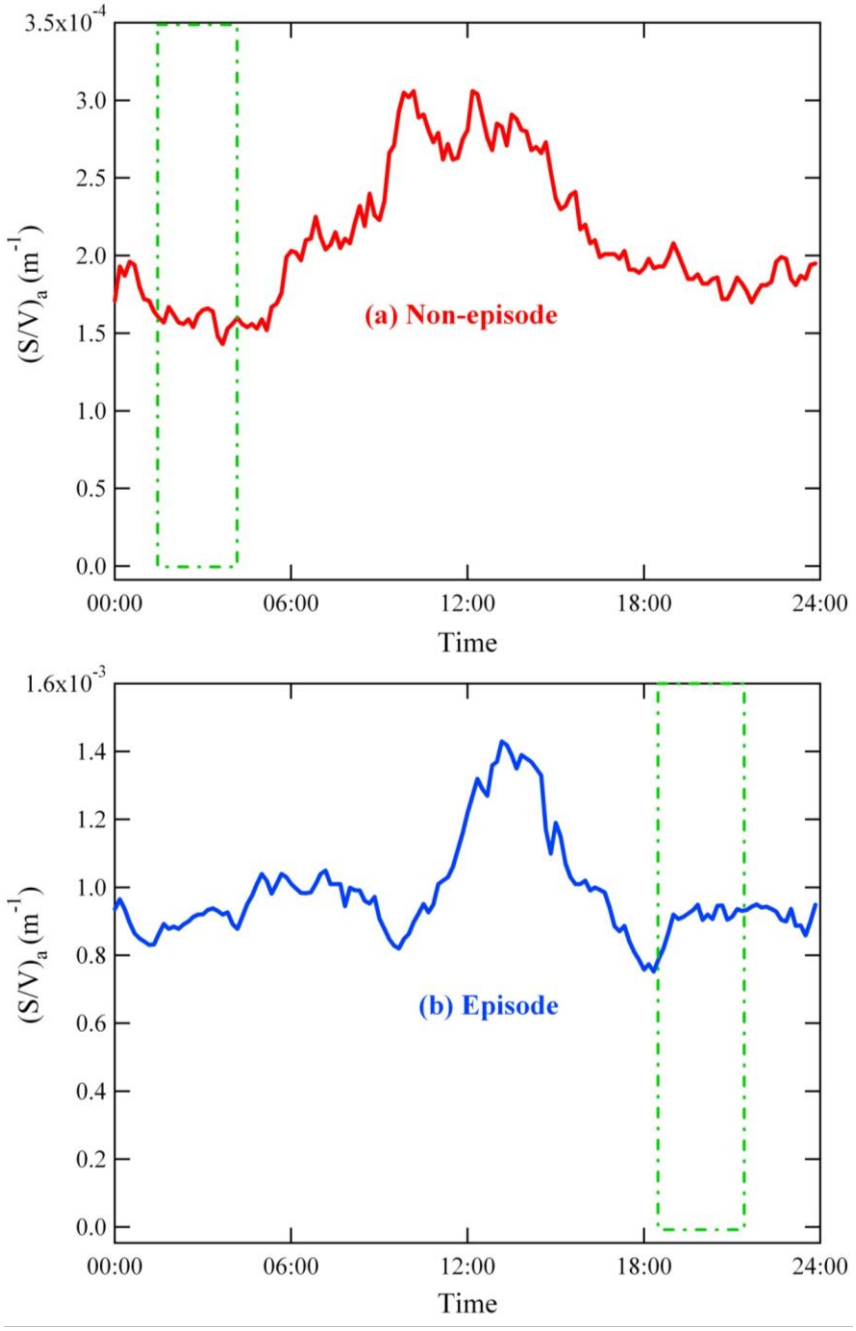

Figure 6.8 Diurnal patterns of surface to volume ratio (surface density) of aerosol in (a) non-episode, (b) episode days.

Selecting the same time periods that used to estimate the NO_2 conversion rates in episode and clear days (Figure 6.6), we found that surface density increased by around 6 times. If the heterogeneous conversion process happened on aerosol surface, the conversion rate should also increase by 6 times according to (E6.2). However, NO_2 conversion rate has increased by only 1.4 times in episode days, as shown in (E6.3). This suggests that NO_2 conversion process at night mainly occurs on solid surfaces (including ground surfaces) in episode days, with minor contribution from aerosol surfaces.

$$\frac{\left(\frac{S}{V}\right)_{a_{episode}}}{\left(\frac{S}{V}\right)_{a_{non-episode}}} \approx \frac{9*\frac{10^{-4}}{m}}{1.5*\frac{10^{-4}}{m}} \approx 6 > \frac{0.4344\%h^{-1}}{0.3072\%h^{-1}} \approx 1.4 \qquad (E6.3)$$

6.3 MCM Model Performances

After examining the nighttime HONO characteristics, it is important to figure out what is responsible for the high daytime HONO level in the episode days. Based on the MCM box model set up (described in chapter 5), numerical simulations are carried out to investigate the daytime HONO chemistry in TC.

Two simulation cases are run to study the possible daytime sources of HONO and its impact to the photochemistry. One simulation case is called Base-case in which only gas-phase chemical reactions are considered in the MCM box model. In other words,

only homogenous reaction between NO and OH (R1.3) is included as the only HONO daytime source in this case. Besides, all observation data except HONO are used as model constraints. Therefore, this case can be used to calculate the daytime HONO PSS concentration. It is also used to calculate the discrepancy between observation and PSS concentration, since only gas-phase source and sink pathways of HONO are included in the model framework (R1.1, R1.2 and R1.3). Another simulation case is referred to as OBM-case which read in all the observation data including HONO in the model. Since real-time measured HONO is among one of the constraints, the simulation results of this observation-based box model can help to study the impact of HONO on OH radical and to calculate the reaction rates of (R1.1), (R1.2) and (R1.3).

Some general simulation results of both Base-case and OBM-case are presented in figure 6.9 and 6.8. Here, because of our specific research interests, only daytime simulation results are shown and analyzed. The simulation time period is from 10th to 31st August which covers both clear and polluted days. Though only daytime results are presented, input data for all observed species are continuous, with ten minutes' time resolution. Besides, ten days' pre-run is conducted to stabilize the active intermediates and parameters in the model.

We can see from figure 6.9 that discrepancy between observation and Base-case PSS HONO concentration in non-episode days are much smaller than that in episode days. This suggests that homogenous source alone already explain a large amount of daytime

HONO during clear days. The averaged simulated HONO to observed HONO ratio in Base-case reaches around 50% in non-episode days. This high contribution from (R1.3) may result from the relatively higher concentrations of both NO and OH in clear days, as presented in figure 6.1 and 6.10, respectively.

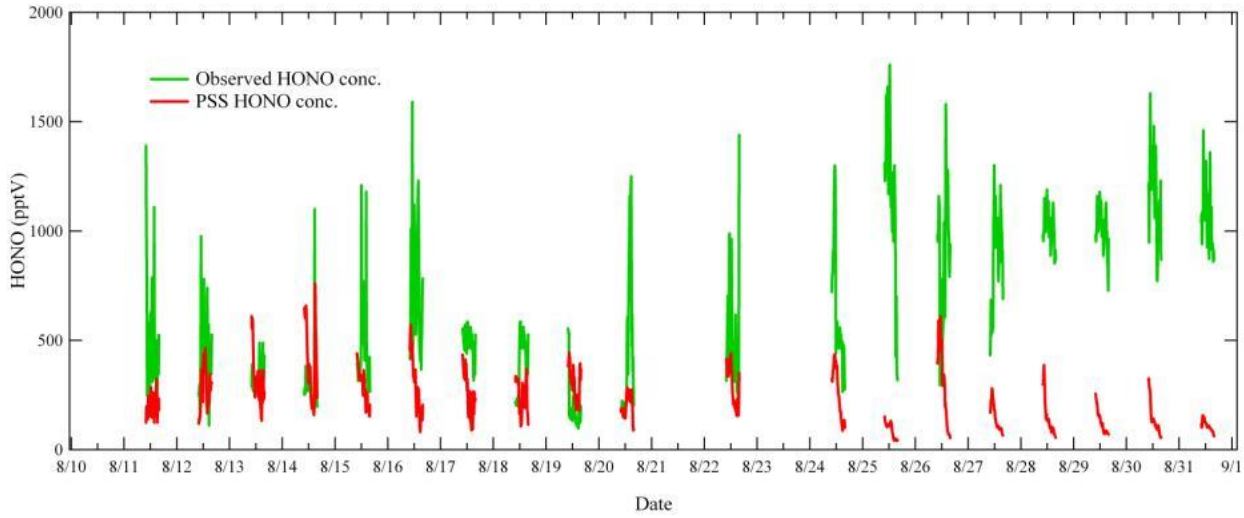

Figure 6.9 Time series for observed and simulated (Base-case) daytime HONO concentrations.

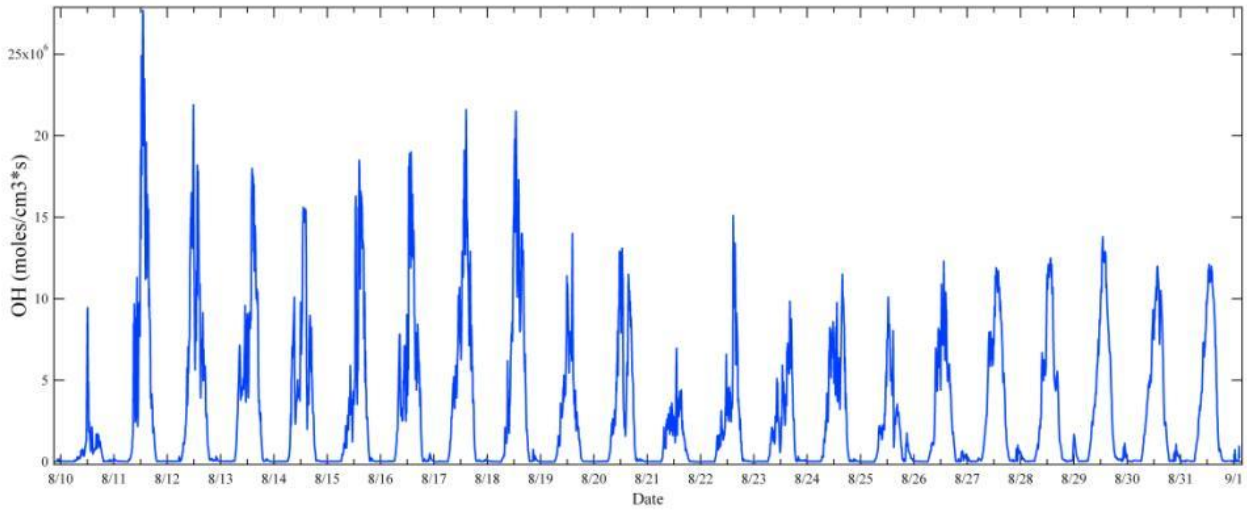

Figure 6.10 Time series for simulated OH concentrations in OBM-case.

However, during episode days, gas-phase PSS HONO concentration simulated by Base-case is far below the observation. This suggests that there exist additional sources which play important roles in the daytime HONO accumulation in polluted days. With an observation-based box model and the PSS analysis approach, the possible additional sources of daytime HONO in episode days will be discussed in detail in section 6.4.

6.4 Daytime HONO source(s) in Episode Days

6.4.1 Method to Calculate Extra Daytime HONO Source(s) Strength

As reviewed in chapter 2, numerous laboratory, modeling and field studies have been conducted to reveal the possible daytime HONO sources. Among all potential sources, NO_2 heterogeneous reactions (R2.8 and R2.9) seem to be the most important two sources of daytime HONO. Yet, whether those reactions take place on solid (referred to as ground surface hereafter) or aerosol surfaces still remains unclear. To investigate the roles of ground and aerosol surfaces in HONO formation in our study site, a daytime HONO budget analysis was carried out using (E6.4) (Su et al., 2008b; Li et al., 2012):

$$\frac{d[HONO]}{dt} = (P_{OH+NO} + P_{extra} + P_{transport} + P_{emission}) - (L_{HONO+hv} + L_{OH+HONO} + L_{depositon} + L_{transport}), \quad \text{(E6.4)}$$

where $\frac{d[HONO]}{dt}$ denotes the variation of observed HONO, P_{OH+NO} denotes HONO production rate from (R1.3), $P_{transport}$ denotes contribution from transport processes,

including horizontal and vertical transport, $P_{emission}$ denotes HONO accumulation from direct emissions of vehicles, and P_{extra} denotes the combination of all extra daytime HONO sources in addition to (R1.3). In the sink terms, $L_{HONO+hv}$ represents HONO photolysis, $L_{OH+HONO}$ represents HONO loss rate from (R1.2), $L_{depositon}$ represents HONO deposition rate, and $L_{transport}$ represents dilution effects through transport processes.

The daytime data we analyzed all satisfy the criteria that photolysis frequency of HONO (J_{HONO}) is greater than 1.0×10^{-3} s^{-1}. Under this circumstance, the lifetime of HONO is in the range of 10-17 minutes. $\frac{d[HONO]}{dt}$ is estimated by approximation of $\frac{\Delta[HONO]}{\Delta t}$ which is the differences of HONO concentrations every 10 minutes (Sörgel et al., 2011). $P_{emission}$ is estimated based on a direct HONO/NO_x emission ratio of 0.8% (Kurtenbach et al., 2001). The latest anthropogenic emission inventory (EI) in Hong Kong with a resolution of 1.5 km was used to estimate the direct NO_x emission in TC. This inventory is obtained from HKEPD (reference year 2010), including monthly emissions from transportation, residential, power plant, industry, and agriculture sectors. A diurnal variation is applied to EI according to the traffic pattern in Hong Kong, due to the fact that the NO_x emission of the grid where TC located (380 mol/km^2h in daily average) is mainly from transportation (>90%). Daytime HONO mixing height is assumed to be 200 m, considering that HONO emitted from ground will undergo fast photolysis during vertical transport (Alicke et al., 2002). $L_{depositon}$ is calculated by assuming a HONO daytime dry deposition velocity of 2 cm/s and a HONO mixing height of 200 m

(Harrison et al., 1996; Chan et al., 2006). Sensitivity studies on different HONO mixing height (20 and 1000 m) are carried out, and results are presented in Table 6.2 (section 6.4.3). During study period, averaged wind speed is 2 m/s. With a short lifetime of HONO when J_{HONO} is greater than1.0×10^{-3} s^{-1}, horizontal transport is assumed to be of minor importance to the observed HONO.

As to the vertical transport effect, (E6.4) is widely adopted to estimate HONO daytime extra sources by considering the negligible role of this term, which leads to reasonable results (Alicke et al., 2002; Zhou et al., 2002; Kleffmann et al., 2003; Vogel et al., 2003; Kleffmann et al., 2005; Acker et al., 2006a; Michoud et al., 2013). Yet, Wong et al. (2012) found strong negative HONO gradient in field measurement. In their following study, by adopting a 1-D transport model, they pointed out that vertical transport is the main sink pathway of HONO in the lower boundary layer (Wong et al., 2013). Though this term may be of great importance in some specific locations, especially in locations where strong HONO gradients are observed, the significance of vertical transport differs from place to place. For example, uniform daytime HONO gradients have been observed in many field measurements (Trick, 2004; Kleffmann, 2007; Häseler et al., 2009; Zhang et al., 2009). If this is the case, vertical transport may be of minor importance. Thus, P_{extra} estimated by (E6.4) is still reasonable. Moreover, in situations where there are no vertical meteorological parameters available and it is difficult to quantify the contribution from vertical transport process, P_{extra} can be considered as the lower limit for the extra HONO source. Therefore, equation (E6.4) is simplified to:

$$P_{extra} \approx \frac{\Delta[HONO]}{\Delta t} + L_{HONO+hv} + L_{OH+HONO} + L_{depositon} - P_{OH+NO} - P_{emission} \quad \text{(E6.5)}$$

To obtain P_{extra}, the other three factors on the right side of (E6.5) ($L_{HONO+hv}$, $L_{OH+HONO}$, and P_{OH+NO}) need to be calculated. In our study, HONO and NO were measured, while OH and J_{HONO} were both simulated by the MCM photochemical box model, as described in chapter 5.

6.4.2 OH and J_{HONO} Simulation

The OH concentration is simulated by a zero-dimensional observation-based box model. The chemical mechanism implemented in the model is the MCM (Master Chemical Mechanism), version 3.1. To reproduce OH concentration in our study site, real-time observation data obtained in the field study are all used to constrain the model. Previous studies show that OH concentrations simulated by the MCM model are comparable with measurements in high-NO_x atmospheres (Mihelcic et al., 2003; Elshorbany et al., 2009; Elshorbany et al., 2012). Therefore, OH simulation result of OBM-case, as presented in figure 6.10, is used in calculation.

J_{HONO} is also simulated by the MCM model, which is based on the method suggested by Saunders et al.:(2003)

$$J = l(cosx)^m \exp(-n.secx) \quad \text{(E6.6)}$$

where x is the solar zenith angle. Jenkin et al. (1997) have discussed optimized parameters for l, m and n. To associate the simulated photolysis frequency with measurement, all modeled J values including J_{HONO} are scaled by a factor defined as $(\frac{J_{NO_2(observed)}}{J_{NO_2(modeled)}})$. The simulation results of both OH concentrations and J_{HONO} values are within reported range, and comparable with measurements in rural and urban sites (Su et al., 2008b; Hofzumahaus et al., 2009; Li et al., 2010; Li et al., 2012).

6.4.3 Analysis of Extra HONO Daytime Source(s) in Episode Days

6.4.3.1 Calculation of Extra Daytime Source(s)

Our study focuses on the polluted period from 25 to 31 August 2011 when daytime HONO frequently exceeds 1 ppbV. Analysis of daytime HONO chemistry was based on daily datasets that satisfy $J_{HONO}>1.0\times10^{-3}s^{-1}$. Under these conditions, a quasi-steady-state for HONO can be reasonably assumed.

The averaged diurnal variation of HONO exhibits a typical pattern, which peaks in the early morning and reaches minimum around noon (Figure 6.5 and Figure 6.11a). However, a HONO mixing ratio of 1.2 ppbV was observed when $J_{HONO}>1.0\times10^{-3}s^{-1}$. Thus, there should be some extra sources to sustain this high HONO level in the daytime. According to (E6.5), the extra daytime source strength of HONO (P_{extra}) is estimated (Figure 6.11b), with an averaged P_{extra} of 1.12 pptV/s at our study site. Figure 6.12

further shows the production and loss rates related to each term in E6.5. P_{extra} is found to be up to five times faster than the homogenous reaction (R1.3). It is also much higher than those observed in other sites, as shown in table 6.1. During this period, a large daytime P_{extra} is expected because of high HONO (up to 1.2 ppbV) and relatively low NO concentrations (<10 ppbV), which results in low contribution from the homogenous reaction (NO+OH) in episode days.

As mentioned above, P_{extra} is calculated without considering the vertical dilution effect. Lacking meteorological parameters to quantify the contribution from vertical transport in our study site, we did a rough estimation of the impact from this process, by adopting the results in Wong et al. (2013) where HONO loss rate from vertical transport is more than three times larger than its photolysis. Result shows that if strong daytime vertical gradient do exist and vertical transport is ineligible, P_{extra} is largely under-estimated (Table 6.2). Thus, the traditional PSS approach is likely to produce only the lower limit of the unknown daytime HONO sources, if vertical dilution effect is very strong. Therefore, future field studies should also take into account the vertical meteorological parameters so as to figure out the contribution of this process.

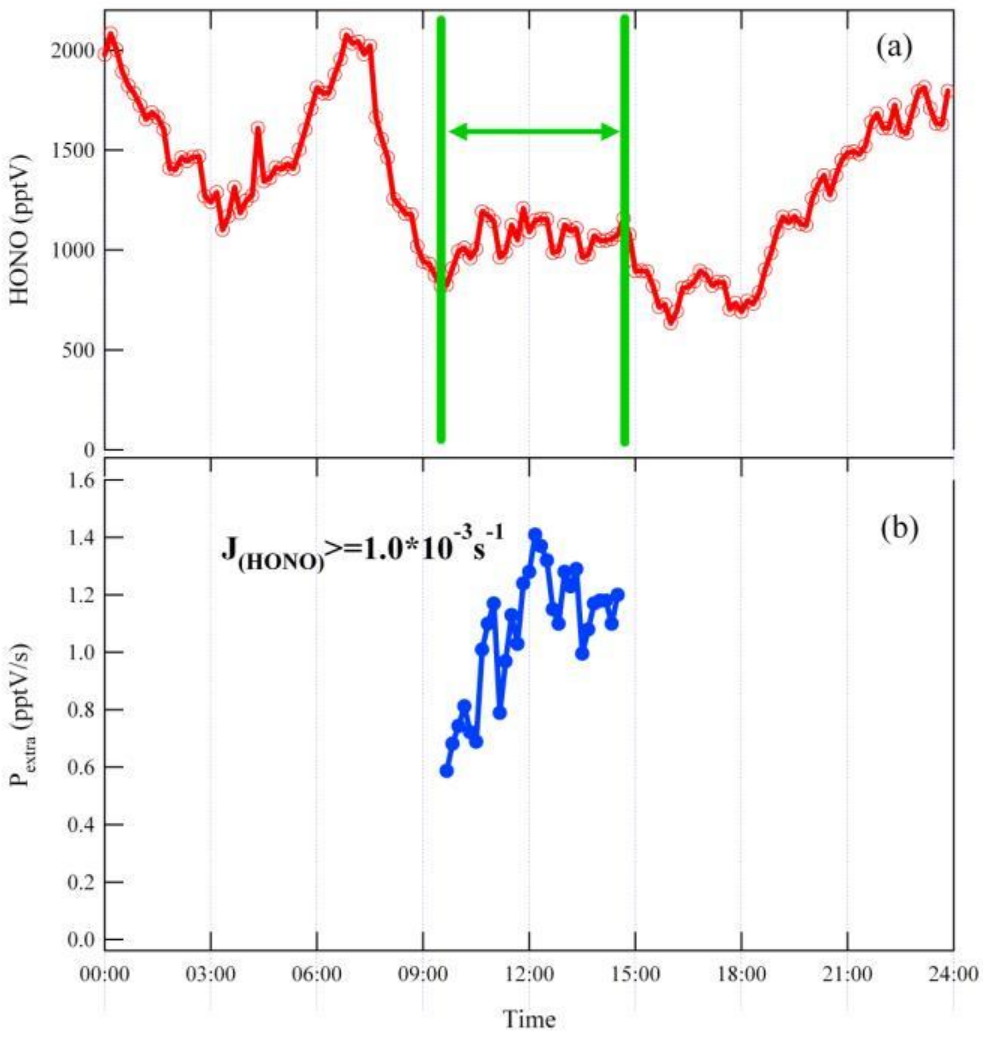

Figure 6.11 (a) Averaged diurnal pattern of HONO; and (b) Averaged P_{extra} when $J_{HONO}>1.0\times10^{-3}s^{-1}$ during study period from 25 to 31 August, 2011.

Table 6.1 Comparison of P_{extra} between Tung Chung and other study sites.

Location	P_{extra} (pptV/s)	Reference
Back Garden (rural)	0.21	Li et al.(2012)
Xin Ken (rural)	0.56	Su et al.(2008b)
Santiago, Chile (downtown)	0.47	Elshorbany et al.(2009)
Houston (downtown)	0.17	Wong et al.(2012)
Julich (forest)	0.14	Kleffmann et al. (2005)
Tung Chung (suburban)	1.12	Our Study

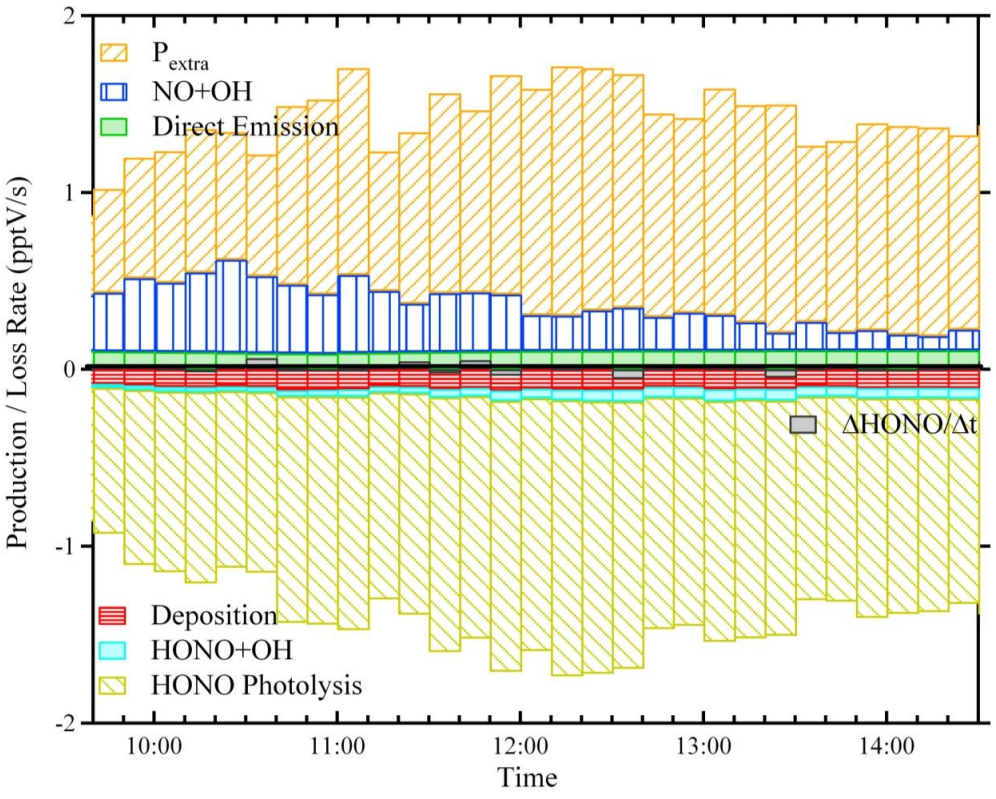

Figure 6.12. Production and loss rates of each process in (E6.5).

Table 6.2 Sensitivity tests of $P_{(extra)}$ and correlation coefficients between $P_{(extra)}$ and various parameters under different HONO mixing heights.

HONO Mixing Height (m)	**P(extra) (pptV/s)**	**Correlation Coefficient (R): P(extra) & various parameters as follows**				
		NO_2	**NO_2*$(S/V)_a$**	**NO_2*$(S/V)_a$*J_{NO2}**	**NO_y**	**NO_x**
20	1.12	0.21	0.70	0.71	0.44	0.01
200	1.12	0.11	0.65	0.67	0.34	-
200	5.00	0.28	0.67	0.72	0.47	0.10
1000	1.18	0.11	0.63	0.67	0.34	-

6.4.3.2 Correlation Analysis between P_{extra} and Different Proxies

In this section we examine the roles of different surfaces that are responsible for the extra daytime source of HONO (P_{extra}). Assuming 100% yield of HONO from redox reactions on aerosol surfaces (R2.9), and 50% yield of HONO from NO_2 heterogeneous reaction (R2.8,) on ground surface, the first order rate constant of these two sources can be calculated by the following formulas (Svensson et al., 1987; Kleffmann et al., 1998):

$$k_a = \frac{1}{4} * V_{NO_2} * \left(\frac{S}{V}\right)_a * \gamma_a \quad \text{(E6.7)}$$

$$k_g = \frac{1}{8} * V_{NO_2} * \left(\frac{S}{V}\right)_g * \gamma_g \quad \text{(E6.8)}$$

where k_a and k_g are rate constants on aerosol and ground surfaces, respectively. V_{NO_2} is the mean molecular speed of NO_2. $\left(\frac{S}{V}\right)_a$ and $\left(\frac{S}{V}\right)_g$ are surface to volume ratio of aerosol and ground surfaces. γ_a and γ_g represent NO_2 uptake coefficients on the two types of surfaces (Kurtenbach et al., 2001; Aumont et al., 2003a; Li et al., 2010; Czader et al., 2012b; Zhang et al., 2012).

When J_{HONO} is greater than $1.0\times10^{-3}s^{-1}$, temperature is high and solar radiation is very strong. Assuming that if the boundary layer is well-developed under such circumstance, the mixing height can be regarded as constant and the volume of the air column per geometric surface is fixed. Thus, it is reasonable to treat $\left(\frac{S}{V}\right)_g$ as a constant. Reaction rates of NO_2 reactions on aerosol and ground surfaces can be derived according to (E6.9) and (E6.10) as follows:

$$R_a = k_a[NO_2] = m * \left(\frac{S}{V}\right)_a * [NO_2] \quad \text{(E6.9)}$$

$$R_g = k_g[NO_2] = n * [NO_2] \quad \text{(E6.10)}$$

where R_a and R_g are reaction rates of NO_2 on two types of surfaces, m and n are two constants denoting values of $(\frac{1}{4} * V_{NO_2} * \gamma_a)$ and $(\frac{1}{8} * V_{NO_2} * \left(\frac{S}{V}\right)_g * \gamma_g)$, respectively. Accordingly, $(\left(\frac{S}{V}\right)_a * [NO_2])$ and $([NO_2])$ are two variables, which can be considered as proxies of NO_2 heterogeneous reactions on aerosol and ground surfaces. Several recent laboratory studies show that these first order surface reactions can be photo-enhanced,

and the uptake coefficient, γ, depends highly on irradiation (George et al., 2005; Stemmler et al., 2006; Stemmler et al., 2007; Ndour et al., 2008; Monge et al., 2010). To take light into account, the reaction rates are thus expressed as:

$$R_a^* = M * J_{NO_2} * \left(\frac{S}{V}\right)_a * [NO_2] \quad \text{(E6.11)}$$

$$R_g^* = N * J_{NO_2} * [NO_2] \quad \text{(E6.12)}$$

where R_a^* and R_g^* are photo-enhanced reaction rates, and M and N are two fitting parameters. Accordingly, $(J_{NO_2} * \left(\frac{S}{V}\right)_a * [NO_2])$ and $(J_{NO_2} * [NO_2])$ are considered as two proxies of photo-enhanced NO_2 heterogeneous reactions on aerosol and ground surfaces. To make it simple, the extra missing sources can be written as:

$$P_{extra} \propto J_{NO_2} * (\frac{S}{V}) * [NO_2] \quad \text{(E6.13)}$$

We first investigate the correlation between P_{extra} and the NO_2 which is the main precursor of HONO. Figure 6.13a indicates small correlation coefficients between P_{extra} and NO_2 (R=0.12). As mentioned above, this figure can also be regarded as the correlation between P_{extra} and NO_2 heterogeneous reaction on ground surfaces (Su et al., 2008b). Poor correlation is found, which is possibly due to the relatively stable and abundant NO_2 concentrations during episode days. After taking $\left(\frac{S}{V}\right)_a$ into account, the correlation has significantly increased, with a much larger coefficient of 0.65 for $(\left(\frac{S}{V}\right)_a * [NO_2])$ (Figure 6.13b). It is further improved to 0.67 after considering

J_{NO_2} (Figure 6.13c). It is noteworthy that this small improvement does not imply a negligible role of light in HONO formation. Because we only analyze the data collected when J_{HONO} is larger than $1.0\times10^{-3}s^{-1}$ and the solar radiation is very strong under such conditions.

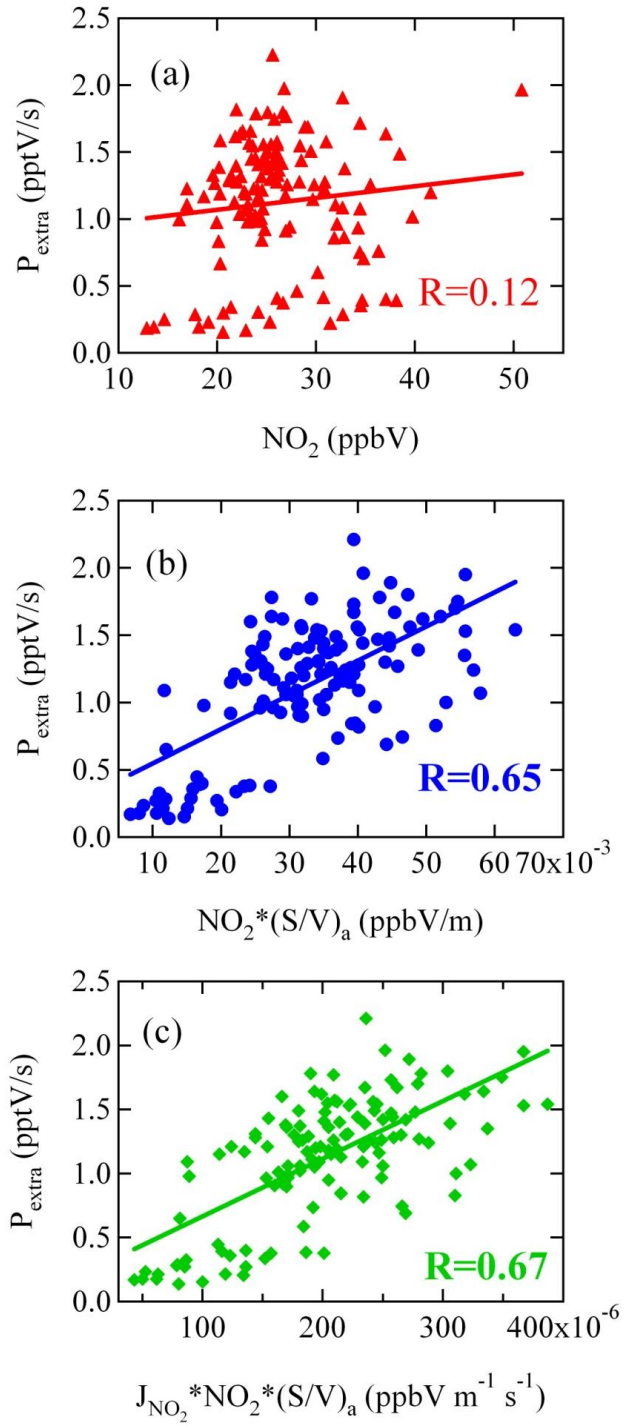

Figure 6.13 Correlations between P_{extra} and proxies of different sources: (a) ground source: ($[NO_2]$); (b) aerosol source: $\left(\left(\frac{S}{V}\right)_a * [NO_2]\right)$; and (c)photo-enhanced aerosol source: $\left(J_{NO_2} * \left(\frac{S}{V}\right)_a * [NO_2]\right)$.

The good correlations in figure 6.13b, c (R=0.65-0.67,) suggest that NO_2 heterogeneous reactions on aerosol surface may contribute significantly to daytime HONO buildup. This is different from the results obtained in central and northern PRD. Su et al. (2008b) found that in Xinken (100 km north of TC), HONO formation tended to be mainly on the ground surface rather than on the aerosol surface. Li et al. (2012) also observed poor correlations between the unknown daytime HONO source and aerosol-related parameters at Back Garden, a rural site in northern PRD. Both studies suggested that aerosol sources are negligible in the formation of HONO.

To verify the good correlations in figure 6.13b and 6.13c are caused by the real source-product relation, rather than by other factors, such as boundary layer variation, correlations analysis between P_{extra} and NO_y, P_{extra} and NO_x are conducted. NOy denotes the sum of NOx and all nitrogen compounds that are oxidation products of NOx in the atmosphere (Seinfeld and Pandis, 2006). Compared to other reactive species, NOy concentration is considered to be relatively constant within the boundary layer. Therefore, if the good correlations in figure 6.13b, c are resulted from simultaneous variation of air pollutants in the developing boundary layer, there should be a good correlation between P_{extra} and NO_y. Similarly, if P_{extra} show good correlation with NO_x, observed HONO and aerosols may share the same near-ground sources, such as emission. Yet, poor correlations are found between P_{extra} and NO_y, P_{extra} and NO_x (R=0.34 and -0.11, respectively). Similar correlation results are found in sensitivity tests under different HONO mixing heights and with/without vertical dilution effects (Table 6.2).

Possible reasons for the importance of aerosol surfaces in our study site include: (1) a large daytime $\left(\frac{S}{V}\right)_a$ (Figure 6.4), (2) high daytime RH with averaged values between 60%-70% (Figure 6.3), and (3) organic coating on aerosols (Figure 6.15). During the study period, the atmosphere was extremely polluted, with very high aerosol loading. The averaged daytime $\left(\frac{S}{V}\right)_a$ reached 1.15×10^{-3} m^{-1}. This indicated that aerosol could contribute more to the HONO production than in clear days, since (S/V) is a determining factor in the first order HONO production rate (Seinfeld and Pandis, 2006). Besides, from the morphology of aerosol during the study period (Figure 6.15), aerosols were observed to be coated with organics. According to George et al. (2005) and Stemmler et al. (2006; 2007), aerosol surfaces containing organics such as phenols, aromatic ketones and humid acid can also help enhance the uptake of NO_2 under irradiated condition.

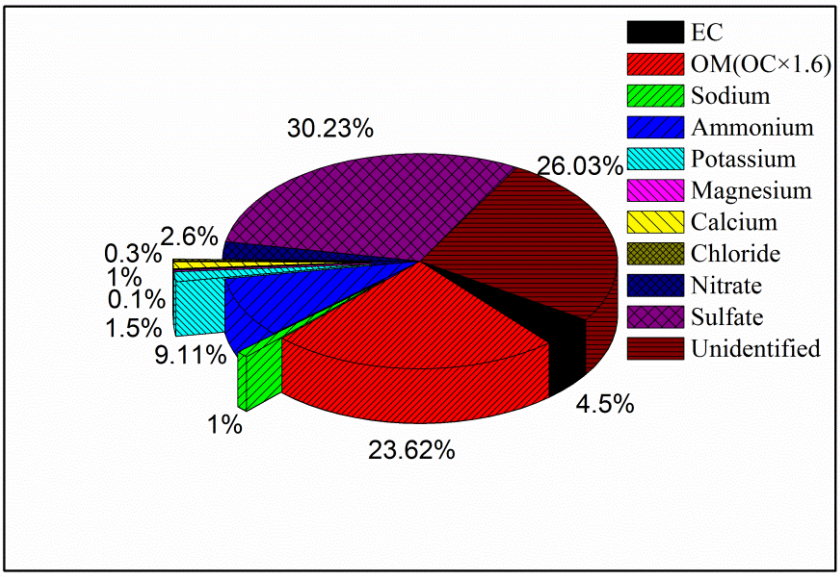

Figure 6.14 Average chemical compositions of $PM_{2.5}$ when $J_{HONO}>1.0\times10^{-3}s^{-1}$ from 25 to 31 August, 2011.

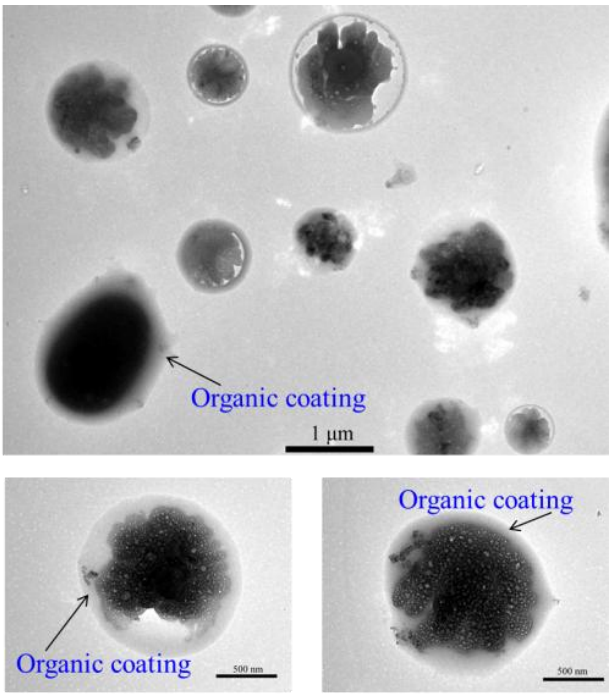

Figure 6.15 TEM (Transmission electron microscope) images of individual particles collected during episode.

6.4.3.3 Correlation Analysis between P_{extra} and Different Components in Aerosol

From the correlation analysis above, we see that aerosol plays an ineligible role in polluted days. In order to have more hints on which component in aerosol is the determining one in HONO production, detailed analysis into various chemical components in $PM_{2.5}$ is conducted.

According to figure 6.14, the major components in $PM_{2.5}$ include sulfate (SO_4^{2-}), undefined and organic matters (OM=organic carbon (OC)*1.6). They take up 30.23%, 26.03% and 23.62% of the total $PM_{2.5}$ mass concentration, respectively. These three top

components are followed by ammonium (NH_4^+) and elementary carbon (EC), which take up 9.11% and 4.5%, respectively. Other components, such as nitrate (NO_3^-), potassium (K^+) and so on, are less than 3% in the total mass concentration.

From table 6.3 and figure 6.16 below, we find that three main components SO_4^{2-}, OM and NH_4^+ all have good correlations with P_{extra}, with R larger than 0.6. Yet, despite the fact that EC is not the most abundant component in $PM_{2.5}$ (only takes up 4.5% of the total mass concentration), the correlation (R) between P_{extra} and EC reaches 0.85, which is the highest correlation compared to all other components. This suggests that EC (or soot) in aerosols may play an important role in the daytime HONO formation during episode days. In fact, Monge et al. (2010) have found that oxidized soot surfaces can be reactivated in the presence of sunlight, and the reaction rate is dramatically increased compared to that in the dark and oxidized conditions.

Table 6.3 Correlations between P_{extra} and different components in $PM_{2.5}$ during episode days.

	Correlations between P_{extra} and different (R)
SO_4^{2-}	**0.77**
OM (represented by OC)	**0.71**
NH_4^+	**0.67**
EC	**0.85**
NO_3^-	0.44
K^+	0.32
Na^+	0.04
Ca^{2+}	0.24
Cl^-	-0.23
Mg^{2+}	0.20

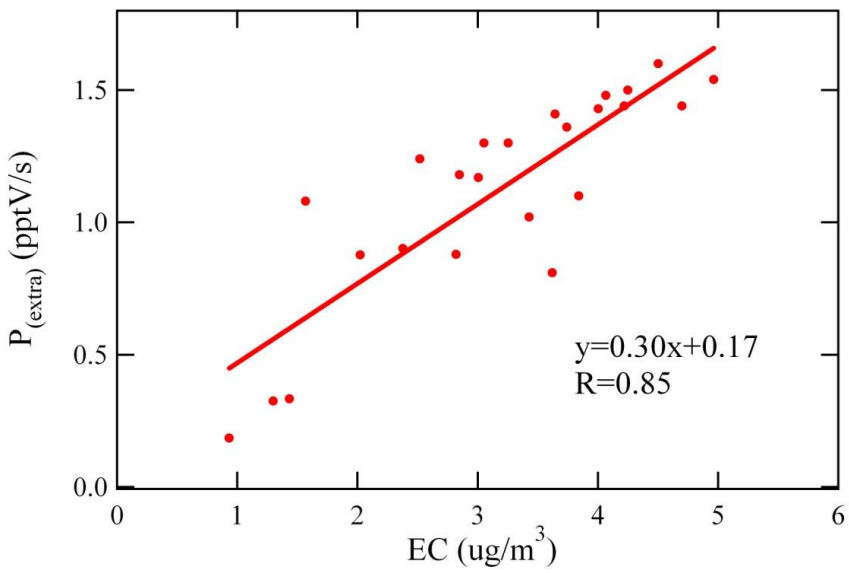

Figure 6.16 Correlations between P_{extra} and observed EC during episode days.

Another very interesting phenomenon is that when ploting HONO to NO_2 data in the episode, we find that the data can be divided into two groups: the large- and small-slope groups (Figure 6.17). When examine the characteristics of these two groups, we discover that most of the data in large-slope group appear in the early morning from 5 to 9 a.m.. The small-slope group of data mainly center around 17 to 19 p.m.. Though slopes are different, the two groups have one thing in commen. That is, time periods for both groups are in the rush hours. This phenomenon suggests that the conversion rates from NO_2 to HONO in these two time periods may be different. In the early morning, large slope indicates a relatively higher conversion rate compared to that in the afternoon, with fewer NO_2 yet more HONO produced.

Conversion rate can be largely affected by the surface types. For example, on the fresh soot surfaces, NO_2 uptake is very efficient, leading to large conversion rate of NO_2 to HONO. Yet, when the soot surfaces are oxidized, the redox reaction rate of NO_2 is greatly reduced to a negligible role (Ammann et al., 1998). Thus, it is likely that in the morning rush hours, due to the fresh emitted gases and particles from vehicles, the reaction interfaces such as ground and aerosol surfaces are covered with various reactive organic and inorganic chemicals, which can promote the HONO production. However, in the afternoon, owing to the accumulation of many photochemical oxidants such as O_3 and OH, the reactive interfaces are oxidized quickly, leading to decreasing conversion efficiency of NO_2 to HONO. Figure 6.16 together with figure 6.17 give us some indications that EC may be one of the most important compounds that largely affect the conversion efficiency of NO_2 heterogeneous reaction. On the other hand, due to the abundant oxidants, the fresh emitted NO in the afternoon rush hour are immedietly oxidized to NO_2. The increasing NO_2 concentration also results in low HONO to NO_2 ratio in the afternoon.

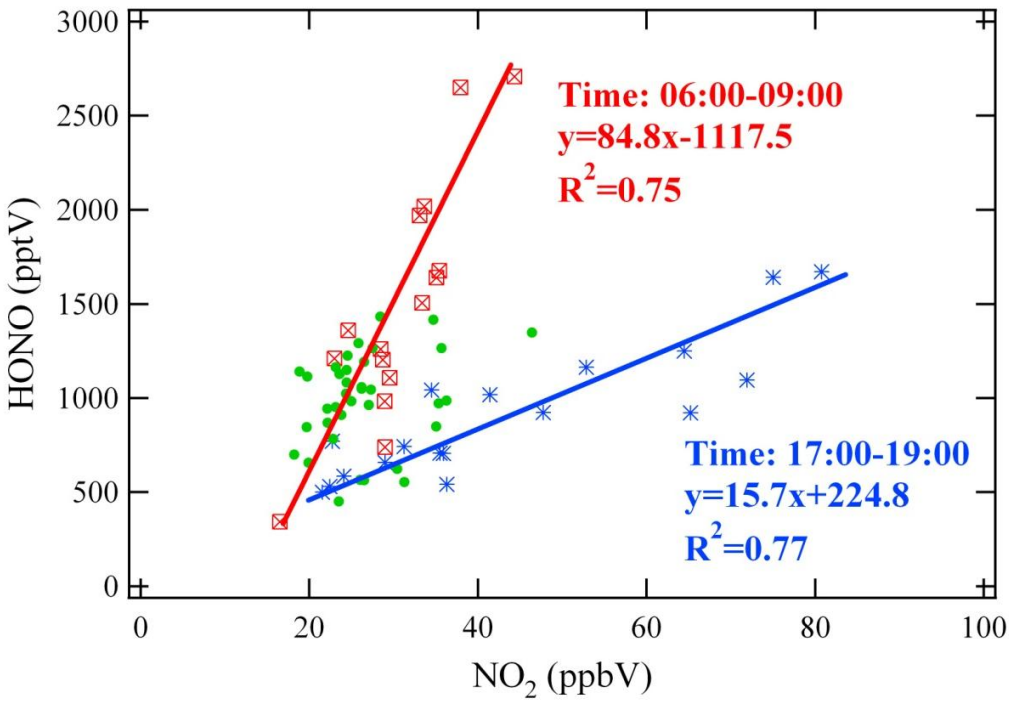

Figure 6.17 HONO to NO_2 plotting in the morning (6-9 a.m.) and afternoon (17-19 p.m.) rush hours.

6.4.4 Estimation of NO_2 Uptake Coefficient on Aerosol (γ_a)

Although NO_2 uptake coefficient (γ_a) has been tested on many different aerosol surfaces, the value adopted in numerical simulations is still in a wide range, from 10^{-7} to 10^{-3} (Jacob, 2000; Aumont et al., 2003a; Vogel et al., 2003; Li et al., 2010; Li et al., 2011b; An et al., 2013; Wong et al., 2013). Here, we try to have some indications of this value from the comprehensive summer field measurement in TC.

Assuming a first order production rate and 100% yield of HONO on aerosol surfaces (E6.7), P_{extra} can be expressed as (E6.14) (Kleffmann et al., 1998; George et al., 2005;

Seinfeld and Pandis, 2006; Stemmler et al., 2006; Stemmler et al., 2007; Ndour et al., 2008). Thus, an 'apparent' γ_a of NO_2 can be derived according to this equation:

$$P_{extra} = R_{aerosol} + R_{other} = (\frac{1}{4} * v_{NO_2} * \gamma_a) * (\left(\frac{S}{V}\right)_a * [NO_2]) + R_{other} \quad \text{(E6.14)}$$

where $R_{aerosol}$ is the first order reaction rate of NO_2 heterogeneous reaction on aerosol, R_{other} is the HONO source strength of all additional sources. From the P_{extra} versus $(\left(\frac{S}{V}\right)_a * [NO_2])$ plot (Figure 6.13b), an observation-based γ_a can be derived from the slope:

$$\frac{1}{4} * v_{NO_2} * \gamma_a = 25.46 * 10^{-3} m/s \quad \text{(E6.15)}$$

Taking an approximation for v_{NO_2} of 400 m/s, γ_a is calculated to be 2.5×10^{-4} ($\pm0.5\times10^{-4}$, within confidence interval, $P<0.001$) in this study (Vogel et al., 2003; Czader et al., 2012b). Although this daytime observation-derived γ_a is 1-2 orders of magnitude larger than the value observed in many recent laboratory studies, some modeling studies adopt very large γ_a which is comparable to 2.5×10^{-4} (Jacob, 2000; Li et al., 2011b; An et al., 2013; Wong et al., 2013).

NO_2 redox reaction on fresh soot surfaces is very fast in the first few seconds, with γ_a up to 10^{-2} (Ammann et al., 1998; Gerecke et al., 1998). Yet, γ_a slows down to 10^{-7}, due to the oxidation of the soot surfaces with reaction time (Kleffmann et al., 1999; Arens et

al., 2001). Even though light can change the reactivity of oxidized soot surfaces, γ_a with a value of 10^{-6} is recorded at maximum (Monge et al., 2010). Higher γ_a in the range from 10^{-6} to 10^{-5} was observed on irradiated aerosol surfaces coated with organics (George et al., 2005; Stemmler et al., 2006; Stemmler et al., 2007). Reaction (R2.3) on pure TiO_2 has been found to be catalyzed under irradiated condition, γ_a of 10^{-4} was derived in laboratory study (Gustafsson et al., 2006). But on mixed TiO_2-SiO_2 aerosols, photo-catalyzed γ_a of NO_2 is only in the order of 10^{-6}, which indicates that γ_a cannot reach 10^{-6} on atmospheric particles where TiO_2 only takes up a few percent of the content (Ndour et al., 2008). Therefore, despite large observation-derived γ_a in our study, it cannot seem to be explained by any known reactions in recent laboratory studies.

However, in some modeling studies, reasonable simulation results were produced only when large γ_a from 10^{-4} to 10^{-3} was used (Jacob, 2000; Li et al., 2011b; An et al., 2013; Wong et al., 2013). The reasons for this discrepancy are unclear. It is possible that some unknown reactions on aerosol exist which have not been tested in laboratory studies yet (Wong et al., 2013). Moreover, though lab-measured γ_a may be more fundamental, an accurate comparison between the observation-derived and lab-measured γ_a is difficult to achieve, due to several factors: (1) different radiation conditions in the laboratory studies and the field study, (2) different methods for determination of $\left(\frac{\mathrm{S}}{\mathrm{V}}\right)_a$, and (3) a non-unity (not equal to one) correlation coefficient between P_m and $\left(\frac{\mathrm{S}}{\mathrm{V}}\right)_a * [NO_2]$ (as shown in Figure 6.13b). The radiation condition is an important parameter that affects

the photo-enhanced uptake coefficient of NO_2 on a surface. Yet, in most cases, the wavelengths of light sources used in laboratory studies differ from visible light in the atmosphere. Besides, in this study, $\left(\frac{S}{V}\right)_a$ was calculated from WPS^{TM} instrument which adopts mobility diameter surface area method (chapter 4). Different surface area calculation methods (geometric, equivalent mobility diameter and BET (Brunauer–Emmett–Teller) surface area) may also lead to different derived γ_a. In addition, the non-unity correlation coefficient in figure 6.13b also introduces some uncertainties on the large derived γ_a. Considering these factors, laboratory studies should carry on examing the NO_2 uptake coefficient on atmospheric particles containing different chemical compositions. Meanwhile, standard criteria should also be set up in order to make an appropriate selection of γ_a in different numerical simulations.

6.5 HONO Impact to OH Radical

HONO has been proved to be a strong source of OH in the early morning when concentrations of other OH precursors, such as O_3 and HCHO, are low (Seinfeld and Pandis, 2006). In this section, we try to examine the impact of the observed high daytime HONO on the overall OH budget. To achieve this, we compare the model simulation results of OBM-case (simulation case constrained with observed HONO) to Base-case (simulation case without HONO constraint). OH concentration simulated by OBM-case is considered as reference for the Base-case, for the reason that in OBM-case all real-time observation data are included in the model. Besides, MCM model

performance of OH is proved to be reliable, as mentioned above (Mihelcic et al., 2003; Elshorbany et al., 2009; Elshorbany et al., 2012).

Simulated averaged diurnal patterns of OH concentrations in the two cases under two different scenarios (episode and non-episode days) are presented in figure 6.18. Peak OH concentration of OBM-case is 1.3×10^{7} and 1.1×10^{7} molecules·cm^{-3}s^{-1} for non-episode and episode days, respectively. These peak concentrations are comparable with the measurement of Hofzumahaus et al. (2009) in a rural site (Back Garden), and simulation result of Su et al. (2008b) in a polluted rural site (Xinken). The simulation case without considering the HONO extra daytime sources (Base-case) underestimates OH concentration by 11% compared to the OBM-case in non-episode days. This underestimation increases to 20% in episode days due to the abundant ambient HONO level. This highlights the importance of integrating a representative HONO heterogeneous formation mechanism into photochemical air quality models so as to obtain a more accurate OH simulation result.

We then compare the OH production rate from the photolysis of HONO with another two major OH sources: photolysis of HCHO and of O_3. All these production rates are calculated by the MCM model (as shown in Figure 6.19). Results demonstrate that photolysis of HONO dominates OH production not only in the early morning, but also throughout the day. In episode days, nearly half (≈46.8%) of the primary OH production rate is attributed to HONO photolysis, followed by O_3 photolysis (≈29.2%) and HCHO

photolysis (≈24.0%). In non-episode days, the impact of HONO on OH radical is even stronger, due to the low concentration of both O_3 and HCHO at this time. It takes up about 53% of the primary rate. This phenomenon contrasts with the results in some rural or remote areas where HCHO or O_3 photolysis was the dominant OH precursor in the whole day (Alicke et al., 2002; Aumont et al., 2003a; Su et al., 2008b). Our results (Figure 6.18 and 6.19) indicate that HONO can be a major OH precursor under certain circumstances, and is therefore of great significance to the photochemistry and formation of the air pollution.

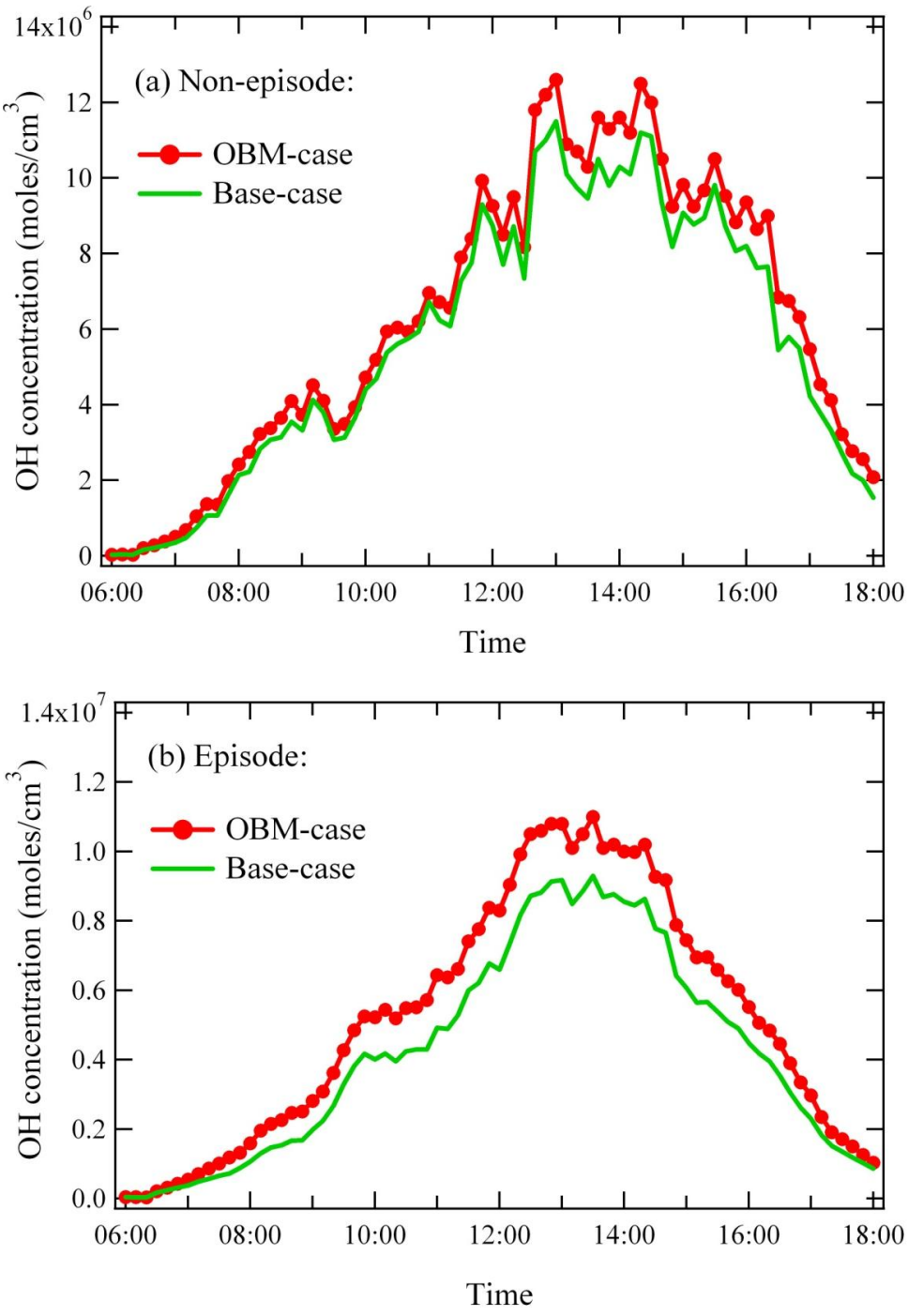

Figure 6.18 Averaged daytime patterns of OH concentrations in two simulation cases in (a) non-episode and (b) episode days: OBM-case (red) and Base-case (green).

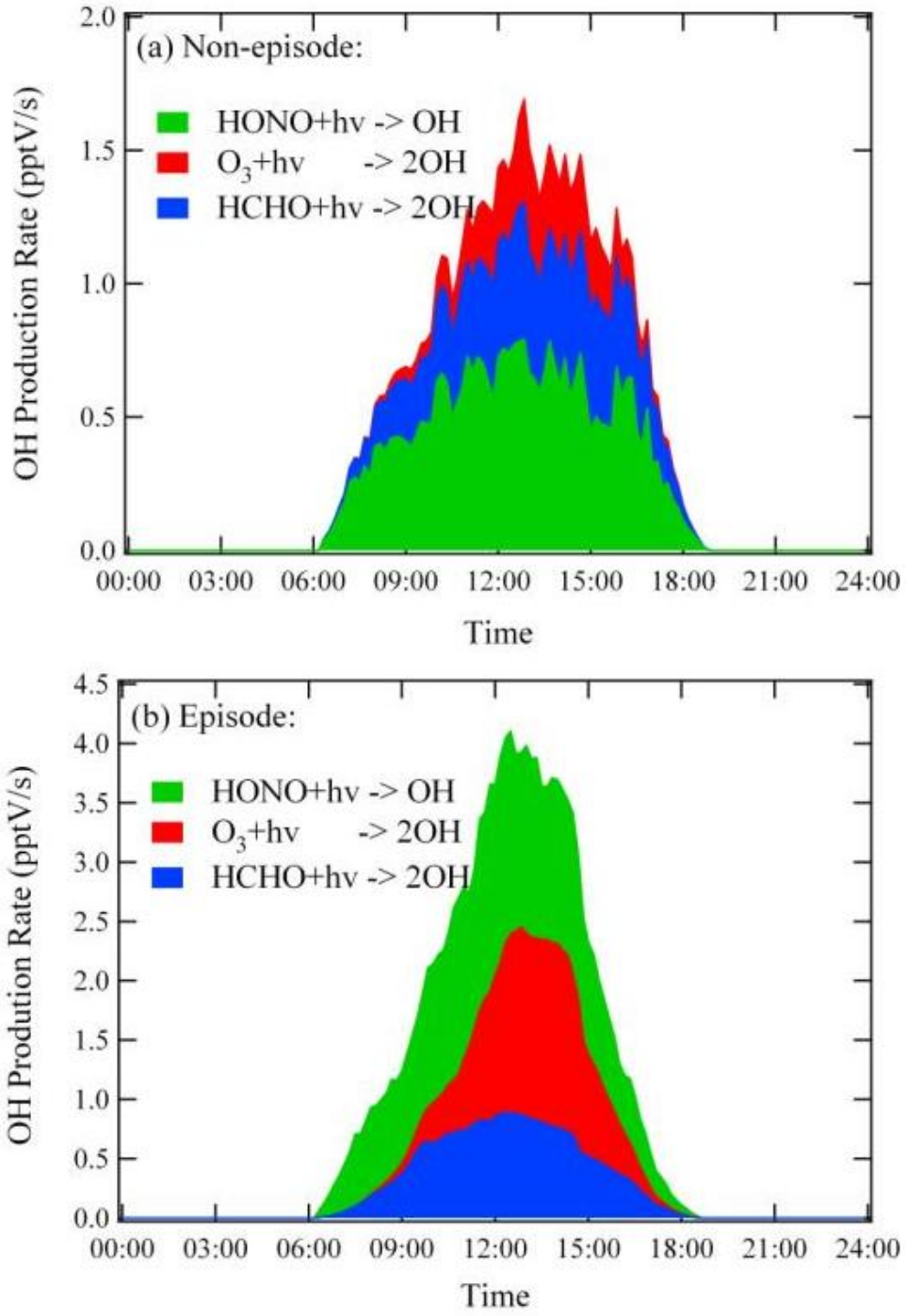

Figure 6.19 Averaged OH production rate for HONO (green), O_3 (red) and HCHO (blue) photolysis in OBM-case in (a) non-episode and (b) episode days.

Chapter 7 Conclusions and Recommendations

7.1 Conclusions

A zero-dimensional photochemical box model has been adopted to investigate the nitrous acid (HONO) chemistry in Hong Kong. The model is coupled with a near explicit chemical mechanism, MCM version 3.1. Besides, it is constrained by data observed during a comprehensive field campaign in a suburban site in Hong Kong. Results of this study have revealed both nighttime and daytime characteristics of HONO in the study site, which contributes to the understanding of the existing knowledge gap in HONO chemistry.

The main findings are summarized as follows:

(1) In the summer field campaign, a multi-day photochemical episode lasting for successive seven days has been observed. High daytime HONO concentrations over 1 ppbV were frequently measured, which is among the highest concentrations in existing records. The observation-based MCM box model has been used to explore the daytime HONO source(s). Large discrepancy exists between the simulated HONO PSS concentration and observation in episode days. Only by considering a significant extra daytime source (P_{extra}) of 1.12 pptV/s, can the high HONO level up to 1.2 ppbV be sustained.

(2) Correlation analysis between P_{extra} and proxies of ground and aerosol sources indicates that heterogeneous reaction on aerosol surfaces appears be of great importance to the daytime HONO accumulation in episode days. This important role of aerosol in daytime HONO formation appears to be resulted from the low NO_2 conversion rate on ground, high aerosol surface density as well as favorable aerosol chemical component (elementary carbon). Based on the good correlation between P_{extra} and aerosol-related source (R=0.65), a NO_2 uptake coefficient (γ_a) of 2.5×10^{-4} on aerosol surfaces is calculated. This value is larger than those obtained in laboratory studies. But it is comparable with the value adopted in many numerical simulations. The large uptake coefficient suggests that more attention should be paid on the role of aerosol in HONO formation.

(3) Nighttime NO_2 to HONO conversion rates of 0.43%/h and 0.31%/h have been estimated for episode and non-episode days, respectively. Conversion rates in this study are relatively lower compared to those in other sites, which indicate a low NO_2 conversion efficiency in TC. Further analysis suggests that the heterogeneous conversion process at night mainly occurs on ground surfaces instead of aerosol surfaces.

(4) Numerical simulation results show that HONO is a significant source of OH radical not only in the early morning, but also throughout the whole day in both scenarios (episode and non-episode). Chemical mechanism including only HONO homogenous source will lead to 20% underestimation of OH concentration in simulation. This suggests the need to incorporate a comprehensive HONO formation mechanism into the model framework in order to obtain a better model performance of OH radical and other related species.

7.2 Recommendations

Since this is the first piece of effort on HONO study in Hong Kong, only certain aspects of HONO have been studied. More focus should be put on this topic in the future to obtain a whole picture of HONO. To obtain extra evidence of the daytime HONO formation mechanism and to reduce the uncertainties of the model simulations, following recommendations are provided for further studies:

(1) Considering the importance of HONO in photochemistry, measurement of HONO, including both horizontal and vertical gradient measurements, should be taken into account in more field campaigns in the future.

(2) In order to improve numerical efficiency, the MCM box model in this study makes some simplification of the physical processes. It is better for the future numerical studies to incorporate the physical framework into the model simulation (such as 1-D or 3-D transport model), so as to minimize the possible calculation uncertainties caused by the physical processes.

(3) NO_2 uptake coefficient on aerosol surfaces (γ_a) has a wide range (10^{-8} to 10^{-4}), when parameterized into the model. In laboratory studies, this value also ranges from 10^{-8} to 10^{-5}. The reasons for this discrepancy are unclear. To reduce the modeling uncertainties caused by artificial factors, future studies should try to derive γ_a based on the field measurements in real atmosphere. Comparison between this observation- and laboratory-derived γ_a is strongly suggested so as to find the most appropriate parameterization scheme in different air quality models under different environments.

(4) HONO can be a significant source of OH radical throughout the whole day. Therefore, to obtain more accurate simulation results of OH and other chemical species, air quality models should include a representative HONO formation mechanism (including both homogeneous and heterogeneous reactions) in the model framework.

References

Acker, K., Möller, D., Auel, R., Wieprecht, W., Kalaß, D., 2005. Concentrations of nitrous acid, nitric acid, nitrite and nitrate in the gas and aerosol phase at a site in the emission zone during ESCOMPTE 2001 experiment. Atmos. Res. 74 (1), 507-524.

Acker, K., Möller, D., Wieprecht, W., Meixner, F.X., Bohn, B., Gilge, S., Plass-Dülmer, C., Berresheim, H., 2006a. Strong daytime production of OH from HNO_2 at a rural mountain site. Geophys. Res. Lett. 33 (2), L02809.

Acker, K., Möller, D., Wieprecht, W., Meixner, F.X., Bohn, B., Gilge, S., Plass‐Dülmer, C., Berresheim, H., 2006b. Strong daytime production of OH from HNO_2 at a rural mountain site. Geophys. Res. Lett. 33 (2).

Acker, K., Möller, D., 2007. Atmospheric variation of nitrous acid at different sites in Europe. Environ. Chem. 4 (4), 242-255.

Alicke, B., Platt, U., Stutz, J., 2002. Impact of nitrous acid photolysis on the total hydroxyl radical budget during the Limitation of Oxidant Production/Pianura Padana Produzione di Ozono study in Milan. J. Geophys. Res. 107 (D22), 8196.

Alicke, B., Geyer, A., Hofzumahaus, A., Holland, F., Konrad, S., Pätz, H., Schäfer, J., Stutz, J., Volz-Thomas, A., Platt, U., 2003. OH formation by HONO photolysis during the BERLIOZ experiment. J. Geophys. Res 108, 8247.

Ammann, M., Kalberer, M., Jost, D., Tobler, L., Rössler, E., Piguet, D., Gäggeler, H., Baltensperger, U., 1998. Heterogeneous production of nitrous acid on soot in polluted air masses. Nature 395 (6698), 157-160.

An, J., Zhang, W., Qu, Y., 2009. Impacts of a strong cold front on concentrations of HONO, HCHO, O_3, and NO_2 in the heavy traffic urban area of Beijing. Atmos. Environ. 43 (22), 3454-3459.

An, J., Li, Y., Chen, Y., Li, J., Qu, Y., Tang, Y., 2013. Enhancements of major aerosol components due to additional HONO sources in the North China Plain and implications for visibility and haze. Adv. Atmos. Sci. 30 (1), 57-66.

Andres-Hernandez, M., Notholt, J., Hjorth, J., Schrems, O., 1996. A DOAS study on the origin of nitrous acid at urban and non-urban sites. Atmos. Environ. 30 (2), 175-180.

Appel, B., Winer, A., Tokiwa, Y., Biermann, H., 1990. Comparison of atmospheric nitrous acid measurements by annular denuder and differential optical absorption systems. Atmos. Environ. Part A. General Topics 24 (3), 611-616.

Arens, F., Gutzwiller, L., Baltensperger, U., Gäggeler, H.W., Ammann, M., 2001. Heterogeneous reaction of NO_2 on diesel soot particles. Environ. Sci. Technol. 35 (11), 2191-2199.

Atkinson, R., Baulch, D., Cox, R., Hampson Jr, R., Kerr, J., Troe, J., 1992. Evaluated kinetic and photochemical data for atmospheric chemistry: Supplement IV. IUPAC subcommittee on gas kinetic data evaluation for atmospheric chemistry. J. Phys. Chem. Ref. Data 21, 1125.

Aumont, B., Madronich, S., Ammann, M., Kalberer, M., Baltensperger, U., Hauglustaine, D., Brocheton, F., 1999. On the NO_2+soot reaction in the atmosphere. J. Geophys. Res. 104 (D1), 1729-1736.

Aumont, B., Chervier, F., Laval, S., 2003a. Contribution of HONO sources to the NOx/HOx/O3 chemistry in the polluted boundary layer. Atmospheric Environment 37 (4), 487-498.

Aumont, B., Chervier, F., Laval, S., 2003b. Contribution of HONO sources to the $NO_x/HO_x/O_3$ chemistry in the polluted boundary layer. Atmos. Environ. 37 (4), 487-498.

Bejan, I., El Aal, Y.A., Barnes, I., Benter, T., Bohn, B., Wiesen, P., Kleffmann, J., 2006. The photolysis of ortho-nitrophenols: a new gas phase source of HONO. Phys. Chem. Chem. Phys. 8 (17), 2028-2035.

Bloss, C., Wagner, V., Jenkin, M., Volkamer, R., Bloss, W., Lee, J., Heard, D., Wirtz, K., Martin-Reviejo, M., Rea, G., 2005. Development of a detailed chemical mechanism (MCMv3. 1) for the atmospheric oxidation of aromatic hydrocarbons. Atmos. Chem. Phys. 5 (3), 641-664.

Brasseur, G., Prinn, R.G., Pszenny, A.A., 2003. Atmospheric chemistry in a changing world: an integration and synthesis of a decade of tropospheric chemistry research: the International Global Atmospheric Chemistry Project of the International Geosphere-Biosphere Programme. Springer Verlag.

Cardelino, C.A., Chameides, W.L., 2000. The application of data from photochemical assessment monitoring stations to the observation-based model. Atmos. Environ. 34 (12-14), 2325-2332.

Carr, S., Heard, D. E., and Blitz, M. A., 2009. Comment on "Atmospheric Hydroxyl Radical Production from Electronically Excited NO_2 and H_2O". Science 324 (5925), 336b.

Carter, W.P.L., 1988. Documentation for the SAPRC atmospheric photochemical mechanism preparation and emissions processing programs for implementation in airshed models. Appendix C, California Air Resource Board.

Carter, W.P.L., 2000. Documentation of the SAPRC-99 chemical mechanism for VOC reactivity assessment. Contract 92 (329), 95-308.

Carter, W.P.L., Division, C.E.P.A.A.R.B.R., University of California, R.C.o.E.C.f.E.R., Technology, 2007. Development of the SAPRC-07 chemical mechanism and updated ozone reactivity scales. California Air Resources Board, Research Division.

Carter, W.P.L., 2010. Development of a condensed SAPRC-07 chemical mechanism. Atmos. Environ. 44 (40), 5336–5345.

Chan, W.H., Nordstrom, R.J., Calvert, J.G., Shaw, J.H., 1976. Kinetic study of nitrous acid formation and decay reactions in gaseous mixtures of nitrous acid, nitrogen oxide (NO), nitrogen oxide (NO_2), water, and nitrogen. Environ. Sci. Technol. 10 (7), 674-682.

Chou, C.C.-K., Liu, S.C., Lin, C.-Y., Shiu, C.-J., Chang, K.-H., 2006. The trend of surface ozone in Taipei, Taiwan, and its causes: Implications for ozone control strategies. Atmos. Environ. 40 (21), 3898-3908.

Cooper, O., Parrish, D., Stohl, A., Trainer, M., Nédélec, P., Thouret, V., Cammas, J., Oltmans, S., Johnson, B., Tarasick, D., 2010. Increasing springtime ozone mixing ratios in the free troposphere over western North America. Nature 463 (7279), 344-348.

Crowley, J.N., Carl, S.A., 1997. OH Formation in the Photoexcitation of NO_2 beyond the Dissociation Threshold in the Presence of Water Vapor. J. Phys. Chem. 101 (23), 4178-4184.

Czader, B., Rappenglück, B., Percell, P., Byun, D., Ngan, F., Kim, S., 2012a. Modeling nitrous acid and its impact on ozone and hydroxyl radical during the Texas Air Quality Study 2006. Atmos. Chem. Phys. Discuss 12, 5851-5880.

Czader, B.H., Rappenglück, B., Percell, P., Byun, D.W., Ngan, F., Kim, S., 2012b. Modeling nitrous acid and its impact on ozone and hydroxyl radical during the Texas Air Quality Study 2006. Atmos. Chem. Phys. 12 (15), 6939-6951.

Elshorbany, Y., Kurtenbach, R., Wiesen, P., Lissi, E., Rubio, M., Villena, G., Gramsch, E., Rickard, A., Pilling, M., Kleffmann, J., 2009. Oxidation capacity of the city air of Santiago, Chile. Atmos. Chem. Phys. 9 (6), 2257-2273.

Elshorbany, Y., Steil, B., Brühl, C., Lelieveld, J., 2012. Impact of HONO on global atmospheric chemistry calculated with an empirical parameterization in the EMAC model. Atmos. Chem. Phys. Discuss 12 (5), 12885-12934.

Febo, A., Perrino, C., Allegrini, I., 1996. Measurement of nitrous acid in Milan, Italy, by DOAS and diffusion denuders. Atmos. Environ. 30 (21), 3599-3609.

Finlayson-Pitts, B., Pitts Jr, J., 1993. Atmospheric chemistry of tropospheric ozone formation: scientific and regulatory implications. J. Air Waste Manage. 43 (8), 1091-1100.

Finlayson-Pitts, B., Wingen, L., Sumner, A., Syomin, D., Ramazan, K., 2003. The heterogeneous hydrolysis of NO_2 in laboratory systems and in outdoor and indoor atmospheres: An integrated mechanism. Phys. Chem. Chem. Phys. 5 (2), 223-242.

Gao, J., Wang, T., Zhou, X., Wu, W., Wang, W., 2009. Measurement of aerosol number size distributions in the Yangtze River delta in China: Formation and growth of particles under polluted conditions. Atmos. Environ. 43 (4), 829-836.

George, C., Strekowski, R., Kleffmann, J., Stemmler, K., Ammann, M., 2005. Photoenhanced uptake of gaseous NO_2 on solid organic compounds: a photochemical source of HONO? Faraday Discuss. 130 (0), 195-210.

Gerecke, A., Thielmann, A., Gutzwiller, L., Rossi, M.J., 1998. The chemical kinetics of HONO formation resulting from heterogeneous interaction of NO_2 with flame soot. Geophys. Res. Lett. 25 (13), 2453-2456.

Gery, M.W., Whitten, G.Z., Killus, J.P., Dodge, M.C., 1989. A photochemical kinetics mechanism for urban and regional scale computer modeling. J. Geophys. Res 94 (12), 925-912.

Gonçalves Ageitos, M., Dabdub, D., Chang, W., Saiz, F., Jorba Casellas, O., Baldasano Recio, J.M., 2010. The impact of different nitrous acid sources in the air quality levels of the Iberian Peninsula. Atmos. Chem. Phys. Discuss 10, 28183-28230.

Gonçalves, M., Dabdub, D., Chang, W., Jorba, O., Baldasano, J., 2012. Impact of HONO sources on the performance of mesoscale air quality models. Atmos. Environ. 54, 168–176.

Gustafsson, J.R., Orlov, A., Griffiths, P.T., Cox, R.A., Lambert, R.M., 2006. Reduction of NO_2 to nitrous acid on illuminated titanium dioxide aerosol surfaces: implications for photocatalysis and atmospheric chemistry. Chem. Comm. (37), 3936-3938.

Gutzwiller, L., Arens, F., Baltensperger, U., Gäggeler, H.W., Ammann, M., 2002. Significance of semivolatile diesel exhaust organics for secondary HONO formation. Environ. Sci. Technol. 36 (4), 677-682.

HAO, N., ZHOU, B., CHEN, D., CHEN, L.-m., 2006. Observations of nitrous acid and its relative humidity dependence in Shanghai. J. Environ. Sci. 18 (5), 910-915.

Harrison, R.M., Kitto, A.M.N., 1994. Evidence for a surface source of atmospheric nitrous acid. Atmos. Environ. 28 (6), 1089-1094.

Harrison, R.M., Peak, J.D., Collins, G.M., 1996. Tropospheric cycle of nitrous acid. J. Geophys. Res. 101 (D9), 14,429-414,439.

Harrison, R.M., Collins, G.M., 1998. Measurements of reaction coefficients of NO_2 and HONO on aerosol particles. J. Atmos. Chem. 30 (3), 397-406.

Häseler, R., Brauers, T., Holland, F., Wahner, A., 2009. Development and application of a new mobile LOPAP instrument for the measurement of HONO altitude profiles in the planetary boundary layer. Atmos. Meas. Tech. Discuss. 2 (4), 2027-2054.

Hofzumahaus, A., Rohrer, F., Lu, K., Bohn, B., Brauers, T., Chang, C.C., Fuchs, H., Holland, F., Kita, K., Kondo, Y., 2009. Amplified trace gas removal in the troposphere. Science 324 (5935), 1702-1704.

Howard, C.J., Evenson, K., 1977. Kinetics of the reaction of HO_2 with NO. Geophys. Res. Lett. 4 (10), 437-440.

Jacob, D.J., 2000. Heterogeneous chemistry and tropospheric ozone. Atmos. Environ. 34 (12), 2131-2159.

Jenkin, M.E., Cox, R.A., Williams, D.J., 1988. Laboratory studies of the kinetics of formation of nitrous acid from the thermal reaction of nitrogen dioxide and water vapour. Atmos. Environ. (1967) 22 (3), 487-498.

Jenkin, M.E., Saunders, S.M., Pilling, M.J., 1997. The tropospheric degradation of volatile organic compounds: a protocol for mechanism development. Atmos. Environ. 31 (1), 81-104.

Jenkin, M.E., Saunders, S.M., Wagner, V., Pilling, M.J., 2003. Protocol for the development of the Master Chemical Mechanism, MCM v3 (Part B): tropospheric degradation of aromatic volatile organic compounds. Atmos. Chem. Phys. 3 (1), 181-193.

Kaiser, E., Wu, C., 1977. A kinetic study of the gas phase formation and decomposition reactions of nitrous acid. J. Phys. Chem. 81 (18), 1701-1706.

Kirchstetter, T.W., Harley, R.A., Littlejohn, D., 1996. Measurement of nitrous acid in motor vehicle exhaust. Environ. Sci. Technol. 30 (9), 2843-2849.

Kleffmann, J., Becker, K., Wiesen, P., 1998. Heterogeneous NO_2 conversion processes on acid surfaces:: possible atmospheric implications. Atmos. Environ. 32 (16), 2721-2729.

Kleffmann, J., Becker, K.H., Lackhoff, M., Wiesen, P., 1999. Heterogeneous conversion of NO2 on carbonaceous surfaces. Phys. Chem. Chem. Phys. 1 (24), 5443-5450.

Kleffmann, J., Heland, J., Kurtenbach, R., Lörzer, J., Wiesen, P., 2002. A new instrument (LOPAP) for the detection of nitrous acid (HONO). Environ. Sci. Pollut. Res. 9 (4), 48-54.

Kleffmann, J., Kurtenbach, R., Lörzer, J., Wiesen, P., Kalthoff, N., Vogel, B., Vogel, H., 2003. Measured and simulated vertical profiles of nitrous acid--Part I: Field measurements. Atmos. Environ. 37 (21), 2949-2955.

Kleffmann, J., Wiesen, P., 2004. Heterogeneous conversion of NO.

Kleffmann, J., Gavriloaiei, T., Hofzumahaus, A., Holland, F., Koppmann, R., Rupp, L., Schlosser, E., Siese, M., Wahner, A., 2005. Daytime formation of nitrous acid: A major source of OH radicals in a forest. Geophys. Res. Lett. 32 (5), L05818.

Kleffmann, J., Wiesen, P., 2005. Heterogeneous conversion of NO_2 and NO on HNO_3 treated soot surfaces: atmospheric implications. Atmos. Chem. Phys. 5 (1), 77-83.

Kleffmann, J., 2007. Daytime sources of nitrous acid (HONO) in the atmospheric boundary layer. Chem. Phys. Chem. 8 (8), 1137-1144.

Kleffmann, J., Wiesen, P., 2008. Technical Note: Quantification of interferences of wet chemical HONO LOPAP measurements under simulated polar conditions. Atmos. Chem. Phys. 8 (22), 6813-6822.

Knipping, E.M., Dabdub, D., 2002. Modeling surface-mediated renoxification of the atmosphere via reaction of gaseous nitric oxide with deposited nitric acid. Atmos. Environ. 36 (36-37), 5741-5748.

Krupa, S.V., Manning, W.J., 1988. Atmospheric ozone: formation and effects on vegetation. Environmental Pollution 50 (1), 101-137.

Kurtenbach, R., Becker, K., Gomes, J., Kleffmann, J., Lörzer, J., Spittler, M., Wiesen, P., Ackermann, R., Geyer, A., Platt, U., 2001. Investigations of emissions and heterogeneous formation of HONO in a road traffic tunnel. Atmos. Environ. 35 (20), 3385-3394.

Lammel, G., Cape, J.N., 1996. Nitrous acid and nitrite in the atmosphere. Chem. Soc. Rev. 25 (5), 361-369.

Lammel, G., 1999. Formation of nitrous acid: parameterisation and comparison with observations.

Lee, B., Wood, E., Herndon, S., Lefer, B., Luke, W., Brune, W., Nelson, D., Zahniser, M., Munger, J., 2013. Urban measurements of atmospheric nitrous acid: A caveat on the interpretation of the HONO photostationary state. J. Geophys. Res.: Atmospheres 118 (21), 12274–12281.

Levy 2nd, H., 1971. Normal atmosphere: large radical and formaldehyde concentrations predicted. Science (New York, NY) 173 (3992), 141.

Li, G., Lei, W., Zavala, M., Volkamer, R., Dusanter, S., Stevens, P., Molina, L., 2010. Impacts of HONO sources on the photochemistry in Mexico City during the MCMA-2006/MILAGO Campaign. Atmos. Chem. Phys. 10 (14), 6551–6567.

Li, S., Matthews, J., Sinha, A., 2008. Atmospheric hydroxyl radical production from electronically excited NO_2 and H_2O. Science 319 (5870), 1657-1660.

Li, X., Brauers, T., Häseler, R., Bohn, B., Hofzumahaus, A., Holland, F., Lu, K., Rohrer, F., Hu, M., Zeng, L., 2011a. Exploring the atmospheric chemistry of nitrous acid (HONO) at a rural site in Southern China. Atmos. Chem. Phys. Discuss 11, 27591-27635.

Li, X., Brauers, T., Häseler, R., Bohn, B., Fuchs, H., Hofzumahaus, A., Holland, F., Lou, S., Lu, K., Rohrer, F., 2012. Exploring the atmospheric chemistry of nitrous acid (HONO) at a rural site in Southern China. Atmos. Chem. Phys. 12 (3), 1497-1513.

Li, Y., An, J., Min, M., Zhang, W., Wang, F., Xie, P., 2011b. Impacts of HONO sources on the air quality in Beijing, Tianjin and Hebei Province of China. Atmos. Environ. 45 (27), 4735-4744.

Liao, W., Case, A., Mastromarino, J., Tan, D., Dibb, J., 2006. Observations of HONO by laser-induced fluorescence at the South Pole during ANTCI 2003. Geophys. Res. Lett. 33 (9).

Ling, Z.H., Guo, H., Zheng, J.Y., Louie, P.K.K., Cheng, H.R., Jiang, F., Cheung, K., Wong, L.C., Feng, X.Q., 2012. Establishing a conceptual model for photochemical ozone pollution in subtropical Hong Kong. Atmos. Environ. 76, 208-220.

Liu, Z., 2012. Characterizing the photochemical environment over China, PhD Dissertation thesis, Georgia Institute of Technology.

Marcia C, D., 2000. Chemical oxidant mechanisms for air quality modeling: critical review. Atmos. Environ. 34 (12–14), 2103-2130.

Mebel, A., Lin, M., Melius, C., 1998. Rate constant of the HONO+ HONO→ H_2O+ NO+ NO_2 reaction from ab initio MO and TST calculations. J. Phys. Chem. 102 (10), 1803-1807.

Michoud, V., Colomb, A., Borbon, A., Miet, K., Beekmann, M., Camredon, M., Aumont, B., Perrier, S., Zapf, P., Siour, G., 2013. Study of the unknown HONO daytime source at an European suburban site during the MEGAPOLI summer and winter field campaigns. Atmos. Chem. Phys. Discuss 13 (9), 23639-23690.

Michoud, V., Colomb, A., Borbon, A., Miet, K., Beekmann, M., Camredon, M., Aumont, B., Perrier, S., Zapf, P., Siour, G., 2014. Study of the unknown HONO daytime source at a European suburban site during the MEGAPOLI summer and winter field campaigns. Atmos. Chem. Phys. 14 (6), 2805-2822.

Mihelcic, D., Holland, F., Hofzumahaus, A., Hoppe, L., Konrad, S., Müsgen, P., Pätz, H.W., Schäfer, H.J., Schmitz, T., Volz‐Thomas, A., 2003. Peroxy radicals during BERLIOZ at Pabstthum: Measurements, radical budgets and ozone production. J. Geophys. Res.: Atmospheres (1984–2012) 108 (D4).

Monge, M.E., D'Anna, B., Mazri, L., Giroir-Fendler, A., Ammann, M., Donaldson, D.J., George, C., 2010. Light changes the atmospheric reactivity of soot. P. Natl. Acad. Sci. USA 107 (15), 6605-6609.

Ndour, M., D'Anna, B., George, C., Ka, O., Balkanski, Y., Kleffmann, J., Stemmler, K., Ammann, M., 2008. Photoenhanced uptake of NO_2 on mineral dust: Laboratory experiments and model simulations. Geophys. Res. Lett. 35 (5), L05812.

Notholt, J., Hjorth, J., Raes, F., 1992. Formation of HNO_2 on aerosol surfaces during foggy periods in the presence of NO and NO_2. Atmos. Environ. Part A. General Topics 26 (2), 211-217.

Oltmans, S., Lefohn, A., Harris, J., Galbally, I., Scheel, H., Bodeker, G., Brunke, E., Claude, H., Tarasick, D., Johnson, B., 2006. Long-term changes in tropospheric ozone. Atmos. Environ. 40 (17), 3156-3173.

Perner, D., Platt, U., 1979. Detection of nitrous acid in the atmosphere by differential optical absorption. Geophys. Res. Lett. 6 (12), 917-920.

Qin, M., Xie, P., Su, H., Gu, J., Peng, F., Li, S., Zeng, L., Liu, J., Liu, W., Zhang, Y., 2009. An observational study of the HONO–NO_2 coupling at an urban site in Guangzhou City, South China. Atmos. Environ. 43 (36), 5731-5742.

Ren, X., Harder, H., Martinez, M., Lesher, R.L., Oliger, A., Simpas, J.B., Brune, W.H., Schwab, J.J., Demerjian, K.L., He, Y., 2003. OH and HO_2 Chemistry in the urban atmosphere of New York City. Atmos. Environ. 37 (26), 3639-3651.

Rivera-Figueroa, A., Sumner, A., Finlayson-Pitts, B., 2003. Laboratory studies of potential mechanisms of renoxification of tropospheric nitric acid. Environ. Sci. Technol. 37 (3), 548-554.

Ryerson, T., Trainer, M., Holloway, J., Parrish, D., Huey, L., Sueper, D., Frost, G., Donnelly, S., Schauffler, S., Atlas, E., 2001. Observations of ozone formation in power plant plumes and implications for ozone control strategies. Science 292 (5517), 719-723.

Sarwar, G., Luecken, D., Yarwood, G., Whitten, G.Z., Carter, W.P.L., 2008a. Impact of an updated carbon bond mechanism on predictions from the CMAQ modeling system: Preliminary assessment. J. Appl. Meteor. Climatol. 47 (1), 3-14.

Sarwar, G., Roselle, S.J., Mathur, R., Appel, W., Dennis, R.L., Vogel, B., 2008b. A comparison of CMAQ HONO predictions with observations from the Northeast Oxidant and Particle Study. Atmos. Environ. 42 (23), 5760-5770.

Saunders, S.M., Jenkin, M.E., Derwent, R.G., Pilling, M.J., 2003. Protocol for the development of the Master Chemical Mechanism, MCM v3 (Part A): tropospheric degradation of non-aromatic volatile organic compounds. Atmos. Chem. Phys. 3 (1), 161-180.

Seinfeld, J.H., 1988. Ozone air quality models. A critical review. JAPCA, J. Air Waste Ma. 38 (5).

Seinfeld, J.H., Pandis, S.N., 1998. From air pollution to climate change: Atmospheric Chemistry and Physics. John Wiley & Sons, New York.

Seinfeld, J.H., Pandis, S.N., 2006. Atmospheric chemistry and physics: from air pollution to climate change. John Wiley & Sons, Inc., Hoboken, New Jersey.

Sillman, S., 1993. Tropospheric ozone: The debate over control strategies. Annu. Rev. Energy Environ. 18 (1), 31-56.

Simon, P.K., Dasgupta, P.K., 1995. Continuous automated measurement of gaseous nitrous and nitric acids and particulate nitrite and nitrate. Environ. Sci. Technol. 29 (6), 1534-1541.

Sörgel, M., Regelin, E., Bozem, H., Diesch, J.-M., Drewnick, F., Fischer, H., Harder, H., Held, A., Hosaynali-Beygi, Z., Martinez, M., 2011. Quantification of the unknown HONO daytime source and its relation to NO_2. Atmos. Chem. Phys. 11, 15119-15155.

Spataro, F., Ianniello, A., Esposito, G., Allegrini, I., Zhu, T., Hu, M., 2013. Occurrence of atmospheric nitrous acid in the urban area of Beijing (China). Sci. Total Environ. 447, 210-224.

Spindler, G., Bruggemann, E., Herrmann, H., 1999. Nitrous acid (HNO_2) concentration measurements and estimation of dry deposition over grassland in eastern Germany. Borrell, PM and Borell, P., Editors, 223-227.

Spindler, G., Hesper, J., Brüggemann, E., Dubois, R., Müller, T., Herrmann, H., 2003. Wet annular denuder measurements of nitrous acid: laboratory study of the artefact reaction of NO_2 with S (IV) in aqueous solution and comparison with field measurements. Atmos. Environ. 37 (19), 2643-2662.

Stemmler, K., Ammann, M., Donders, C., Kleffmann, J., George, C., 2006. Photosensitized reduction of nitrogen dioxide on humic acid as a source of nitrous acid. Nature 440 (7081), 195-198.

Stemmler, K., Ndour, M., Elshorbany, Y., Kleffmann, J., D'anna, B., George, C., Bohn, B., Ammann, M., 2007. Light induced conversion of nitrogen dioxide into nitrous acid on submicron humic acid aerosol. Atmos. Chem. Phys. 7 (16), 4237-4248.

Stockwell, W.R., Calvert, J.G., 1983. The Mechanism of NO_3 and HONO formation in the nighttime chemistry of the urban atmosphere. J. Geophys. Res. 88 (C11), 6673-6682.

Stockwell, W.R., 1986. A homogeneous gas phase mechanism for use in a regional acid deposition model. Atmos. Environ. (1967) 20 (8), 1615-1632.

Stockwell, W.R., Middleton, P., Chang, J.S., Tang, X., 1990. The second generation regional acid deposition model chemical mechanism for regional air quality modeling. J. Geophys. Res. 95 (D10), 16343-16367.

Stockwell, W.R., Kirchner, F., Kuhn, M., Seefeld, S., 1997. A new mechanism for regional atmospheric chemistry modeling. J. Geophys. Res. 102 (D22), 25847-25879.

Stutz, J., Alicke, B., Neftel, A., 2002. Nitrous acid formation in the urban atmosphere: Gradient measurements of NO_2 and HONO over grass in Milan, Italy. J. Geophys. Res. 107 (D22), 8192.

Stutz, J., Wong, K.W., Tsai, C., 2013. Field Observations of Daytime HONO Chemistry and Its Impact on the OH Radical Budget. Disposal of Dangerous Chemicals in Urban Areas and Mega Cities, 1-14.

Su, H., Cheng, Y.F., Cheng, P., Zhang, Y.H., Dong, S., Zeng, L.M., Wang, X., Slanina, J., Shao, M., Wiedensohler, A., 2008a. Observation of nighttime nitrous acid (HONO) formation at a non-urban site during PRIDE-PRD2004 in China. Atmos. Environ. 42 (25), 6219-6232.

Su, H., Cheng, Y.F., Shao, M., Gao, D.F., Yu, Z.Y., Zeng, L.M., Slanina, J., Zhang, Y.H., Wiedensohler, A., 2008b. Nitrous acid (HONO) and its daytime sources at a rural site during the 2004 PRIDE-PRD experiment in China. J. Geophys. Res. 113 (D14), D14312.

Su, H., Cheng, Y., Oswald, R., Behrendt, T., Trebs, I., Meixner, F.X., Andreae, M.O., Cheng, P., Zhang, Y., Pöschl, U., 2011. Soil nitrite as a source of atmospheric HONO and OH radicals. Science 333 (6049), 1616-1618.

Svensson, R., Ljungström, E., Lindqvist, O., 1987. Kinetics of the reaction between nitrogen dioxide and water vapour. Atmos. Environ. (1967) 21 (7), 1529-1539.

Trick, S., 2004. Formation of nitrous acid on urban surfaces, Ph.D. Dissertation thesis, Ruperto-Carola University of Heidelberg, Germany.

Tyndall, G.S., Orlando, J.J., Calvert, J.G., 1995. Upper Limit for the Rate Coefficient for the Reaction HO_2+NO_2. fwdarw. HONO+O_2. Environ. Sci. Technol. 29 (1), 202-206.

Veitel, H., 2002. Vertical profiles of NO_2 and HONO in the planetary boundary layer, Ph.D. Dissertation thesis, Ruperto-Carola University of Heidelberg, Germany.

Villena, G., Kleffmann, J., Kurtenbach, R., Wiesen, P., Lissi, E., Rubio, M.A., Croxatto, G., Rappenglück, B., 2011. Vertical gradients of HONO, NO_x and O_3 in Santiago de Chile. Atmos. Environ. 45 (23), 3867-3873.

Vingarzan, R., 2004. A review of surface ozone background levels and trends. Atmos. Environ. 38 (21), 3431-3442.

Vogel, B., Vogel, H., Kleffmann, J., Kurtenbach, R., 2003. Measured and simulated vertical profiles of nitrous acid--Part II. Model simulations and indications for a photolytic source. Atmos. Environ. 37 (21), 2957-2966.

Wang, T., Cheung, T.F., Lam, K.S., Kok, G.L., Harris, J.M., 2001. The characteristics of ozone and related compounds in the boundary layer of the South China coast: temporal and vertical variations during autumn season. Atmos. Environ. 35 (15), 2735-2746.

Wang, T., Cheung, T., Li, Y., Yu, X., Blake, D., 2002. Emission characteristics of CO, NO_x, SO_2 and indications of biomass burning observed at a rural site in eastern China. J. Geophys. Res 107 (D12), ACH 9-1–ACH 9-10.

Wang, T., Kwok, J.Y., 2003. Measurement and analysis of a multiday photochemical smog episode in the Pearl River delta of China. J. Appl. Meteorol. 42 (3), 404-416.

Wang, T., Poon, C., Kwok, Y., Li, Y., 2003. Characterizing the temporal variability and emission patterns of pollution plumes in the Pearl River Delta of China. Atmos. Environ. 37 (25), 3539-3550.

Whitten, G.Z., Hogo, H., Killus, J.P., 1980. The carbon-bond mechanism: a condensed kinetic mechanism for photochemical smog. Environ. Sci. Technol. 14 (6), 690-700.

Wong, K.W., Oh, H., Lefer, B., Rappenglück, B., Stutz, J., 2011. Vertical profiles of nitrous acid in the nocturnal urban atmosphere of Houston, TX. Atmos. Chem. Phys. 11 (8), 3595-3609.

Wong, K.W., Tsai, C., Lefer, B., Haman, C., Grossberg, N., Brune, W.H., Ren, X., Luke, W., Stutz, J., 2012. Daytime HONO vertical gradients during SHARP 2009 in Houston, TX. Atmos. Chem. Phys. 12 (2), 635-652.

Wong, K.W., Tsai, C., Lefer, B., Grossberg, N., Stutz, J., 2013. Modeling of daytime HONO vertical gradients during SHARP 2009. Atmos. Chem. Phys. 13 (7), 3587-3601.

Wu, H.W.Y., Chan, L., 2001. Surface ozone trends in Hong Kong in 1985-1995. Environ. Int. 26 (4), 213-222.

Xu, Z., Wang, T., Xue, L., Louie, P.K.K., Luk, C.W.Y., Gao, J., Wang, S., Chai, F., Wang, W., 2013. Evaluating the uncertainties of thermal catalytic conversion in measuring atmospheric nitrogen dioxide at four differently polluted sites in China. Atmos. Environ. 76, 221-226.

Yarwood, G., Whitten, G.Z., Rao, S., 2005. Updates to the Carbon Bond 4 photochemical mechanism. Environ. Int. Corp.

Yu, Y., Galle, B., Panday, A., Hodson, E., Prinn, R., Wang, S., 2009. Observations of high rates of NO_2-HONO conversion in the nocturnal atmospheric boundary layer in Kathmandu, Nepal. Atmos. Chem. Phys. 9 (17), 6401-6415.

Zhang, B., Tao, F.-M., 2010. Direct homogeneous nucleation of NO_2, H_2O, and NH_3 for the production of ammonium nitrate particles and HONO gas. Chem. Phy. Lett. 489 (4), 143-147.

Zhang, J., Wang, T., Chameides, W., Cardelino, C., Kwok, J., Blake, D., Ding, A., So, K., 2007. Ozone production and hydrocarbon reactivity in Hong Kong, Southern China. Atmos. Chem. Phys. 7 (2), 557-573.

Zhang, N., Zhou, X., Shepson, P.B., Gao, H., Alaghmand, M., Stirm, B., 2009. Aircraft measurement of HONO vertical profiles over a forested region. Geophys. Res. Lett. 36 (15), L15820.

Zhang, R., Sarwar, G., Fung, J., Lau, A., Zhang, Y., 2011. Impact of nitrous acid chemistry on air quality modeling results over the Pearl River Delta region. Atmos. Chem. Phys. Discuss. 11, 15075–15117.

Zhang, R., Sarwar, G., Fung, J.C.H., Lau, A.K.H., Zhang, Y., 2012. Examining the Impact of Nitrous Acid Chemistry on Ozone and PM over the Pearl River Delta Region. Adv. Meteor. 2012, 1-18.

Zheng, J., Zhong, L., Wang, T., Louie, P.K.K., Li, Z., 2010. Ground-level ozone in the Pearl River Delta region: Analysis of data from a recently established regional air quality monitoring network. Atmos. Environ. 44 (6), 814-823.

Zhou, X., Civerolo, K., Dai, H., Huang, G., Schwab, J., Demerjian, K., 2002. Summertime nitrous acid chemistry in the atmospheric boundary layer at a rural site in New York State. J. Geophys. Res. 107 (D21), 4590.

Zhou, X., Gao, H., He, Y., Huang, G., Bertman, S.B., Civerolo, K., Schwab, J., 2003. Nitric acid photolysis on surfaces in low-NO_x environments: Significant atmospheric implications. Geophys. Res. Lett. 30 (23), 2217.

Zhou, X., Zhang, N., TerAvest, M., Tang, D., Hou, J., Bertman, S., Alaghmand, M., Shepson, P.B., Carroll, M.A., Griffith, S., 2011. Nitric acid photolysis on forest canopy surface as a source for tropospheric nitrous acid. Nat. Geosci. 4 (7), 440-443.

Ziemba, L.D., Dibb, J.E., Griffin, R.J., Anderson, C.H., Whitlow, S.I., Lefer, B.L., Rappenglück, B., Flynn, J., 2010. Heterogeneous conversion of nitric acid to nitrous acid on the surface of primary organic aerosol in an urban atmosphere. Atmos. Environ. 44 (33), 4081-4089.